AD-A040 265   NAVAL RESEARCH LAB WASHINGTON D C   F/G 17/2
EXPERIMENTAL INVESTIGATION OF THE CHARACTERISTICS OF PC1 MICROP--ETC(U)
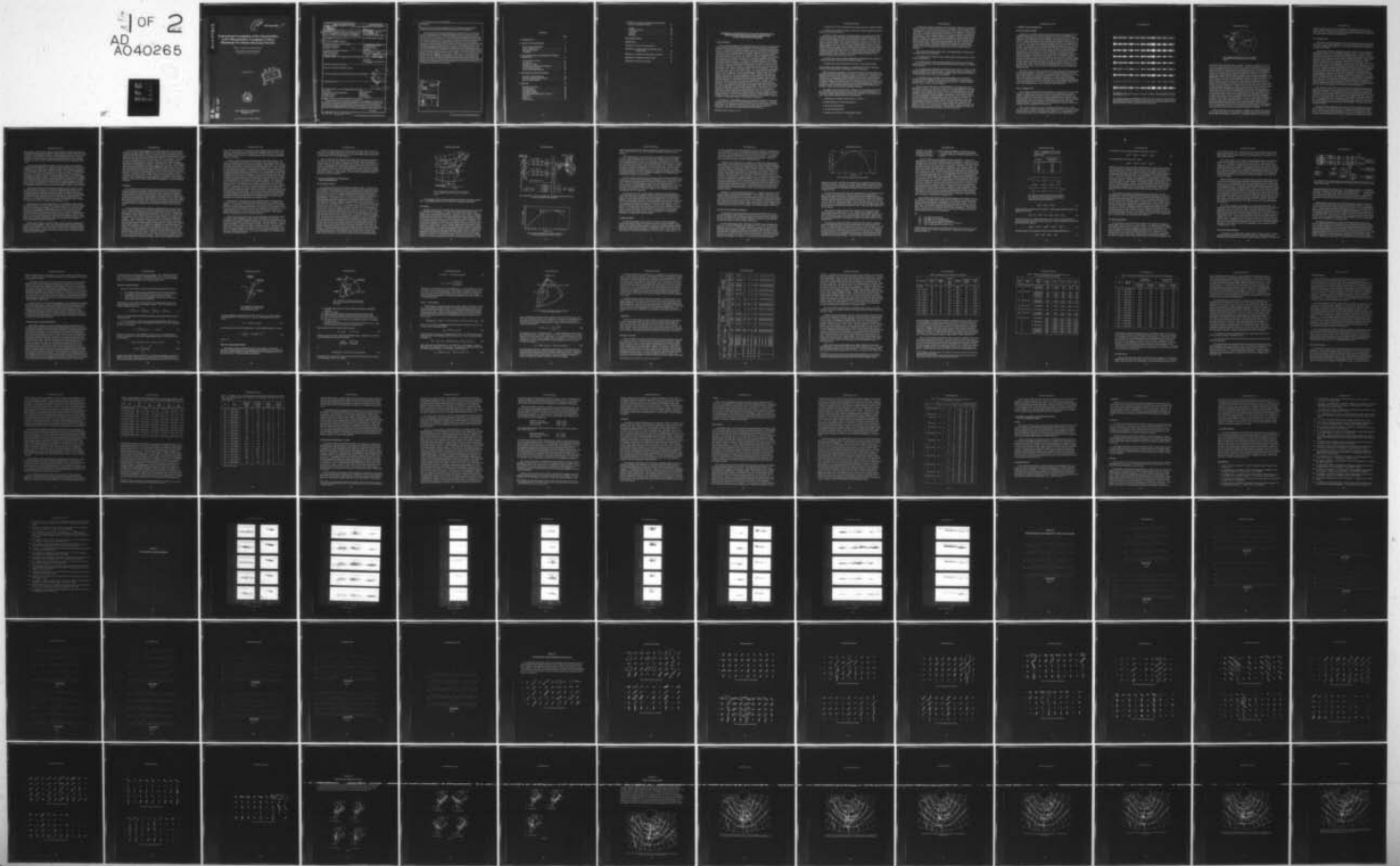MAY 77   E L ALTHOUSE, J R DAVIS

UNCLASSIFIED   NRL-8086   NL

1 OF 2
AD
A040265

NRL Report 8086

Experimental Investigation of the Characteristics of Pc1 Micropulsation Propagation Using a Midlatitude Five-Station Receiving Network

EDWIN L. ALTHOUSE AND JOHN R. DAVIS

Electromagnetic Propagation Branch
Communications Sciences Division

May 18, 1977

DDC

JUN 8 1977

C

NAVAL RESEARCH LABORATORY
Washington, D.C.

REPORT DOCUMENTATION PAGE		READ INSTRUCTIONS BEFORE COMPLETING FORM
1. REPORT NUMBER NRL 8086	2. GOVT ACCESSION NO.	3. RECIPIENT'S CATALOG NUMBER
4. TITLE (and Subtitle) EXPERIMENTAL INVESTIGATION OF THE CHARACTERISTICS OF Pc1 MICROPULSATION PROPAGATION USING A MIDLATITUDE FIVE-STATION RECEIVING NETWORK		5. TYPE OF REPORT & PERIOD COVERED Final report on one phase of a continuing NRL problem
		6. PERFORMING ORG. REPORT NUMBER
7. AUTHOR(s) Edwin L. Althouse and John R. Davis		8. CONTRACT OR GRANT NUMBER(s)
9. PERFORMING ORGANIZATION NAME AND ADDRESS Naval Research Laboratory Washington, D.C. 20375		10. PROGRAM ELEMENT, PROJECT, TASK AREA & WORK UNIT NUMBERS NRL Problem R07-29 ONR Program Element 61153N-21
11. CONTROLLING OFFICE NAME AND ADDRESS Department of the Navy Office of Naval Research Arlington, Va. 22217		12. REPORT DATE May 18, 1977
		13. NUMBER OF PAGES 96
14. MONITORING AGENCY NAME & ADDRESS(if different from Controlling Office)		15. SECURITY CLASS. (of this report) Unclassified
		15a. DECLASSIFICATION/DOWNGRADING SCHEDULE

16. DISTRIBUTION STATEMENT (of this Report)

Approved for public release; distribution unlimited.

17. DISTRIBUTION STATEMENT (of the abstract entered in Block 20, if different from Report)

18. SUPPLEMENTARY NOTES

19. KEY WORDS (Continue on reverse side if necessary and identify by block number)

Alfven waves
Communications to submerged submarines
Geomagnetic variations
Ionospheric ducting

Magnetic field sensors
Magnetosphere
Micropulsations
Ultralow frequencies

20. ABSTRACT (Continue on reverse side if necessary and identify by block number)

An experimental study has been made of the characteristics of the propagation of midlatitude Pc1 micropulsations for the purpose of assessing the applicability of the 0.5-2.0 Hz frequency band to naval communications. Naturally occurring hydromagnetic emissions were the object of study because no effective way of artificially generating these waves is known. Observations were made using a five-station receiving network stretching from New York to Florida and from Maryland to Illinois. All data were

(Continued)

DD FORM 1473 EDITION OF 1 NOV 65 IS OBSOLETE
i
S/N 0102-014-6601

20 (Continued)

telemetered in real time over telephone data lines to NRL for centralized recording and analysis. Amplitude, spectral, and polarization characteristics are presented for the data analyzed.

Cross-correlation was used to determine propagation time delays between sites. The time delays were used as input parameters for three methods of propagation analysis to determine the speed and direction of arrival of the Pc1 waves. The first analysis method considers the propagation to be that of a plane wave traveling over a flat Earth; the second method considers the propagation to be that of a plane wave traveling over a spherical earth. The third method (called the source location method) assuems that the wave front spreads radially over a spherical earth from a localized source. Of the three analysis methods, the source location method satisfied the data best, had smaller standard deviations for the values of propagation velocity determined, and was more consistent in computed direction of arrival. No case of east-to-west propagation was observed, but this is primarily due to the mid-latitude location of the observation sites. The directions of propagation that were detected tended to coincide approximately with that of the geomagnetic meridian in the vicinity of the particular site. This directional tendency was most pronounced for the source location method of analysis. Propagation group velocities ranging from 440 to 1523 km/s were observed. Variation in group velocity for a given event over a period of an hour was typically less than 10%. Attenuation rates ranging from 0 to 13 dB/1000 km, with an average of 6.5 dB/1000 km, were observed. Because of the high attenuation rate relative to the ELF band, the large variability in attenuation rate, the limited period of time during which ionospheric ducting is effective, and the apparent directionality associated with ducted propagation, the use of the 0.5-2.0 Hz frequency band for long-range communications is not recommended.

CONTENTS

EXPERIMENTAL INVESTIGATION OF THE CHARACTERISTICS OF Pc1 MICROPULSATION PROPAGATION USING A MIDLATITUDE FIVE-STATION RECEIVING NETWORK

1. INTRODUCTION

The use of electromagnetic waves with frequencies below 100 Hz for communications between land-based sites and deeply submerged terminals has received much attention in the 1970s. The interest in this frequency band is due to its potential for delivering information over distances of thousands of kilometers with only a few decibels of attentuation and because of the increased penetration of seawater obtainable at the lower frequencies. At ELF frequencies (6 Hz-3 kHz) the low attenuation rates for propagation between land-based or airborne sites are due to the existence of efficient waveguide modes between the ionosphere and the surface of the earth [1]. Attenuaticn along the vertical path, from the air-seawater boundary to the depth of the receiving terminal, can be calculated using simple skin-depth equations. At a frequency of 60 Hz, which is the center of the 40- to 80-Hz band of the proposed SEAFARER system, the attenuation loss incurred in penetration to depths of 100 and 300 m would be 26.7 and 80.2 dB, respectively, assuming a seawater conductivity of 4 mho/m. Dropping still lower in frequency, to the ULF band (below 6 Hz), results in much smaller losses. At 1 Hz the attenuation values would be 3.5 dB at 100 m and 10.4 dB at 300 m. Hence, by dropping from the SEAFARER band to the lower frequency of 1 Hz, a 23-dB advantage in signal strength could be realized at 100 m depth and a 70-dB advantage at 300 m, *assuming comparable signal strengths at the surface.* The signal strength at the surface depends on the power and radiation efficiency of the generation mechanism and the propagation losses incurred along the transit path. At ELF frequencies the waveguide duct is bounded on the lower side by the surface of the earth and on the upper side by the E- or F-layer of the ionosphere. At ULF frequencies waveguide ducting is also theoretically possible [2-5]. The ULF duct boundaries are usually within the ionosphere itself, with the center of the duct at the height of the F_2 layer maximum plasma density. Manchester [6] has calculated that for nighttime conditions at frequencies below 0.7 Hz the E layer may be transparent, so that the duct includes the free-space layer down to the surface of the earth. When the duct boundaries are entirely contained within the ionosphere, the signal strength observed at a site below the ionosphere depends on leakage through the lower waveguide boundary. Hence, at ULF frequencies excessive duct containment of the wave could lead to small signal strengths at subionospheric receiving sites.

The utility of an electromagnetic wave for communications depends on the signal-to-noise ratio and also on the rate at which information can be conveyed on it. The latter consideration is of substantial concern for ULF, for which the carrier frequency is of the order of only 1 Hz. Whether a ULF-band communications system could ever be considered an alternative to the SEAFARER ELF system depends on ·

1

1. Attainment of a ULF wave-generation mechanism that can be suitably modulated

2. Existence of an efficient propagation mode that will allow omnidirectional propagation in the horizontal direction.

Generation of ULF waves by the conventional means of an antenna and associated electronic driving system is probably impractical because the radiation efficiency of an antenna decreases roughly as the square of the frequency radiated. The radiation efficiency for the SEAFARER system is approximately 10^{-4}, and at 1 Hz it would be three orders of magnitude smaller. The prospect of generating propagating waves in the 1-Hz region probably would not have been seriously considered were it not that a naturally existing background of nearly coherent emissions that range from 0.5 to 2 Hz, commonly known as Pc1 micropulsations, have been observed and recorded for many years, indicating that a generation mechanism does exist. Whether or not such a mechanism can be controlled is still uncertain. Davis et al. [7] describe possible methods by which ULF emissions might be created artificially. These methods include perturbation of the ambient ionospheric dynamo currents by means of

1. E- and F-region electron density modifications accomplished by the technique of "ionospheric heating," using a powerful HF radar installation

2. Artificial cesium ionization implants in the 90- to 140-km altitude range.

Also considered is the possible stimulation of a magnetospheric VLF-ULF three-wave interaction using appropriately located high-power VLF transmitters.

Willis and Davis [8] expanded on the VLF-ULF three-wave interaction theory and presented experimental results obtained in October of 1973 and 1974. Although the data suggested a link between VLF transmitter modulation intervals and commencement or enhancement of micropulsations, these indications were weak and not always repeatable. A research effort by Fraser-Smith and Cole [9] also has had some limited success in statistically correlating ULF emissions with VLF transmitter operation at the Siple station in Antarctica. Willis and Davis concluded that the most promising method of ULF wave generation would be conventional large antenna and power transmitter hardware; this, however, is impractical with present technological constraints.

The purpose of the research described in this report is to investigate the characteristics of ULF ducting, which, as pointed out previously, are equally as important for a successful long range communications system as is the attainment of a generation mechanism. The particular properties studied were the following:

1. Experimental confirmation of the existence of the duct

2. Preferred directions of travel within the duct

3. Group and phase velocities

4. Observed attenuation rates

5. Suitability of the duct as a communications channel.

To make the necessary observations, a five-site network consisting of two orthogonal single-axis induction antennas at each location was established. The site locations were Canandaigua, New York; Indian Head, Maryland; Wayne, West Virginia; Champaign, Illinois; and Panama City, Florida. Site separations ranged from 450 to 1600 km. All data were telemetered on dedicated telephone data lines to NRL for centralized recording and subsequent analysis. Cross-correlation techniques were applied to determine time-of-arrival differences between sites. This information was subsequently used for determination of direction of arrival and propagation speed by least-square error analysis methods using data from all five sites. Three different analysis methods were used: The usual plane-wave, flat-earth method, a plane-wave, spherical-earth method, and a spherical-earth, curved-wavefront method. Polarization histories were prepared for each data window analyzed. Spectral and amplitude-time developments of the Pc1 emissions are also illustrated.

The network of observation stations used in this research differs in several respects from others reported in the literature:

1. The spacing of the stations is closer, allowing superior spatial resolution of micropulsation characteristics.

2. The larger number of sites used (five instead of two or three, as in most other studies) creates redundancy in the observables and allows greater confidence in conclusions derived from them.

3. A two-way (duplex) telephone line telemetry system is used from all sites to NRL to permit simultaneous recording of all data on a single tape recorder. This eliminates the greatest potential source of error—the need to maintain precision timing at each site and to later synchronize data records for cross-correlation.

4. A calibration system using half of the duplex telephone line is employed to quantify phase shifts through the entire system, including filters, telemetry components, and tape recorder. In addition, it permits an NRL-activated check on antenna phasing, system frequency response, and gain calibration.

The next section of this report is a brief introduction to the phenomenon of Pc1 hydromagnetic emissions, for the benefit of those who have little background in this area. The current concepts of the origin of the emissions in the magnetosphere and of ducted propagation in the ionosphere are reviewed. In Sec. 3 a detailed description of the data acquisition system and data processing system is presented. For the benefit of readers who may be interested in similar installations, the description of the data acquisition system includes identification and approximate costs of key components. Section 4 is devoted to description of three different methods used for analyzing the data to determine propagation speed and direction of arrival. The fifth section discusses the data obtained from the five-station network, the results obtained from applying the three methods of analysis to the data, and the conclusions inferred. Section 6 summarizes the results of the last section and relates them to the feasibility of establishing a naval communications system which uses frequencies in the 0.5- to 2-Hz band.

2. THEORY AND BACKGROUND

The Pc1 Micropulsation Band

Because it is not possible at present to generate controlled ULF emissions for duct propagation studies, the class of natural emissions known as Pc1 micropulsations was studied to permit deductions about duct properties. The term "Pc" refers to "pulsation continuous" and is distinguished from the irregular class of pulsations known as Pi's. The suffix "1" indicates the frequency band, defined by international convention as 0.2 to 5 Hz. Pc2, Pc3, and Pc4's are also defined and designate bands that are progressively lower in frequency. An example of an amplitude-time display of a typical Pc1 event is shown in Fig. 1. The display at the top of the illustration represents the signal observed on the induction antenna oriented along a magnetic north-south direction at the Canandaigua, New York (NY), receiving site. The second display from the top represents the data obtained from the antenna oriented in an east-west direction. Proceeding downward similarly in groups of two displays, the data received from the Champaign, Illinois (IL), Indian Head, Maryland (MD), Wayne, West Virginia (WV), and Panama City, Florida (FL), sites are shown. The time scale of the display (running from left to right) is compressed to the extent that the carrier frequency (1.25 Hz) cannot be resolved and appears as a blur under the modulation envelope. The actual time window shown is 10.6 min. With this choice of time scale the modulations appear as beads on a string; hence they are often called "pearls." The data shown were bandpass filtered at a Q of 50, and the displays serve well to show that this amount of filtering does not severely broaden the modulation detail.

The choice of the Pc1 band as a vehicle of ULF communications research stems from the following observations. In the class of natural continuous emissions, the Pc1 band has the highest frequency and therefore can support the highest information rate. In contrast to lower frequency micropulsation bands, the Pc1 class of emissions appear to represent electromagnetic disturbances characteristic of traveling rather than standing waves. Pc1 events can be observed at sites separated by several thousand kilometers without losing identifying features. Close observation of envelope modulation sequences has shown that propagation group velocities range from 500 to 2000 km/s.

Theory of Origin of Pc1's

Current theory places the generation-amplification mechanism of Pc1's in the magnetosphere at a distance of about 4 to 10 earth radii and at approximately equatorial latitude. Several generation mechanisms have been proposed, but the one that is currently most widely accepted involves a cyclotron instability process within the energetic equatorial proton belt. Jacobs' book on geomagnetic micropulsations [10] and references contained therein present an explanation of the mechanism as well as earlier, less plausible postulates. In-depth perspective can be obtained from papers by Criswell [11], Campbell [12], and Troitskaya and Gul'elmi [13].

The cyclotron resonance mechanism is indicated schematically in Fig. 2. Shown here is the earth, a concentric ionosphere, several magnetic field lines that extend outward 10 earth radii at the equator, and the equatorial proton belt. If a hydromagnetic wave enters the proton belt it can be amplified by transferral of kinetic energy from the
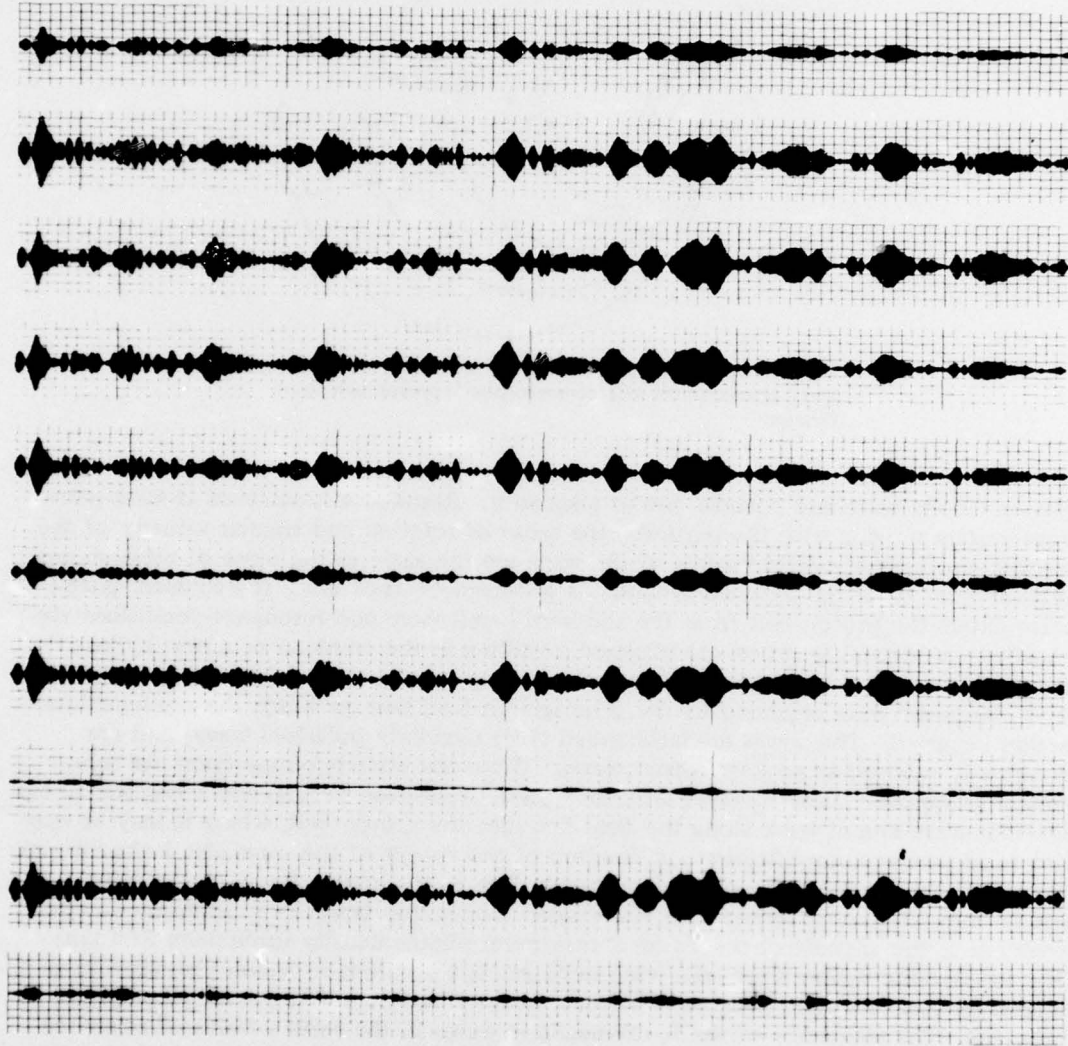
4

Fig. 1—Typical appearance of an amplitude-time record of a Pc1 event. From top to bottom the strip recordings alternate north-south and east-west horizontal components for the stations located at New York, Illinois, Maryland, West Virginia, and Florida. The data are from day 119 and were filtered at a center frequency of 1.25 Hz at a Q of 50. A window of 10.6 min of data is shown.
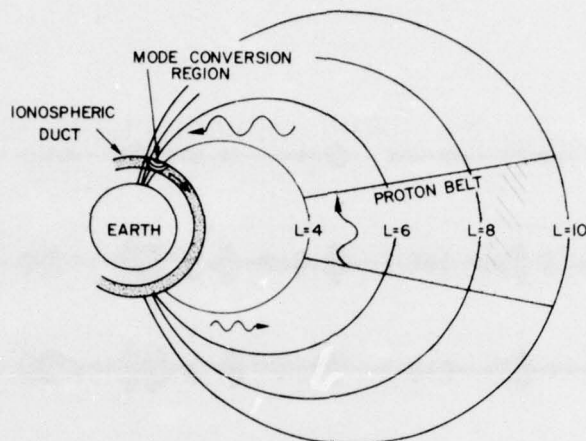
5

Fig. 2—Schematic representation of the earth, ionosphere, and magnetosphere with magnetospheric proton-belt amplification

protons if the wave and particles are in resonance. Resonance is achieved if (in a reference system moving with the particles) the sense of rotation and angular velocity of the electric and magnetic field vectors of the wave are the same as the sense of rotation and angular velocity of the particles around the geomagnetic field line. If a hydromagnetic wave enters the proton belt from the southern hemisphere and resonance conditions are satisfied, an instability process is triggered, resulting in the emission of a new hydromagnetic wave coherent with the first and traveling toward the northern hemisphere. The hydromagnetic wave is guided by the geomagnetic field line on which the resonant interaction occurred. The waves are left-handed (LH) circularly polarized waves and are commonly referred to as slow Alfven waves. When the wave impinges upon the ionosphere at approximately F_2-layer altitude a partial reflection occurs, and a fraction of the incident wave is sent back along the field line into the proton belt, where it may or may not again undergo amplification. A fraction of the energy of the wave also leaks through the ionosphere and can be detected on the surface of the earth. Some of the wave energy may also be converted into waveguided modes that travel in an ionospheric duct centered at the altitude of the F_2-layer maximum plasma density (nominally 350 km). The ionospheric region where the wave impingement occurs is sometimes referred to as a secondary source region, because it is from this localized area that ducted propagation proceeds. The frequency of the hydromagnetic waves in the earth's frame of reference is only about 50% of the ion cyclotron frequency because of the Doppler shift caused by the motion of the protons along the field lines. If only one wave packet is bouncing between hemispheres, then the period of the envelope modulation is related to the bounce time along the field line from the ionospheric reflection point in one hemisphere to the conjugate reflection point in the other hemisphere and back again. When several wave packets are active, however, the modulation periods will be irregular.

When an instability or resonant interaction is triggered, the resultant wave amplitude growth is generally nonlinear. T. Watanable [14] has shown that if the nonlinear terms are included in the Boltzmann equations for a cold plasma background of electrons and

protons in which is also included a small fraction of nonthermal protons, then the apparent observed frequency of the wave increases with time when the wave amplitude grows with time. As with all such instabilities, the growth continues only as long as conditions are favorable, and then the process decays.

The Ionospheric Duct

The existence of natural waveguide ducts in the ionosphere has been given theoretical credence by Dessler [15], Manchester [4, 6], Tepley and Landshoff [5], Kawamura [16], and Greifinger and Greifinger [2, 3]. The following results are due primarily to Greifinger and Greifinger.

During daytime conditions, when large ion-neutral collision frequencies prevail, the mathematical complexity of the propagation equations is severe. To obtain tractable mathematics it is necessary to consider the geomagnetic field to be vertical. The conclusions obtained, therefore, are less valid at low latitudes than at high ones. The important feature of the analysis is that under daytime conditions attenuation is high and propagation in the duct extends to distances of only hundreds of kilometers. Under nighttime conditions the ion-neutral collision frequency is small compared to the ion cyclotron frequency, and the propagation equations simplify. The restriction of a vertical magnetic field is relaxed. Low attenuation is computed (less than 1 dB/1000 km) in the plane of the magnetic meridian, and propagation is expected to extend for thousands of kilometers. In directions off the magnetic meridian, coupling between the slow Alfven mode (field guided) and the fast Alfven mode (ducted) occurs, producing resonant absorption peaks. The frequency of the resonances depends on ionospheric properties and geomagnetic dip angle (and consequently on geomagnetic latitude), but not on the angle of propagation relative to the magnetic meridian. The magnitude of the resonance, however, does depend on the angle of propagation and increases rapidly as E-W propagation is approached. This suggests that off-meridian propagation may be restricted to certain passbands. But since the passbands are different for different geomagnetic latitudes, it is questionable whether propagation can continue without severe attenuation for directions other than geomagnetic N-S or possibly exactly geomagnetic E-W.

Over a frequency range of 0.5 to 5.0 Hz, at least three waveguide modes may propagate, but the attenuation rate for the lowest mode is the smallest and is only weakly dependent on frequency. Each propagating mode has a low-frequency cutoff that is a characteristic of the boundary conditions of the waveguide (specifically the finite thickness of the vacuum layer) and is not a consequence of increasing attenuation. The cutoff frequency for the lowest mode is around 0.5 Hz and is higher at night than during the day. For measurements of Pc1 micropulsations at the surface of the earth, which is outside the waveguide duct, there is an effective high-frequency cutoff in any band because of an exponential decrease with frequency of the transmission coefficient of the lower waveguide boundary.

Along the magnetic meridian the phase velocity is a monotonically decreasing function of frequency. At the low-frequency cutoff the phase velocity approaches infinity. Above cutoff it decreases rapidly and appears to approach an asymptote of constant velocity. By varying ionospheric parameters in such a way as to represent the extremes of sunspot maximum and minimum conditions, Greifinger and Greifinger [2] obtained

group velocities of 400 km/s for nighttime sunspot maximum conditions and 720 km/s for nighttime sunspot minimum conditions. Phase velocities well above cutoff were about 30% higher. Manchester [6] calculated a corresponding group velocity of 800 km/s with a phase velocity of 1000 km/s well away from cutoff but made no effort to ascertain the effects of sunspot conditions. Apparently the difference between phase and group velocity can be at least 100 to 200 km/s well away from cutoff and much greater near cutoff.

For off-meridian propagation the phase velocity is no longer a monotonically decreasing function of frequency [3]. Significant anomalies characteristic of resonance behavior appear in the phase velocity-vs-frequency graphs. The anomalies become greater as E-W propagation is approached. Deviations in phase velocity for E-W propagation can be ± 30% to 40% over the corresponding velocity along the meridian. Over an 0.15-Hz bandwidth it is possible to have a 67% change in phase velocity for E-W propagation, 29% change at an angle of 45 degrees off the geomagnetic meridian, and only 8% change for propagation along the meridian. Off-meridian propagation may therefore be plagued with both possible high attenuation and high dispersion. Nevertheless, there are regions where the effects of attenuation and dispersion for off-meridian propagation are less extreme than the example given above. The question of whether ducted Pc1 micropulsation propagation is limited in direction along the geomagnetic meridian is still unresolved.

Experimental observations with land-based equipment have been made by several workers to evaluate the character of Pc1 ducting. Manchester [6] analyzed data from two Australian stations separated by 1200 km and within 2.6 degrees of the same geomagnetic meridian. He assumed that duct propagation was limited to the geomagnetic meridian plane and made deductions of group velocity from cross-correlations of the envelopes of Pc1 signals observed at each site. Group velocities ranging from 460 to 800 km/s were determined, and an inverse relationship between group velocity and the critical frequency of the F_2 ionospheric layer was shown to exist.

Wentworth et al. [17], made observations of Pc1 micropulsations using a basically N-S-oriented network of five sites located at College, Alaska; Palo Alto, California; Kauai, Hawaii; Canton Island; and Tongatapu. The latter two stations lie in the South Pacific, are south of the geomagnetic and geographic equator, and were most useful for transequatorial and interhemispheric studies. All sites lie close to the same geomagnetic meridian except Palo Alto, which lies 40 degrees to the east. Based on a statistical summary of six events containing a combined total of 60 pearls observed at Palo Alto and Kauai and of three events containing 91 pearls observed at College and Kauai, an average group velocity of 900 km/s was reported. Again the assumption that propagation is along the geomagnetic meridian was invoked.

Campbell and Thornberry [18], were the first to report observations suggesting the occurrence of E-W propagation. They used a widely separated network of five stations located at Great Whale River, Quebec; Boulder, Colorado; Newport, Washington; College, Alaska; and Maui, Hawaii. From a 14-min sample of one Pc1 event they concluded that east-to-west propagation occurred for this event at a group velocity of 2300 km/s with a standard deviation of 500 km/s.

8

A second claim to E-W propagation is reported by Fraser [19] who used a widely separated three-station network with locations of Great Whale River, Quebec; Boulder, Colorado; and College, Alaska. Because of a judicious system of data selection that retained only those data samples that had near-linear polarization (small ellipticity), constant polarization major-axis orientation, and high cross-correlation coefficients, a set of some 40 Pc1 events was thinned to 2 useful ones. Since a Pc1 event frequently consists of several sets of rising elements that can interfere with one another, Fraser (as well as Campbell) narrow-band filtered the signals to a bandwidth of the order of hundredths of hertz before cross-correlating the envelopes to obtain group time delays. Both of Fraser's events indicated approximately east-to-west propagation and group velocities from 570 to 2500 km/s, depending on which data sample and frequency band was used. However, the data presented have some disturbing qualities. For one of the events analyzed, within a time span of 31 min and a frequency span from 0.58 to 0.70 Hz, there is a factor of four difference in computed velocities. Within a time span of 22 min and within a single narrow frequency band centered on 0.58 Hz, a factor of two difference in velocity was computed. These observations of E-W propagation pose a dilemma. Is E-W propagation higher in velocity and more highly variable than N-S propagation, or are the observations inaccurate?

Polarization

The polarization of the field-line guided, or slow, Alfven wave is left-hand (LH) circular in the northern hemisphere. Sites at high latitudes that are directly below the ionospheric reflection point would most likely see similar polarization characteristics. Sites at middle and low latitudes have polarization characteristics that are modified by ionospheric mode conversions, ducting properties, and interference from refracted waves and from waves originating from other secondary source regions. Because of the relatively high conductivity of the surface of the earth, the vertical component of the hydromagnetic emissions observed is usually small. Consequently, polarization determinations are frequently made from measurements from two orthogonal antennas in the horizontal plane.

Altman and Fijalkow [20, 21] determined mathematically that if the slow Alfven wave is vertically incident on the ionosphere, LH polarization will be observed at the surface of the earth at high latitudes, but as the distance from the source increases this will gradually change to right-hand (RH) polarization at lower latitudes. Greifinger [22, 23], assuming a vertical magnetic field, analyzed the consequences of activation of the ionospheric duct by a wave from a finite source incident obliquely on the high-latitude ionosphere. Again LH elliptical polarization is predicted for earth-based observations beneath the source. This changes to RH polarization as the distance from the source increases and degenerates to linear polarization at large distances. Baranskiy [24] analyzed the polarization properties of Pc1 pulsations propagating in a homogeneous boundless plasma. The polarization in the medium was considered to be linear. The effects of the boundaries of the actual ionospheric duct were neglected and assumed to be of secondary importance. He determined that the direction of the horizontal projection of the pulsation magnetic field vector (which is equivalent to the direction of the polarization observed on earth with orthogonal horizontal sensors) tends to point toward the secondary source region at *high* and *middle* latitudes. Another interesting property pointed out from the observations of Lyatskiy and Selivanov [25] is that the polarization tends to

9

aline toward the direction of the magnetic meridian during the intensity maxima of the pulsations. This relationship between polarization orientation and the intensity of the signal suggests that under some circumstances the polarization direction can be attributable to the properties of the source mechanism rather than to the relative geographical location of the source.

Polarizations observed at middle and high latitudes are generally elliptical. Comparison of polarization characteristics such as ellipticity, sense of phasor rotation, and orientation of major axes have been largely inconsistent at high latitudes. This inconsistency is generally ascribed to proximity to the secondary source region, where competition between the direct and ducted wave produces highly variable results. As lower latitudes are approached better consistency in observations is achieved for narrow-band events or for narrow-band-filtered segments of broad-band events. The importance of bandwidth in analyzing amplitude-time and polarization records is well illustrated by Pope [26]. Pope noted that Pc1 events consist of a multitude of rising tones (spectrogram fine structure) of different frequencies that may overlap with respect to time. He showed that beating occurred between different frequency components that overlapped temporarily, causing a substantial distortion of the amplitude-time envelope modulation. To investigate the effect of beating on the polarization he considered the summation of two elliptically polarized waves of two different frequencies which increased linearly with time and of two different major axis orientations but with the same ellipticities and senses of phasor rotation. He determined that as time progressed the ellipticity of the resultant wave varied cyclically through the extremes of linear to elliptical to circular and that the major axis orientation varied by 90 degrees. At each point in time at which linear polarization occurred the phasor rotation reversed. These important results demonstrate that when comparing polarizations or amplitude-time data among various sites it is imperative that the event be either naturally narrow-band or electronically filtered to produce narrow-band sections in which the rising tones do not overlap in time.

Observations of Pc1 polarizations at low and middle latitudes by Baranskiy [24], Troitskaya et al. [27] and Summers and Fraser [28] have shown a consistent diurnal variation of the orientation of the major axis of the polarization ellipse. In the northern hemisphere an early morning counterclockwise (CCW) rotation of the polarization major axis occurs from an initial northeast direction to a subsequent northwest direction. In the southern hemisphere the rotation is in the clockwise (CW) direction. Baranskiy [24] suggests (with caution due to the limited data analyzed) that the Pc1 source regions follow the morning side of the dawn day-night terminator.

Summers [29] showed that the path of the hydromagnetic wave undergoes significant refraction when propagating through a medium with changing plasma density. He considered the effect of increasing plasma density as the equator is approached and found that if the density gradient is along the meridian, then as the wave propagates in the duct toward the equator it is refracted toward the meridian. The farther the wave is originally angled away from the meridian, the harder it is refracted toward it. Observations by Tepley [30] and Smith [31], which indicated that the polarization approaches the direction of the magnetic meridian as the latitude of the observation point decreases, tend to support the refraction phenomenon if one accepts the hypothesis that polarization direction indicates propagation direction.

Summers and Fraser [28] have determined from observations that there does not appear to be any significant dependence of the polarization ellipse major axis orientation on frequency and that there does not seem to be any relationship between phasor rotation and time of day or event signal frequency.

Fraser and Summers [32] suggested the possibility that for near-linear polarization the direction of the major axis may also point to the source region for propagation directions away from the magnetic meridian at low latitudes. This hypothesis appears to conflict with Baranskiy [24] and ignores the effects of refraction mentioned above. In support of this hypothesis four case studies were presented. Of the four only two had linear polarization data at three sites simultaneously that could be projected to attempt source region location. Of these two cases only one succeeded in having the polarization projections converge in a common region. We do not believe that the data presented adequately support the hypothesis.

3. DATA ACQUISITION AND PROCESSING SYSTEMS DESCRIPTION

The Five-Station Network

The locations of the five ULF receiving sites are shown in Fig. 3. The L-shell contours associated with the geomagnetic McIlwain coordinates are also included for an altitude of 200 km. Data for these contours were extracted from the 1970 NASA publication SP-3054 [33]. The New York site (hereafter denoted by the symbol NY) was located on the property of the Federal Communications Commission, Canandaigua, N. Y. The geographic coordinates are $42.90°N$, $77.27°W$, and the geomagnetic L-shell value is approximately 3.1. The Illinois site (IL) was located at the University of Illinois Monticello Road field station, Champaign, Ill. (coordinates $40.02°N$, $88.32°W$; $L \approx 2.7$). The Maryland site (MD) was situated in a quiet area of the Naval Ordnance Station, Indian Head, Md. (coordinates $38.55°N$, $77.24°W$; $L \approx 2.7$). The West Virginia site (WV) was located on a farm in Wayne, W. Va. (coordinates $38.25°N$, $82.43°W$; $L \approx 2.6$). The Florida site (FL) operated from the nonmagnetic site of the Naval Coastal Systems Laboratory, Panama City, Fla. (coordinates $30.17°N$, $85.75°W$; $L \approx 1.9$). The five-station network was in continuous operation from April 9, 1975, to February 19, 1976. A four-station network consisting of the NY, MD, WV, and FL sites was operated prior to that period from December 16, 1974, to April 8, 1975. An initial three-site grid consisting of the NY, MD, and WV sites was in operation from November 5, 1973, to December 15, 1974. Identical receiving systems that operated unattended were used at each location. From each site data from two antennas oriented orthogonally in magnetic north-south and east-west directions in a horizontal (level) plane were telemetered continuously to NRL over type-C2 conditioned telephone data lines using FM-modulated carriers. The consequent ten channels of data received at NRL were demodulated and recorded on analog and digital recorders along with time information accurate to within a few milliseconds. A calibration system that was activated at NRL and that excited all five stations simultaneously was used to measure differences in phase shift between pairs of field systems and telemetry links. The calibration circuit was also used to measure overall system frequency response at all sites and to provide a check on amplitude calibration.
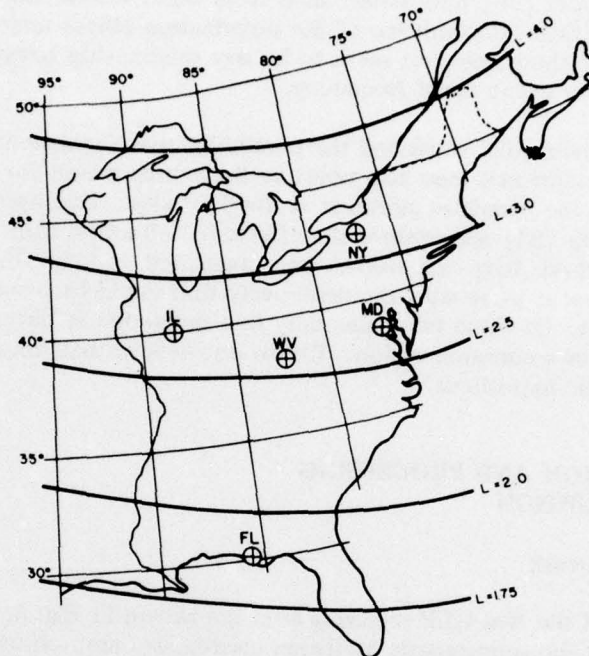
Fig. 3—The geographic locations of the five receiving sites and the McIlwain L-shell contours for an altitude of 200 km

A block diagram of the entire receiving system from field to laboratory is shown in Fig. 4. A detailed description of each of the block components follows below.

The Antenna

The antenna used was of the induction type, with thousands of turns of wire wound on a laminated moly-permalloy core. They were purchased from Geotronics Corp., Austin, Tex., at a cost of $2150 each (1974). The entire coil is encased in a type-304 stainless steel cylindrical jacket and potted in polyurethane rubber. There is a Faraday shield between the case and coil. The outside dimensions are approximately 2-m length by 7.6-cm cross-sectional diameter. The antenna inductance is 605 H, resistance is 438 Ω, distributed capacitance is 0.00134 μF, and unloaded sensitivity is 137 μV/Hzγ. An effective shunt resistance of 58.7 kΩ across the inductance must be included for analytical equivalent circuit analysis. For good transient response the antenna must be shunt loaded with a resistance of 1 to 2 kΩ; a 1.45-kΩ loading resistor was used for the measurements reported here. The loaded antenna response is shown in Fig. 5. The addition of the loading resistor reduces the initial +6-dB/octave response from 137 μV/Hzγ to approximately 100 μV/Hzγ and ultimately flattens the response at 50 μV/γ above 2 Hz. Additional roll-off attained by using either a 2-μF (curve B) or 10-μF (curve A) shunt capacitor is also shown. A quality nonelectrolytic 10-μF capacitor was used in all field installations to assure adequate rejection of 60-Hz and other high-frequency noise. The
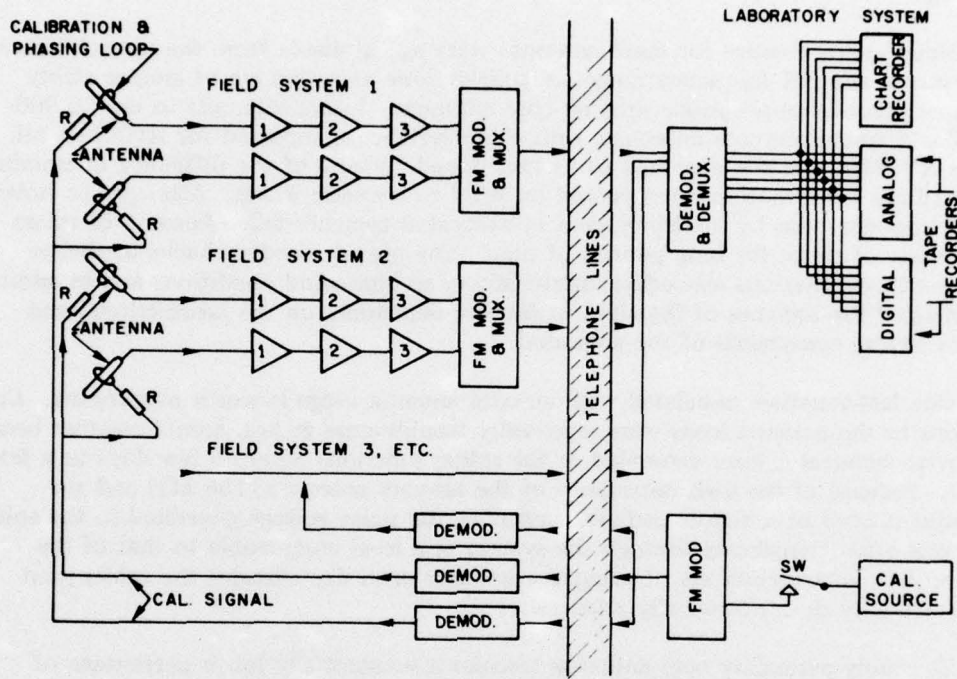
12

Fig. 4—Block diagram of the entire receiving system, including the telephone data lines, FM
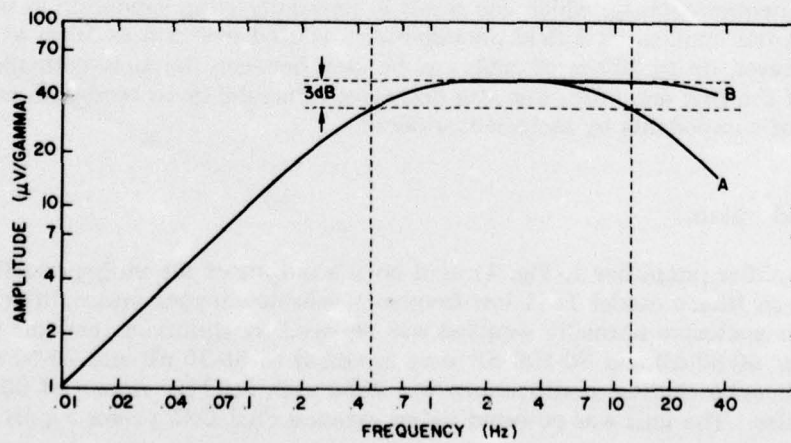modulators, multiplexers, and demodulators

Fig. 5—Antenna response with shunt loading of a resistance of
1.45 kΩ and a capacitance of (A) 10 μF or (B) 2 μF

13

effective 3-dB bandwidth of the resistive and capacitive loaded antenna covers the approximate interval of 0.45 to 12 Hz. This bandwidth is altered by subsequent stages of filtering.

Noise characteristics for these antennas were not available from the manufacturer. However, in the Pc1 frequency range we believe these antennas are of greater utility for most practical applications than air-core antennas. Initial attempts to use 16 000-turn-2-m-diameter air-core antennas, with characteristics as reported for style 5 in ref. 34, at the NY, MD, and WV sites had to be abandoned because of the difficulty of isolating the antennas from motion noise caused by wind or acoustic waves. Attempts to isolate the air-core antennas by installing them in excavated trenches failed because of retain several feet of water for long periods of time. The use of wooden shacks to shelter above-earth installations was often unsatisfactory in high wind conditions and in addition complicated the logistics of the site installation, depending on the jurisdictional and environmental constraints of the area used.

One last vexation associated with air-core antenna usage is worth mentioning. Connections to the antenna leads were repeatedly troublesome in *hot, humid weather* because of electrochemical actions generated in the solder junctions within a few days to a few weeks. Because of the high impedance of the air-core antennas (138 kΩ) and the consequent need of a high-impedance amplifier, the noise voltage generated in the solder joint was often transferred through the system at a level comparable to that of the induced Pc1 micropulsations. During dry weather or in dry climates the solder-joint noise difficulty does not usually arise.

The moly-permalloy core antennas transfer a substantially lower percentage of cable-lead junction noise (from thermal, contact potential, or electrochemical origin) because of the lower antenna impedance and lower input impedance of the subsequent amplifier. (In the present application the effective amplifier input impedance will be that of the loading resistor (1.45 kΩ.) The moly-permalloy antennas are waterproof and can be buried in the ground without fear of ground-water leakage problems. An additional advantage of the physical configuration of these antennas is that they can be buried very inconspicuously, which can result in immunity from vandalism in uncontrolled areas. In our application a field preamplifier was used within 5 to 10 m of the antennas. However, up to 330 m of cable can be used between the moly-permalloy antennas and the first amplifier; this also decreases vulnerability to vandalism and destruction of components by inclement weather.

Amplifier and Filters

The amplifier (amplifier 1, Fig. 4) used on the output of the moly-permalloy antenna was an Ithaco model 1541 low-frequency seismic chopper preamplifier. The magnetic case enclosure normally supplied was replaced by aluminum, and the standard gain ranges of 60-80 dB and 80-100 dB were modified to 50-70 dB and 70-90 dB. The procurement cost including modifications was $950 each (1974). A gain of 60 dB was used at all sites. The unit was powered by an external dual D.C. power supply at $\pm$ 20

V, 10 mA each supply. The 3-dB bandwidth was nearly 100 Hz, with -3-dB points at 0.01 Hz and 100 Hz. The input was balanced and had an impedance of 4 MΩ shunted by 0.01 μF. The maximum noise specified over the band 0.1-100 Hz is 0.16 μV rms with input shorted and 0.66 μV rms with 200 kΩ source impedance. The amplifiers were located within 5 to 10 m of each antenna and were enclosed in waterproof aluminum boxes containing a dessicant for dehumidification.

Amplifier 2 was of unity gain and consisted of a 12-dB/octave multiple-feedback low-pass active filter (-3-dB point at 2 Hz) followed by a passive 6-dB/octave high-pass filter (-3-dB point at 0.04 Hz). The high-pass filter was constructed using two 1000-μF electrolytic capacitors in series back-to-back configuration, with an empirically selected termination resistor of approximately 5-10 kΩ in value. This filter was intended primarily for d.c. blocking. It was checked in the laboratory for frequency response and stability of phase-shift characteristics with varying temperature and was found to be acceptable. The low-pass filter used a 2-μF and a 10-μF nonelectrolytic capacitor, each of which was obtained from a parallel combination of 1- to 2.5-μF, 50-V dipped capacitors. The correct combinations were determined with a capacitance bridge. The frequency response of the filter was checked in the laboratory, but the temperature stability of the phase-shift characteristics was not. It was discovered after all the field installations were complete that the temperature stability of the dipped capacitors was not as good as is customary with the larger tubular varieties. This may explain the nonconstant system phase-shift differences between members of pairs of sites, observed by means of the calibration system.

Amplifier 3 is a Neff model 123 general-purpose d.c. amplifier with selective calibrated gain positions and low-pass filter bandwidths. A d.c.-to-10-Hz (-3 dB at 10 Hz, 12 dB/octave) filter bandwidth was used at all sites. A gain of 200 was used at NY; a gain of 500 was used at all other sites. The overall frequency response of the system including that of the telemetry system is shown in Fig. 6. This response was determined by inductive coupling of a constant rms magnetic field into the antenna at various frequencies with subsequent observation of the rms level change at the laboratory (output) terminal. The overall response was optimized for Pc1 reception in the frequency range of 0.5-2.0 Hz.

The Data Lines and Telemetry Equipment

Full duplex type-C2 conditioned data lines were used from NRL to each of the five receiving stations. Signals could be sent from NRL to all sites without interrupting the flow of returning data. All telemetry equipment was hard-wired to the telephone lines through telephone company interface equipment; no acoustic couplers were used. The lines were active 24 h each day without interruption.

Type-C2 conditioning provides a bandwidth of 300-3000 Hz with maximum variations of -2 to +6 dB or 500-2800 Hz with variations of -1 to + 3 dB. The maximum frequency error is ±5 Hz. Absolute phase shifts are not specified. A minimum of 40 dB dynamic range was usually maintained. Greater detail of specifications for C2 and other grade lines is available from Bell System publications [35]. Data lines to the FL and IL sites were provided by Western Union at an approximate cost of $505 and $421, respectively, per month. The lines to the NY and WV sites were provided by American Telephone and Telegraph Co. (AT&T) at a cost of approximately $342 and $327,
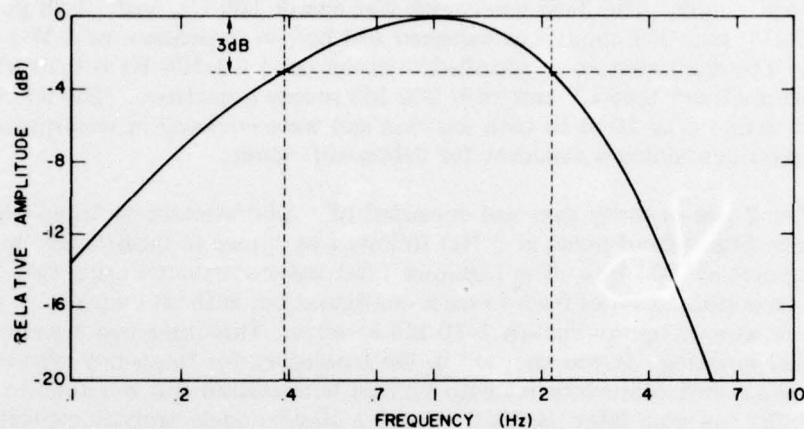
Fig. 6—Relative frequency response of overall system

respectively, per month. The MD line was provided by the Chesapeake and Potomac Telephone Company at a monthly cost of $136. Initial installation charges are usually of the order of a few hundred dollars, provided telephone lines of quality sufficient to meet the desired grade of conditioning exist within a few hundred feet of the circuit termination points.

Pc1 data received at the field sites, which were amplified and conditioned as discussed previously, were telemetered to NRL on the data lines in an analog form on frequency-modulated (FM) carriers in standard IRIG proportional-bandwidth channels. Data from all north-south (NS) oriented antennas were sent as a carrier center frequency of 960 Hz, and data from all east-west (EW) oriented antennas was sent at a center frequency of 1300 Hz. Maximum modulation of the carrier center frequencies was ± 7.5%. At each site the two FM-modulated carriers were summed and transmitted along the same data line and then separated and demodulated at NRL to regain the original signal form for each antenna.

The telemetry modulation/demodulation equipment was purchased from Data-Control Systems, Inc. (DCS), Danbury, Conn. Models GOV-5 modulators, GFD-17 demodulators, GFD-17L-51 low-pass filters, and GMA5 housing module assemblies were used. A send/receive system for five sites as depicted in Fig. 4 with no spares would cost approximately $24,000. The equipment is capable of providing a 60-dB noise-free dynamic range.

The telemetry send-lines from NRL to the field sites were used for a calibration system that would probe all five systems simultaneously at the same frequency and phase. A synthesizer at NRL was used to select a test sine wave in the region of 0.5-2.0 Hz. This was FM modulated on a 1700-Hz center-frequency carrier and telemetered to all field sites where it was demodulated to regain the 0.5-2.0 Hz sine wave. This signal was then induced into each of the antennas by means of a calibration loop consisting of a single turn of wire wound tightly around the antenna outer circumference at the middle of the antenna axis (see Fig. 4). A 1000-Ω resistor was inserted in series with

16

the leads to each single-turn inductor to ensure maintenance of constant-rms current through the calibration loop over a 0.1-20 Hz range. The demodulators automatically disconnected themselves from the calibration loop when no carrier was present (i.e. when no calibration was being sent from NRL).

Use of the calibration system allowed site-to-site comparisons of overall-system phase differences to be made at will without leaving the laboratory. However, any delays originating in the send system (including modulator, demodulator, and data line) must not be variable with time and must be known as a function of frequency so that they can be subtracted from the total two-way delay. Demodulation of the calibration signal in the field was accomplished using FM reproduce boards from a Bell & Howell tape recorder. The low-pass filter on each demodulator was of sufficient bandwidth that negligible phase shift occurred at that stage. Also the DCS modulators produced insignificant phase shifts. The low-pass filters associated with the DCS demodulators, however, introduced significant (but constant) phase shifts—52 ms for the 960-Hz channel (14-Hz bandwidth) and 32 ms for the 1300-Hz channel (20-Hz bandwidth). These delays were essentially constant over the band 0.5-2.0 Hz. The delays over the data lines were measured by temporarily wiring the calibration signal output of the demodulator at the field site directly into the input of the modulators. With the receiving system eliminated from the telemetry loop and with the measured equipment delays accounted for, the one-way data-line delays were determined; they are shown in Table 1. Repetition of these measurements during occasional site visits showed the delays to be invariant with time and frequency over the band 0.5-2.0 Hz. Caution must be exercised in associating data-line delays with great-circle distances between termination points because the actual line routing may deviate vastly from this arc and also because part of the delay is attributable to electrical apparatus as opposed to actual transit time along the line.

Cross-correlation lags computed from Pc1 data originating at two different sites must be corrected for time lags caused by phase shifts in the data lines, the receiving system, and the telemetry demodulators if the highest accuracy is desired. Figrue 7 shows schematically the flow of data from the field (point b) to the laboratory (point c), as well as the flow of the calibration signal from the laboratory (point a) to the field and back again. Where arrows are shown without labels the delay is insignificant. The expression for the correction factors to be applied to the cross-correlation lags determined for Pc1 data from different sites can now be determined.

Let

Δt_l = time delay for the data line
Δt_s = time delay for the receiving system
Δt_m = time delay for the telemetry demodulator
Δt_t = time for calibration signal to go from (a) to (b) to (c)
Δt_r = time for data signal to go from (b) to (c).

A single superscript will be used on all quantities when they refer to one site only, and a double superscript will be used if the quantity refers to differences in that parameter between two sites, i.e.,

Table 1—Propagation Delays Determined for the Data Lines and Interfacing Circuitry

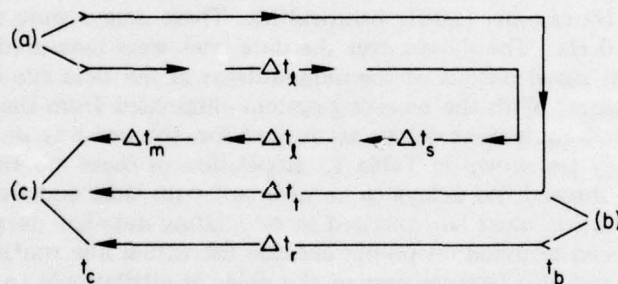| Station	One-Way Data-Line Delay (ms)
NY	8.5
IL	11.7
MD	3.5
WV	9.0
FL	12.2

Fig. 7—Schematic showing system delays over the calibration link (from point a to point b) and over the data-return link (from point b to point c). Multiple paths are shown for the purpose of alternate grouping visualizations.

$$\Delta t_s^{(2)} - \Delta t_s^{(1)} = \Delta t_s^{(2,1)}. \tag{1}$$

If the actual time of arrival of the Pc1 at site "i" is $t_b^{(i)}$ and that actually observed at the laboratory is $t_c^{(i)}$, then

$$t_b^{(i)} = t_c^{(i)} - \Delta t_r^{(i)} = t_c^{(i)} - \Delta t_m^{(i)} - \Delta t_l^{(i)} - \Delta t_s^{(i)}. \tag{2}$$

If arrival times $t_c^{(i)}$ for two different sites (say, sites "l" and "m") are observed for an event that occurred in the field at times $t_b^{(l)}$ and $t_b^{(m)}$, then the difference in observed and actual arrival times is given by

$$\Delta t_b^{(l,m)} = \Delta t_c^{(l,m)} - \Delta t_m^{(l,m)} - \Delta t_l^{(l,m)} - \Delta t_s^{(l,m)}. \tag{3}$$

The system delay can be expressed in terms of the calibration signal delay as

$$\Delta t_s^{(i)} = \Delta t_t^{(i)} - 2\Delta t_l^{(i)} - \Delta t_m^{(i)}. \tag{4}$$

18

The difference in these quantities relative to sites l and m is given by

$$\Delta t_s^{(l,m)} = \Delta t_t^{(l,m)} - 2\Delta t_l^{(l,m)} - \Delta t_m^{(l,m)}. \tag{5}$$

By substituting Eq. (5) into Eq. (3) we obtain

$$\Delta t_b^{(l,m)} = \Delta t_c^{(l,m)} - \Delta t_t^{(l,m)} + \Delta t_l^{(l,m)}. \tag{6}$$

Equation (6) states that the actual time-of-arrival difference is equal to that observed in the laboratory minus a correction factor equal to the cross-correlation lag between calibration signals returned from two different sites plus a factor equal to the one-way difference in data-line lag. This equation would require an additional term representing the calibration field-demodulator lag if it were nonnegligible. The calibration delay $\Delta t_t^{(l,m)}$ is a function of frequency and must therefore be determined at the same frequency as the Pc1 event analyzed. Since significant day-to-day variations in this parameter are also observed, it is important to determine the correction factor in close temporal proximity to the Pc1 event of interest. The temporal variations are attributed to the effect of diurnal temperature variations on temperature-sensitive electronic components at the sites. The chief candidate for these variations are the high-capacity dipped-ceramic filter capacitors (amplifier 2, Fig. 4) and the moly-permalloy antenna. The maximum range of all delay correction-factors lumped together for the events reported on was 0-77 ms.

One additional accounting of telemetry delay must be dealt with. The DCS demodulators for the NS and EW data channels had initially bandwidths of 14 and 20 Hz, respectively. This was a consequence of the difference in FM carrier frequency and proportional bandwidth equipment. This difference in bandwidth introduced a 26-ms shift between the NS and EW data channels. Equation (6) still holds if NS(EW) is compared to NS(EW), but an undeterminable error ranging from 0 to 26 ms arises if the NS and EW components are combined before correlation with the equivalent from another site. Since a component combination technique of squaring and summing was used extensively in the work, the bandwidth of the EW channel was decreased to 14 Hz to eliminate this source of error. However, because of a lengthy procurement time for the lower bandwidth filters, only the Pc1 events labeled with Julian day 338 (to be discussed below) are not affected. Inclusion of this small delay uncertainty in the remaining data does not seriously affect the computations and conclusions.

The Recording Equipment

The 10 channels of data received at the laboratory were recorded on analog and digital magnetic tape recorders and on chart recorders. A Gould/Brush model 480 eight-channel chart recorder was used at a speed of 0.1 mm/s for visual monitoring of incoming data. This speed was too slow to distinguish individual cycles of the carrier but permitted recognition of the pearllike envelope modulation of Pc1 emissions. The NS channels from all sites as well as the EW channels from IL, WV, and FL were recorded 24 hours a day on one chart recorder. These records were not destroyed regardless of the presence or absence of Pc1 activity, provided most of the sites were operational. The

19

NY and MD EW channels were monitored for a short period of time each day to verify proper receiver operation only. These records were too brief to retain. Analog and digital magnetic tape records were saved only when high-quality Pc1 emissions were observed at all five stations.

The analog recorder was a 1-in.-tape, 14-channel Bell and Howell model CPR 4010. All data were recorded at a speed of 15/16 in./s with 4600 ft (1402 m) of tape per 10.5-in. reel. The length of recording time per tape was 16 h. Each of the ten data channels was recorded on a separate track via FM intermediate-band electronics (312-Hz bandwidth, 1688-Hz center frequency 37-dB signal-to-noise ratio, and flutter less than 1% p-p (2 sigma) in band 0.2-312 Hz). An IRIG-B standard amplitude-modulated time code from a chronometer (Datatron model 3000 time code generator/translator) and an IRIG standard servo track signal were recorded on direct record channels. The chronometer was synchronized within 1 ms daily with the Canadian broadcast CHU and drifted no more than 5 ms/day.

Digital recording was done on a modified Monitor Labs (ML) 9100 system having a 12-bit word size (11 bits plus sign) and having a recording dynamic range slightly in excell of 60 dB. Two Digidata model 1500 seven-track digital tape drives were interfaced with the system for automatic switchover. Recording could be done at a density of 556 or 800 characters per inch. The tape decks had dual 1000-word (2000-character) buffers, which filled and unloaded onto tape alternately in order to avoid time gaps and sampling incoherency across the interrecord-gaps of the magnetic tape records. Twelve characters of time, hundreds of days through units of milliseconds from the parallel digital output of the Datatron chronometer, were recorded at the beginning of each record. The 1-MHz source used for the chronometer was also used to derive the sampling timing for the ML 9100 system. The system is simple to operate and reasonably compact, requiring (with the exception of the tape decks) less than $0.08 m^3$ ($3 ft^3$) of rack space. The logic is hard-wired with front panel controls. No computer is used. Up to 32 analog channels can be sampled.

Two modes of operation are selectable on the modified ML 9100 system. The sequential-scan mode, which allows the fastest continuous sampling rate (1000 channels/s), samples and records at a uniform rate within a scan (first through last channels of analog input) and from scan to scan. The scan-and-pause mode, which permits attainment of minimum time skew among all samples of a given scan, can sample at rate up to 5000 channels/s within a scan, but the time between successive scans must be equal to or greater than 0.01 s. The scan-and-pause mode was used to record the 10 channels of analog Pc1 data. An intrascan rate of 1 kHz and an interscan rate of 20 Hz were used. The time skew in sampling among any combination of channels was therefore not greater than 10 ms and was removable in subsequent correlation studies. The Nyquist sampling bandwidth is 10 Hz, which is well above the high-frequency roll-off edge of the field-conditioned data (≈ 2 Hz).

The Data-Processing Equipment

A schematic of the analog data-processing equipment is shown in Fig. 8. The same analog tape recorder was used to both reproduce and record. Cross-correlations were performed using a Federal Scientific model UC-202C 512-point Ubiquitous Correlator with
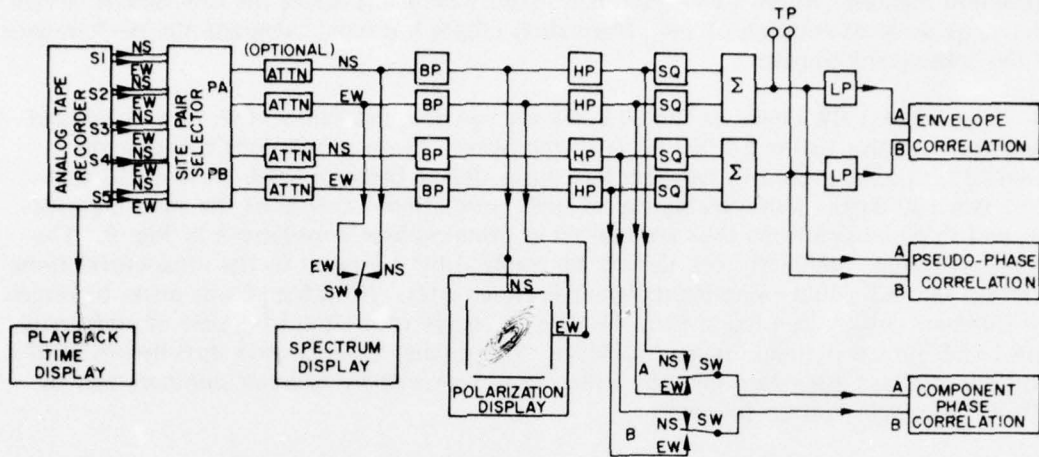
Fig. 8—Schematic of the analog data-processing equipment. S1-S5 designate selected pairs A and B. ATTN signifies "attenuator," BP—"bandpass filter," HP—"high-pass filter," LP—"low-pass filter," SQ—"squarer," and Σ—summer

a reproducing analog tape speed of 30 in./s. Data intervals of interest were located by observing the Datatron model 3000 display of the translated IRIG-B time code recorded on the tape. A switching box was constructed to allow selection of reproduced NS and EW outputs from any pair of sites. When it was necessary to achieve reduced signal levels, the four data channels were fed into attenuators of identical manufacture. The attenuators for the NS and EW channels were always set to the same value for a given site.

Spectral analysis was carried out on the signals from the output of the attenuator. A Federal Scientific model UA-6B 500-line spectrum analyzer was used in conjunction with an option 66-2A 3-D automatic display control and Tektronix 611 storage display scope. A Polaroid camera was used to photograph the display. Z-axis intensity modulation was used to enhance the prominence of large-amplitude frequency components. A 500-Hz analysis range was used; it had an inherent 1-Hz resolution and 1-s memory time. At a playback speedup factor of 32 this translates to a resolution of 0.03125 Hz and a memory time of 32 s. The frequency axis of the display was expanded so that the interval of 0 to 3 Hz was displayed. Individual frequency displays were incremented approximately every 8 s, referred to unity speedup factor.

Following the attenuators the four data channels were band-pass filtered using Princeton Applied Research selective amplifiers model 189 that were precisely adjusted for zero relative phase-shift by observation of linear Lissajous displays among all outputs with a common test signal input. All polarization displays shown in this report of the band-pass filtered signals were obtained by digitizing the data with the ML 9100 system in the scan-and-pause mode with a time skew between NS and EW channels of 4 ms. The polarization ellipses were then plotted on a Calcomp plotter, and the sense of phasor rotations computed by successive arctangent computations on a CDC 3800 computer. A small d.c. offset present at the output of the band-pass filters was removed by passive 6

21

dB/octave high-pass filters. The small d.c. offset would not affect the orientation, eccentricity, or sense of rotation of the polarization ellipse but would degrade the performance of the subsequent squarer.

The NS and EW channels for each site are squared and summed to form a squared magnitude relative to the horizontal receiving plane. Cross-correlations between the summed outputs are used to measure Pc1 phase delays between sites. It is noted that there is a 180 degree phase ambiguity in such correlations because of the squaring process, and these comparisons thus are labeled as pseudo-phase correlations in Fig. 8. The 180-degree phase ambiguity can usually be resolved by reference to the cross-correlations between the individual component signals between sites. No attempt was made to return the summed output to a linear form by using a square-root circuit because of additional offset and limited dynamic range problems. The squarer circuits used Burr-Brown 4203K multiplier/divider integrated circuits, which were followed by resistive summers and an output unity-gain voltage follower.

Envelope detection of the squared signal magnitude was accomplished at the low-pass filter following the summer. For some data samples these filters were Kronhite model 3750 devices adjusted for satisfactory ripple removal and acceptably small difference in phase shift characteristics in the expected envelope fluctuation frequency band. The remaining data samples were envelope detected using a NRL-fabricated two-stage, multiple-feedback, low-pass filter with an ultimate roll-off of 24 dB/octave. Each low-pass stage had a 3-dB high-cut point at 0.469 Hz, referred to unity tape speedup factor. All components were hand selected to achieve minimal phase shift differences from 0-0.5 Hz between the two respective channels.

4. PROPAGATION ANALYSIS METHODS

Three different methods were used to determine direction of arrival and speed of propagation from propagation time differences determined between pairs of sites by the cross-correlation method. The first and simplest method was a plane-wave analysis based on a flat-earth approximation. In this approximation distances and azimuthal angles between sites are computed from chords joining the site locations on a spherical earth. The second method attempts to account for earth curvature by using a hybridization of the plane-wave method with spherical trigonometry. It is assumed that the plane wave travels along a great-circle path with a wavefront lying along another great-circle path perpendicular to the first. The third method allows for curvature of the earth as well as a form of curvature of the wavefront. It assumes that the wave propagates from a localized secondary source region with a wavefront that expands with a circular (or cylindrical) symmetry. The first two methods require at least three sites to make a determination of speed and direction of arrival. The third method requires four sites. When the minimum number of sites was used with any analysis method for determining speed and direction of arrival, the solutions obtained using various combinations of the five stations were sometimes inconsistent. A better approach for obtaining a solution to the propagation problem was obtained by using a least-square, error-minimizing technique with the data from all five sites. This approach reduced the impact of small errors in the data (or deviations of actual propagation conditions from the simplified concepts employed in the analysis methods) on the propagation properties determined. Values of speed

and arrival direction computed represent overall averages. The inconsistencies alluded to above are represented as a variance or standard deviation in one of the solution parameters. The scalar velocity parameter was chosen for this purpose in all three propagation models. The mathematical details for each method are given below.

Plane-Wave, Flat-Earth Method

Between the ith site and the reference site the following parameters are known:

d_i = the distance measured along a chord from the ith site to the reference site

t_i = the propagation time delay between the ith site and the reference site (t_i is negative by convention if the wave arrives at the reference site last)

α_i = the azimuthal angle between the geographic meridian plane and the chord between the ith site and the reference site.

With reference to Fig. 9, assume that the plane wave is traveling with a speed v at an azimuthal angle ϕ with respect to the geographic meridian. Then the following scalar relation is mathematically exact:

$$V = \frac{-d_1}{t_1} \cos \theta_1 = \frac{-d_2}{t_2} \cos \theta_2 = \frac{-d_3}{t_3} \cos \theta_3 = \frac{-d_4}{t_4} \cos \theta_4 \qquad (7)$$

where θ_1 is the angle between the plane-wave direction and the baseline between the ith and reference sites.

In Eq. (7) the indices 1-4 refer to the four possible combinations of pairs of sites relative to a common reference site. By expressing θ in terms of φ and α and substituting into Eq. (7), one obtains

$$V = \frac{-d_i}{t_i} \cos (\alpha_i - \phi) \qquad i = 1, 2, 3, 4. \qquad (8)$$

Because inaccuracies exist in the measurement of d_i, t_i, and α_i, the multiple equality indicated in equations 4.1 and 4.2 is only approximately realized. We define error functions as follows:

$$e_{ij}(\varphi) = [d_i \cos (\alpha_i - \phi)/t_i - d_i \cos (\alpha_j - \phi)/t_j]^2 \qquad (9)$$

$$\text{err} (\varphi) = \left(\sum_{\substack{i,j \\ j > i}} e_{ij}(\phi) \right)^{1/2}. \qquad (10)$$

Equation (9) represents the squared difference in prediction of propagation speed for two different pairs of sites. Equation (10) is a composite error function that represents the rms error characteristic of all possible differences between the four predictions of velocity.
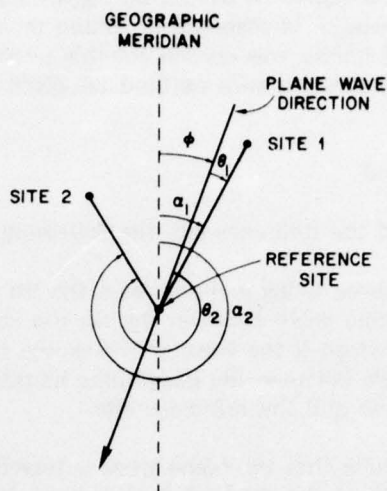
23

Fig. 9—Schematic of coordinate system
and variables used for the planewave,
flat-earth propagation model

A computer algorithm was generated to determine the value of φ (to within 1 degree) that minimized err (ϕ). For this value of $\varphi = \varphi_{min}$ the corresponding four values of velocity,

$$V_i = -d_i \cos(\alpha_i - \varphi_{min})/t_i \qquad (11)$$

were determined, as well as the average velocity v and the standard deviation in velocity,

$$\sigma = \left[\left(\sum_i V_i^2 - N\overline{V}^2 \right) \Big/ (N-1) \right]^{1/2} \qquad (12)$$

with $N = 4$.

Plane-Wave, Spherical-Earth Method

This method is shown schematically in Fig. 10. The direction of wave travel is assumed to lie along a great-circle path passing through the reference site. The wave front (also along a great-circle path) that passes through the ith site is perpendicular to the ray direction at point P. We define the following symbols as

24
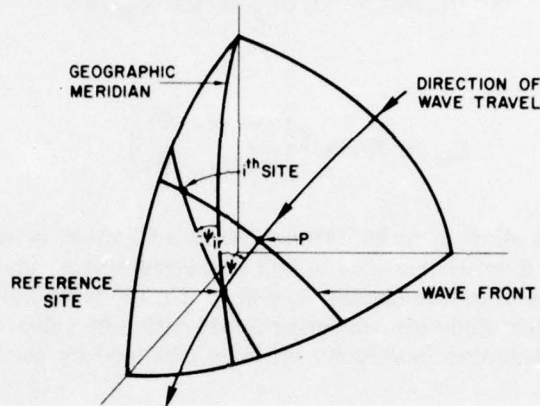
Fig. 10—Schematic of coordinate system and variables used for the planewave, spherical-earth propagation model

Ψ—azimuthal angle of arrival of wave at reference site relative to geographic meridian

R—radius of the earth

d_{ir}—great-circle distance between ith site and reference site (known value)

d_{ip}—great-circle distance between ith site and point P (must be calculated)

d_{pr}—great-circle distance between reference site and point P (must be calculated)

Ψ_{ir}—azimuthal angle of arc d_{ir} relative to the geographic meridian at the reference site (known value)

t_i—propagation time between ith site and reference site (known value); t_i is negative by convention if wave arrives last at reference site.

Individual speed values are obtained from the relation

$$V_i = d_{pr}/t_i \qquad i = 1, 2, 3, 4. \tag{13}$$

Distance d_{pr} must be related to the known parameter values. Using the law of sines for a spherical triangle one may write the relation

$$\frac{\sin 90°}{\sin (d_{ir}/R)} = \frac{\sin (\Psi - \Psi_{ir})}{\sin (d_{ip}/R)}$$

or

$$\text{angle } (d_{ip}/R) = \sin^{-1}[\sin (\Psi - \Psi_{ir}) \sin (d_{ir}/R)]. \tag{14}$$

By using the law of cosines and noting that one of the terms involved drops out because of the right angle at point P, one obtains

$$\cos\left(d_{ir}/R\right) = \cos\left(d_{ip}/R\right)\cos\left(d_{pr}/R\right) \tag{15}$$

or

$$d_{pr} = R\cos^{-1}\left[\frac{\cos\left(d_{ir}/R\right)}{\cos\left(d_{ip}/R\right)}\right].$$

Equations (14) and (15) allow v_i to be determined as a function of azimuth Ψ of arrival of the wave. Since the four estimates of v_i will in general not be identical at any common value of Ψ, an error function similar to that in Eq. (9) is defined. The determination of the value of Ψ for minimum rms error in velocity, the value of the average velocity, and standard deviation in velocity are then obtained by the same procedure as for the flat-earth model.

Source Location Method

The geometrical construction for the source location method is illustrated in Fig. 11. The wave is assumed to spread uniformly from a localized source region to the ith and jth sites along great-circle paths d_{si} and d_{sj}. The associated propagation times from the source are Δt_{si} and Δt_{sj}. These are always positive quantities. By using the spherical triangle defined by the meridians from the geographic pole to the source and to the ith site and by the great-circle path d_{si} the following useful relation is obtained from the law of cosines:

$$\text{angle}\left(d_{si}/R\right) = V\Delta t_{si}/R = \cos^{-1}\left[\cos\theta_i\cos\theta_s + \sin\theta_i\sin\theta_s\cos\left(\varphi_i - \varphi_s\right)\right] \tag{16}$$

where V is the velocity of propagation and R is the radius of the earth. From Eq. (16) one may write an abbreviated relation:

$$\Delta t_{si} = Rf(\theta_i, \theta_s, \varphi_i, \varphi_s)/V \tag{17}$$

where the function f is given by the right-hand side of Eq. (16). The actual observable quantity in time is the propagation delay between two sites. This can be determined by subtraction, as

$$\Delta t_{ij} = \Delta t_{si} - \Delta t_{sj} = R[f(\theta_i, \theta_s, \varphi_i, \varphi_s) - f(\theta_j, \theta_s, \varphi_j, \varphi_s)]/V. \tag{18}$$

Here i and j denote two different sites. The value of Δt_{ij} can be positive or negative, depending on the magnitudes of Δt_{si} and Δt_{sj}. The same sign convention for Δt_{ij} holds as for the other two methods. We now define an error function as

$$e_{ij} = R[f(\theta_i, \theta_s, \varphi_i, \varphi_s) - f(\theta_j, \theta_s, \varphi_j, \varphi_s)]/V - \Delta t_{ij} \tag{19}$$

GEOGRAPHIC POLE

j^{th} SITE

SOURCE LOCATION

i^{th} SITE

d_{sj}

d_{si}

θ_i θ_s
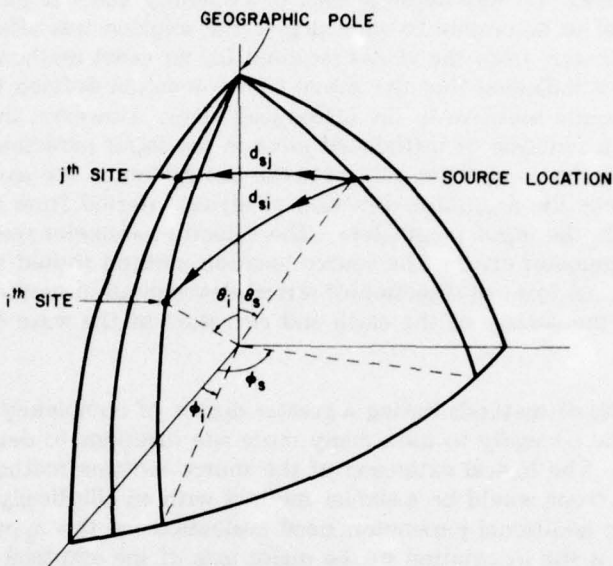
ϕ_s

ϕ_i

Fig. 11—Schematic of coordinate system and variables used
for the source location method

where j represents the reference site and i represents any of the four other sites. The first term on the right side of Eq. (19) represents the prediction of the propagation time delay between sites i and j for a given choice of θ_s, φ_s, v, and the second term, Δt_{ij}, represents the experimentally determined value. Equation (19) is used to form a composite rms error function.

$$\text{err}(\theta_s, \varphi_s, V) = \left(\sum_{i \neq j} e_{ij}^2 \right)^{1/2}. \tag{20}$$

The summation is over i, with j held constant. A computer algorithm is used to search a three-dimensional table of candidate values of θ_s, φ_s, and V to determine the set of these parameters for which function err is a minimum. In our analysis the increment in θ was 1 degree, the increment in φ was 2 degrees, and the increment in V was 3% of the plane-wave solution velocity. Upon determination of source parameters θ_s, φ_s, and V, the velocities V_{ij}, defined as

$$V_{ij} = R[f(\theta_i, \theta_s, \varphi_i, \varphi_s) - f(\theta_j, \theta_s, \varphi_j, \varphi_s)]/\Delta t_{ij} \tag{21}$$

were determined for the four combinations of pairs of sites. The standard deviation in velocity was then determined in the same manner as indicated in Eq. (12). It should be emphasized that the standard deviations calculated in this manner indicate a measure of internal consistency between model and data. They do not represent a measure of consistency obtained by repeated measurement of the same quantity.

27

As will be discussed in more detail in Sec. 5, a stability test was performed on the source location model to determine to what degree the solution was affected by variation of the t_{ij} input parameters from the values required for an exact mathematical solution. The results of the test indicated that the actual source location defined by the coordinates θ_s and φ_s was quite sensitive to the introduced error. However, the movement of the source region as a function of introduced error in the input parameters was closely constrained to fall on the great-circle path between the reference site and the zero-error source location. Hence the azimuthal direction of arrival inferred from this method is insensitive to errors in the input parameters. The velocity parameter was not strongly affected by input parameter error. The source location method should realistically be considered to be a third form of direction-of-arrival determination method that allows for the curvature of the surface of the earth and curvature of the wave front toward the source region.

Propagation analysis methods having a greater degree of complexity were not considered because of the necessity to have many more site locations to determine the propagation parameters. The logical extension of the source location method with a circularly spreading wave front would be a similar method with an elliptically expanding wave front. However, two additional parameters need evaluation for this approach. One is the ellipticity; the other is the orientation of the major axis of the elliptical wave front. Complete determination of parameters for this method would require a minimum of six sites.

5. RESULTS

A total of 18 time windows of data of either 8- or 18-min duration were analyzed in detail. These samples were taken from seven different days over the period from April 15 to December 4, 1975, and represent the best quality Pc1 events observed simultaneously at all five sites during the interval from April 9, 1975, to February 19, 1976. All times used are universal times (UT) in units of hours and minutes unless indicated otherwise. Julian days are listed with the calendar dates because it was considered more convenient to use Julian day only for identification in other areas of the report.

Discussion of the Data

Table 2 summarizes the dates and time windows of the events analyzed, the geomagnetic activity K_p index, the center-frequency of the narrow-band spectral slice utilized, and the apparent direction of arrival in azimuth, apparent group velocity and standard deviation in group velocity for three different mathematical models. All data appear to be taken during relatively quiet geomagnetic conditions by implication of the low K_p* values. Pc1 frequencies range from 0.838 to 1.281 Hz. The last three headings blocked off at the top of Table 2 refer to the three different analysis methods used to determine propagation speed and direction of arrival. The plane-wave, flat-earth method computes the azimuth of arrival and speed of propagation parameter values in a manner that minimizes the internal discrepancy in velocity between all sites with respect to the Florida

*For a discussion of the significance of the K_p index, see Ref. 36.

Table 2—Summary of Data Windows Analyzed and Computed Propagation Model Parameters

Julian Day	Calendar Date	Analysis Interval (UT)	K_p	Pc1 Frequency (Hz)	Plane-Wave Flat-Earth Az (deg)	Plane-Wave Flat-Earth Vel (km/s)	Plane-Wave Flat-Earth Dev (km/s)	Plane-Wave Spherical Earth Az (deg)	Plane-Wave Spherical Earth Vel (km/s)	Plane-Wave Spherical Earth Dev (km/s)	Source-Location Spherical Earth Lat (deg)	Source-Location Spherical Earth Long (deg)	Source-Location Spherical Earth Vel (km/s)	Source-Location Spherical Earth Dev (km/s)	Source-Location Spherical Earth Az (deg)
105	15 Apr 75	0345/0403	2−	.838	4	1106	122	2	1114	129	46	82	1006	56	9
		0915/0923	1+	1.242	6	1373	79	4	1383	86	52	80	1318	46	9
106	16 Apr 75	0630/0648	2+	.878	6	1187	86	4	1196	92	46	82	1080	43	9
		0650/0708	2+	.878	27	1202	46				54	72	1202	42	19
		0700/0718	2+	.878	42	1495	249	41	1523	254	44	76	1436	184	27
		0710/0728	2+	.878	−12	1457	189				48	84	1457	145	4
119	26 Apr 75	0808/0826	1	1.250	6	817	75	4	823	79	44	82	706	27	11
		0816/0824	1	1.250	7	758	105	5	764	107					
122	2 May 75	0757/0805	3	.883	22	502	39	20	509	41	70	46	517	42	18
195	14 July 75	0754/0802	2+	1.281	−4	772	83	−6	774	87	46	84	703	39	4
196	15 July 75	0440/0448	2	.909	−20	517	92	−22	514	95	42	84	465	30	6
		0510/0518	2	1.090	−1	754	66	−3	757	71	48	84	697	38	4
338	4 Dec 75	0241/0259	3	1.019	16	523	72	14	529	74	44	82	444	47	11
		0250/0308	3	1.031	14	530	60	12	535	62	44	82	450	39	11
		0300/0318	3	1.019	11	538	69	9	543	71	44	82	458	36	11
				1.031	0	507	66	−2	510	69	44	82	461	30	11
				1.019	11	675	41	9	682	44	44	82	594	38	9
		0315/0333	3	1.031	−2	643	79	−4	646	82	44	82	585	44	11
				1.031	18	639	29	16	648	32	64	68	640	31	13
		0630/0648	2+	1.259	−20	643	129	−24	576	103	44	84	662	55	5
		0642/0700	2+	1.259	−15	694	96	−18	683	98	46	86	652	50	−1

29

(FL) site.[†] In principle only three sites are required for this calculation. We have found that the redundancy of two extra sites increases the reliability of the solution. The plane-wave, spherical-earth method functions in an analogous way but allows for the curvature of the earth's surface. Again only three sites are required for the calculation, but five sites or four time differences are always used. The difference in results from these two methods is insignificant. The third (source location) method allows for curvature of both the earth's surface and of the wavefront itself. Four sites are required for this calculation, and the inclusion of the fifth creates one redundancy. It should be understood that azimuth (AZ) values listed for the three methods refer to the azimuth of arrival at the FL site relative to the geographic meridian. A 0-degree azimuth implies propagation from north to south along the geographic meridian. For the plane-wave, flat-earth method the arrival azimuth would be the same at all sites. Because of earth curvature the arrival azimuths would be slightly different at the other sites for the plane-wave, spherical-earth method. Since the source location method uses a curved wave front the arrival azimuths could be very different at the other sites, depending on the proximity of the source to the network of sites. The columns labelled "Dev" in Table 2 represent the standard deviation of the variation of the velocity between pairs of sites from the root-mean-square velocity (Vel) determined by application of the analysis method.

Thus the standard deviations represent an internal variance peculiar to the model employed. They do not represent variation observed from repeated measurements of the same data window.

A stability test was performed for the source location method to ascertain the effect on the solution parameters of latitude, longitude, and velocity caused by varying degrees of error in one of the input time delay parameters. The results of the stability test are shown in Table 3. Propagation time delays between each of the other sites and the FL site were computed for a velocity of 800 km/s from a source at 60°N latitude 60°W longitude. These values were –1.999, –1.180, –1.444 and –1.088 sec for NY/FL, WV/FL, MD/FL, and IL/FL, respectively. The root-mean-square deviation from these times and the calculated source location latitude and longitude and azimuth of arrival at the FL site were calculated for introduced errors of ± 0.10 s for the WV/FL input parameter and ± 0.05 to ± 0.30 s for the NY/FL parameter. The computed latitudes and longitudes representing the solution with introduced input parameter errors move away from the exact or zero-error solution location in a manner such that the *azimuth* between the source location and the FL site is nearly invariant. Hence the most meaningful solution parameter for the former date in Table 2 for the source location method is the azimuth of arrival of the wave at the FL site rather than the specific geographical location of source region itself.

Table 4 lists the actual cross-correlation time delays obtained for all data time windows analyzed. These data were used with the analysis methods in Sec. 4 to calculate the velocity and direction of arrival results in Table 2. A "minus" sign before the data value implies that the signal arrived at the other site prior to arrival at the reference site.

[†]It was found that if any other site was used as a common reference the baseline was too short and the propagation times between sites were too small compared to measurement accuracy and compared to deviations in computed temporal model parameters from actual complex propagation conditions.

Table 3—Stability Study of Source Location Method

Perturbation	Latitude (deg)	Longitude (deg)	Azimuth of Arrival (deg)	Velocity (km/s)	Standard Deviation (km/s)	rms Time Error (s)
NONE	60	60	22.6	800.0	0.3	0.001
NY + 0.050	58	64	22.0	800.0	10.6	0.048
NY - 0.050	52	72	21.0	776.0	11.5	0.041
NY + 0.100	66	46	22.4	824.0	19.0	0.065
NY - 0.100	52	72	21.0	776.0	18.1	0.065
WV + 0.100	46	78	18.8	752.0	16.1	0.063
WV - 0.100	66	40	24.2	824.0	34.0	0.091
NY + 0.200	66	48	21.6	848.0	41.2	0.138
NY - 0.200	50	74	20.7	752.0	33.6	0.129
NY + 0.300	66	50	20.9	872.0	66.2	0.210
NY - 0.300	46	76	23.0	728.0	55.0	0.191

All cross-correlation time delays were obtained on data that were narrow-banded at a Q of 50, with subsequent squaring and summing of NS and EW components followed by low-pass filtering to accomplish a form of envelope detection. This detection method was compared to full-wave rectification followed by low-pass filtering for a single axial component. Negligible differences in terms of cross-correlation results were observed when a single component was used for both methods.* The squaring method tends to weight the importance of the large amplitude data at the expense of the lower amplitude constituents. A square-root device was not used after the squaring method detector because of problems with dynamic range and offsets inherent in these analog devices.†

Table 5 lists the apparent attenuation constants in decibels per/1000 km for most of the previously listed data time-windows. The word "apparent" is used because the observed signal strength between two sites depends upon the attenuation of the hydromagnetic wave in the ionospheric medium as well as the transmission (or leakage) coefficient from the ionospheric medium to the surface of the earth. The constants were calculated with the assumption that the wave field strengths were attenuated exponentially with distance. All amplitude ratios were with respect to the FL site. The amplitude values

---

* It is not possible to vectorially combine two components of data with conventional rectification low-pass filtering detection methods.

† Since the cross-correlation was performed with analog apparatus, the squaring, summing, filtering (and square-rooting if applied) were also accomplished with analog devices.

Table 4—Summary of Propagation Time Delays Between Sites
for Group Velocity Determinations

Julian Day	Calendar Date	Analysis Interval (UT)	Pc1 Frequency (Hz)	NY/FL (sec)	WV/FL (sec)	MD/FL (sec)	IL/FL (sec)
105	15 Apr 75	0345/0403	.838	-1.323	- .980	- .823	- .911
		0915/0923	1.242	-1.122	- .715	- .692	- .754
106	16 Apr 75	0630/0648	.878	-1.147	- .852	- .861	- .891
		0650/0708	.878	-1.272	- .821	- .955	- .735
		0700/0718	.878	-1.240	- .618	- .658	- .438
		0710/0728	.878	- .866	- .680	- .486	- .688
119	26 Apr 75	0808/0826	1.250	-1.634	-1.270	-1.257	-1.289
		0816/0824	1.250	-1.649	-1.301	-1.538	-1.414
122	2 May 75	0757/0805	.883	-2.815	-1.990	-2.389	-1.906
195	14 July 75	0754/0802	1.281	-1.553	-1.277	-1.201	-1.410
196	15 July 75	0440/0448	.909	-1.801	-1.844	-1.287	-1.939
		0510/0518	1.090	-1.691	-1.329	-1.246	-1.430
338	4 Dec 75	0241/0259	1.019	-2.489	-2.041	-2.290	-1.914
			1.031	-2.520	-1.978	-2.180	-1.914
		0250/0308	1.019	-2.411	-1.978	-2.103	-1.914
			1.031	-2.395	-2.041	-1.978	-2.101
		0300/0318	1.019	-2.083	-1.479	-1.603	-1.539
			1.031	-1.864	-1.557	-1.524	-1.679
		0315/0333	1.031	-2.301	-1.556	-1.759	-1.539
		0630/0648	1.259	-1.364	-1.354	-1.181	-1.601
		0642/0700	1.259	-1.442	-1.260	-1.149	-2.586

Table 5—Observed Attenuation Constants in Decibels per 1000 Kilometers

Day	Analysis Interval	Plane-Wave Azimuth Used		Source-Location Azimuth Used	
		Attenuation Constant	Standard Deviation	Attenuation Constant	Standard Deviation
105	0345–0403	5.30	2.41	5.18	2.33
105	0915–0923	7.63	4.52	7.52	4.46
106	0650–0708	2.81	1.54	2.80	1.57
106	0700–0718	2.29	1.34	2.15	1.29
106	0710–0728	2.40	1.74	2.05	1.54
119	0808–0826	6.70	2.75	6.62	2.80
122	0757–0805	8.01	4.38	8.02	4.40
195	0754–0802	5.30	2.34	5.10	2.48
196	0440–0448	-0.47	3.28	-0.59	2.22
196	0510–0518	6.06	2.50	5.92	2.52
338	0241–0259	12.76	2.89	12.88	3.07
338	0250–0308	13.05	3.63	13.05	3.63
338	0300–0318	12.03	4.39	12.07	4.42
338	0315–0333	9.25	3.92	9.33	4.02
338	0630–0648	10.09	4.48	8.01	3.63

were manually extracted from strip-chart plots of vectorially summed NS and EW components that were previously bandpass filtered with a Q of 20. Ratios were determined on the average of once every 0.3 to 1.0 min. of data window. No attenuation constants were calculated for events 106 0630/0648 and 338 0642/0700 because the amplitude ratios were not very stable as a function of time. All values of amplitude ratio for a given site pair were averaged over the data window before the attenuation constant was computed. The standard deviation listed is a measure of internal consistency of the average attenuation constant calculated for the four pairs of site combinations. Calculated values are shown for arrival azimuths based on the plane-wave and source-location models but the differences are insignificant.

The Data Spectra

The spectral characteristics of the data are presented in Appendix A. No additional filtering was used in the spectral presentations over the actual passband of the receiving system, which was 0.39-2.1 Hz (-3-dB points). The horizontal line just above 1.5 Hz is a

display calibration marker at 1-9/16 Hz. The spectral display was intensity modulated, which tends to produce a somewhat thresholded appearance. A 32-s memory time was used; it consequently provides 0.03125-Hz frequency resolution. The raster is composed of individual amplitude-frequency displays incremented approximately every 9 s in time. The spectra were generated using the largest amplitude component at each site (usually the NS component). The amplitude of the signal input to the spectrum analyzer was carefully adjusted to retain most of the fine structure detail, with second priority given to displaying the weaker signal components and noise background. A 2-dB adjustment often made an appreciable difference in the display. A weak input emphasized the discrete fine structure but made the overall bandwidth seem narrow. A strong input bloomed out the fine structure detail but often brought to view an apparent wider emission band structure. The rather small dynamic range of the display (not the electronics) should be kept in mind when comparing spectra.

The narrow-band fine structure that rises in frequency with increasing time, a well-known feature of Pc1 emissions, is evident in most of the displays but is especially prominent in Fig. A6 (an "A" before the figure number implies that the figure occurs in Appendix A). Note that the frequency scale does not start at zero in this example. The narrow vertical bands that somewhat degrade the appearance of Fig. A5 are caused by transient impulses in the data from atmospheric discharges, or "spherics," which momentarily overloaded the spectrum analyzer. Most of the events are relatively narrow band (defined in this context as less than 0.5 Hz) with the exception of the events on Julian days 106 (Fig. A2) and 122 (Fig. A4). All data that were analyzed for polarization characteristics and velocity/direction-of-arrival analysis were narrow-band filtered at a Q of 50 with a center frequency near the center of the spectral bands shown in Figs. A1-A8. The data used to compute attenuation constants were filtered at the same center frequencies but with a Q of only 20. The narrow-band filtering was employed to diminish beating effects on the shape of the Pc1 amplitude-time envelope and on the eccentricity, orientation, and phasor rotation of the polarization ellipse. Obviously it is undesirable to eliminate all beating effects, since if this were done there would be no envelope modulation at all and cross-correlation techniques would not be possible except for carrier phase comparisons. Narrow-band filtering is beneficial in several ways:

1. It equalizes the spectral bandwidths at all sites, whereas without filtering they would be unequal because of propagation effects.

2. It reduces the effect of local interferences such as powerline transients and electrical storm discharges.

In all cases the filters were carefully adjusted so that phase shifts between all filter pair combinations at the center frequency ± 0.5 Hz were minimal and insignificant. This was accomplished by observing the Lissajous figure resulting from a test signal in the manner described in Sec. 3. The detrimental effects of beating in broad-band signal analysis sre discussed in Sec. 2 under the subheading "Polarization." Other investigators employing narrow-band filtering in Pc1 analysis were Fraser [19] and Campbell and Thornberry [18].

The Data Envelopes

The envelopes of the narrow-band filtered amplitude-time data for all but the last data window for day 338 are shown in Appendix B. These illustrations represent envelope magnitudes in the horizontal plane. The narrow-band filtered NS and EW components at each site were squared, summed, low-pass filtered, and then digitized. A computer algorithm was used to take the square root before plotting. Careful attention was employed to eliminate d.c. offsets and drifts in this processing. The envelope magnitude method of data presentation has the advantage of reducing the number of illustrations by a factor of two (by virtue of the combination of NS and EW components). In addition it is a better form to use for making comparisons between sites because component-to-component comparisons can lead to confusing and sometimes erroneous conclusions. Comparison of a NS component at one site to an EW component at another site can lead to an error of up to ± 1/4 cycle (0.25 s at 1 Hz) for an elliptically polarized wave (an explanation follows under the heading "Phase Analysis"

The general appearance of the envelope magnitudes requires some explanation. For example, a very obvious change in appearance occurs at the 9-min tick mark in Fig. B7 (data sample on Julian day 119). This change is accompanied by a change in spectral characteristics of the event as shown at approximately 0819 UT in Fig. A3. Here a lower emission band fades out, leaving only the slightly higher frequency band that commenced at approximately 0814 UT. The envelope modulation is caused by beating of the various frequency components that compose the emission and that are not rejected by filtration. If only two frequency components are present and the center frequency of the band-pass filter is placed midway between them, the maximum beating of the envelope will be observed. If on the other hand the center frequency of the filter is placed close to one of the two component carrier frequencies the envelope modulation will be greatly diminished. In Fig. B7 the center frequency of the filter is held constant at 1.25 Hz. The beating pattern varies from slow to rapid to slow again, concurrently with the broadening and subsequent narrowing of the spectrum.

The envelope magnitude illustrations, which are presented with synchronism among all five sites, provide the reader with an excellent opportunity to judge the quality of the data used in the cross-correlations for determining group velocity and direction of arrival. The time scales for each of the five sites have been adjusted to remove the propagation delays so that the modulation peaks are aligned vertically. From purely visual and somewhat subjective observation the greatest similarity in envelope modulation patterns among all five sites occurs in Figs. B2, B6-B11, and B16.

The Data Polarizations

The polarization characteristics of all the data presented in this report are shown in Appendix C. Each polarization ellipse represents 5s of data, and the start of each subsequent ellipse is exactly 1 min from the start of the previous one. The upward ordinate direction is toward magnetic north; the right abscissa direction points toward magnetic east. All data were band-pass filtered at a Q of 50. Careful attention was paid to tuning the identically constructed filters to eliminate phase shifts between NS and EW channels, which would affect the eccentricity of the polarization ellipses. The time sequence is from left to right and the starting and ending times are as given in the figure captions.

The amplitudes at each site were adjusted to yield comparable average magnitudes among all sites. The polarization displays for the 18-min. data windows were divided into two sections for illustration purposes. Graphical display of the data facilitates rapid visual determination of the polarization linearity, the orientation of the polarization ellipse, and the rotation of the ellipse as a function of time and site location. The polarization displays show that there is a slight tendency for the FL site to have more linear polarization than do the more northerly sites. This effect is not pronounced, however, over the latitudes spanned by our network of receiving sites. The characteristics of the polarization phasor rotation were also analyzed in detail by computer analysis of the digitized data. Both right-hand and left-hand polarizations were observed at all sites. The percentage of time, statistically, that each site exhibited right-handed phasor rotation was calculated and the following results were found: NY, 37%; IL, 52%; MD, 45%; WV, 52%; and FL, 50%. A transition from LH phasor rotation at the higher latitudes to predominantly RH rotation at the lower latitudes was not observed. Failure to observe predominantly RH phasor rotation at the lower latitudes leads one to conclude that either RH polarization does not dominate at low latitudes, as has been postulated by theorists, or the effect is masked by the beating effect discussed in Sec. 2, despite the fact that the data were heavily filtered.

Table 6 lists the average angle of projection of the major axis of the polarization ellipse relative to the geographic meridian for a selected group of events that had reasonable temporal stability in polarization characteristics over the interval shown. These angles will be used subsequently to test the hypothesis of Baranskiy that the polarization alines toward the secondary source region. Note that the time intervals in Table 6 are either 8 or 9 min long and are in some cases smaller time windows than previously associated with data from the same day. In each case the smaller time window matches that of the corresponding polarization illustration in Appendix C. The angle of inclination of the eight to nine polarization ellipses in the illustration was averaged for each site. These averages, which represent inclinations from magnetic north, were then adjusted for the magnetic declination at the respective sites to give angles relative to the geographic meridian. A positive angle denotes inclination east of the geographic meridian, and a negative angle, west. In cases where a given polarization ellipse could not be assigned a definite inclination because of extremely small amplitude or because of erratic behavior, it was ignored. Data windows that exhibited much erratic behavior were not included in the table.

The hypothesis of Baranskiy implies that the polarization projections tend to point toward the secondary source region at high and middle latitudes. This tendency was derived from theoretical calculations for linear polarized waves in a homogeneous boundless plasma. In reality neither homogeneous nor boundless conditions are accurate physical descriptions, and exactly linear polarization is seldom observed (although it must be conceded that most polarization measurements are made outside the ionosphere). The NY, IL, MD, and WV sites can certainly be considered midlatitude sites. The FL site is probably borderline between middle and low latitude.

To test this hypothesis, we plotted the data in Table 6 on the maps shown in Appendix D. They have a simplified outline of northeast America and use the same projection as was used in Fig. 3 and in Appendix E (to be discussed). On this projection great-circle paths from any of the sites to distances of a few thousand kilometers can be

Table 6—Average Inclination of the Polarization Ellipse to the Geographic Meridian. Positive
Value Indicates Inclination to the East; Negative Value Indicates Inclination to the West

Day	Time	NY (deg)	IL (deg)	MD (deg)	WV (deg)	FL (deg)
105	0916–0924	58.4 ± 3.8	50.0 ± 2.7	27.8 ± 3.4	27.9 ± 2.7	10.1 ± 4.7
106	0720–0728	26.9 ± 11.7	49.8 ± 2.6	16.1 ± 7.1	28.9 ± 2.8	11.3 ± 3.9
119	0809–0818	-86.7 ± 7.6	43.0 ± 7.7	-35.9 ± 12.7	-7.0 ± 4.6	9.1 ± 10.3
119	0819–0827	-104.6 ± 9.3	36.3 ± 8.7	-42.0 ± 8.5	-14.4 ± 5.7	-1.9 ± 7.2
122	0800–0808	83.8 ± 9.5	50.0 ± 9.5	44.9 ± 3.3	40.6 ± 3.8	29.9 ± 9.0
196	0441–0450	-73.4 ± 13.5	-40.2 ± 5.4	-50.6 ± 11.1	-50.1 ± 6.6	-19.2 ± 6.1
196	0511–0520	-86.3 ± 5.8	-12.3 ± 23.0	-50.2 ± 6.4	-35.7 ± 8.7	-21.1 ± 9.2
338	0241–0250	30.8 ± 9.6	53.5 ± 6.4	28.9 ± 8.4	31.7 ± 5.8	22.4 ± 10.6
338	0251–0300	42.8 ± 25.9	59.0 ± 4.5	33.5 ± 19.6	26.9 ± 6.0	25.6 ± 30.0
338	0301–0310	48.3 ± 15.0	65.7 ± 15.3	30.8 ± 8.5	32.7 ± 11.3	32.8 ± 11.6
338	0631–0639	-66.2 ± 3.5	-19.3 ± 2.6	-15.3 ± 2.7	-20.7 ± 2.7	8.2 ± 5.1

represented by straight lines with sufficient accuracy for the purpose at hand.* The solid
lines emanating from each site position in the illustrations in Appendix D represent the
projections of the major axis of the polarization ellipses. The dashed line (longer dashes)
represents the direction of arrival at the FL site using the plane-wave, flat-earth method
and propagation time-delay data. The dotted line (or shorter dashes) represents the
direction of arrival at FL using the source location method. A glance at all the illustra-
tions in Appendix D immediately shows a strong tendency for alinement of the polariza-
tion projections. While the alinement is often too poor to allow any firm deductions it
is obvious that the polarization orientation is not random. In two cases, 119 0809/0818
and 196 0441/0450, the intersection of all five polarization projections in a relatively
small area appears to support the Baranskiy hypothesis, in spite of the fact that the
polarizations are not exactly linear. In all the other cases shown the tendency to con-
verge is still apparent. Strangely enough, some of the worst examples in terms of
convergency have the smallest standard deviations listed in Table 7 (for example, 105
0916/0924 and 338 0631/0639). Comparison of the polarization projections to the
plane-wave and source location directions of arrival is not consistent. Sometimes one or
the other direction of arrival methods gives good corroboration, but at other times both
methods are in disagreement. Thus it must be concluded that the directional indications
of the polarization data from the five-station network do not usually point to or intersect
on a source region which is in agreement with the direction of arrival computed from

---

*The type of projection is unknown. The straight-line approximation was checked by computing and
 plotting trajectories of several great-circle paths using spherical trigonometry.

Table 7—Comparison of the Average Inclination of the Polarization Ellipse at the Florida Site to the Calculated Direction of Arrival for the Plane-Wave, Flat-Earth and Source Location Models

Day	Time (UT)	Polarization Azimuth (deg)	Standard Deviation (deg)	Plane Azimuth (deg)	Source Azimuth (deg)
105	0346-0354	33.3	7.5	4	9
105	0355-0403	28.9	14.7	4	9
105	0916-0924	10.1	4.7	6	9
106	0631-0639	28.3	5.9	6	9
106	0640-0648	6.4	4.4	6	9
106	0651-0659	12.4	10.4	27	19
106	0700-0708	12.5	10.5	27	19
106	0710-0718	12.4	5.7	-12	4
106	0720-0728	11.3	3.9	-12	4
119	0809-0818	9.1	10.3	6	11
119	0819-0827	-1.9	7.2	7	*
122	0800-0808	29.9	9.0	22	18
195	0755-0804	-17.8	8.3	-4	4
196	0441-0450	-19.2	6.1	-20	6
196	0511-0520	-21.1	9.2	-1	4
338	0241-0250	22.4	10.6	16	11
338	0251-0300	25.6	30.0	11	11
338	0301-0310	32.8	32.8	11	9
338	0311-0320	29.2	15.4	11	9
338	0631-0639	8.2	8.2	-20	5
338	0640-0648	8.2	6.2	-15	-1

*Value not determined.

time delay measurements. Summers [29] predicted that because of refractive effects the farther a wave proceeds toward the equator the more the polarization should approach the geomagnetic meridian (which we estimate to be about $11°E$ at the FL site). This prediction was corroborated by observations of Tepley [30] and Smith [31], and this trend can also be seen in our determinations of direction of arrival and polarization projection.

Fraser and Summers [32] suggested the possibility that for near-linear polarization the projection of the major polarization axis for *low-latitude* stations might point to the source region. This hypothesis is in conflict with the prediction of Baranskiy, who thought the method would work only at high and middle latitudes. It also seems less plausible because of the refraction effect. Table 7 compares the average polarization inclination of the FL site with the direction of arrival azimuths computed using the plane-wave and source location methods based on time-delay measurements. There are more entries in Table 7 than in Table 6 because the FL site polarizations taken alone satisfy more frequently the criterion of approximate linearity and consistency in orientation than when polarizations from all five sites are considered as a whole, as was done for Table 5.5. Some of the average polarizations shown have large standard deviations, however, and should be accepted only with caution. Inspection of the table shows that there is poor agreement between the polarization inclinations and the computed directions of arrival. In addition, there is no better agreement with the polarization inclinations for either the plane-wave or source location method.

Result Summary Maps/Direction of Arrival

The results of Table 2 are displayed pictorially in the illustrations of Appendix E. The straight lines terminating at the FL site represent the computed direction of arrival for the plane-wave, flat-earth method. When solutions for more than one time interval are plotted on the same illustration they are tagged with a label that is referred to the applicable data window in the figure caption. The tagged circles represent the computed locations of the secondary source region for the hydromagnetic wave propagation in the ionospheric medium. It is emphasized again that the *azimuthal angle* of arrival at the FL site for the source location method is a more reliable parameter than the actual source location point. Specification of the source location region on the illustrations allows a rapid visual qualitative comparison of arrival directions associated with the two methods of computation, as well as an association of a geographical area of origin. The arclike curves labeled L = 2, 3, 5, and 10 included on the illustrations are the McIlwain L-shell contours for an altitude of 200 km.* The contours do not change significantly for the purpose at hand for altitude up to 400 km. As mentioned in Sec. 2 the secondary source regions have been reported to be observed most frequently between L-shell values of 4 and 10.

There is evidence that observation of Pc1 micropulsation characteristics is dependent upon a solar time-of-day scale. Baranskiy [24], Troitskaya et al. [27], and Summers and Fraser [28] indicate that in northern latitudes the major axis of the polarization ellipse rotates in a counterclockwise manner with time in early morning hours. This rotation is

---

*The L-value is the geocentric distance measured in earth radii to the place where the field line crosses the equatorial plane and is the same parameter as is used in McIlwain coordinates. For a discussion of McIlwain coordinates, see Ref. 37.

attributed to a westward movement of the secondary source region as the dawn day-night terminator migrates westward. In an attempt to associate observed Pc1 characteristics with solar-time conditions at ionospheric F_2 layer altitude, contours representing the demarcation of astronomical twilight and sunrise at a given instant of time and at an altitude of 350 km are plotted on the illustrations of Appendix E. The stippled area represents the transition region from total darkness on the left to sunlight on the right. The two stippled areas on Fig. E1 represent the twilight-sunrise conditions for the two data windows for day 105. Several other illustrations indicate the advance in the twilight contour by a dashed line for two or more data windows following closely in time.

The data for these contours were taken from tables issued by the Nautical Almanac Office as a supplement to the *American Ephemeris* in 1946 [38]. The correction factor to account for altitude above the surface of the earth had to be extrapolated mathematically because the tabular values extended only to 1525 m (5000 ft). A constant factor of -29 min of arc was used for correction for refraction effects. This value represented the tabular entry for the lowest temperature and pressure combination, -60°F and 102 mbar, respectively.

Inspection of the illustrations of Appendix E shows no consistent tendency for angular dependence of the incoming wave on the location of the twilight-sunrise contours. Contours primarily west of the network of stations do not cause waves to arrive along a westward-tilted azimuth, and contours primarily east of the network of stations do not cause waves to arrive along an eastward-tilted azimuth. On the other hand, Table 2 suggests a tendency for counterclockwise (CCW) rotation of the angle of arrival on a much shorter time scale for the overlapping data sequences taken on two different days (106 0630/0728 and 338 0241/0333). For day 106 the CCW rotation tendency established by the first three data windows is somewhat negated on the last window, which indicates a substantial rotation to the east. The polarizations for this time period are too unsettled to allow determining a rotation tendency. For day 338 the CCW rotation tendency is weak. For the data processed at 1.019 Hz over the time span 0241/0318 a maximum of 5 degrees of rotation is observed for the plane-wave method and only 2 degrees for the source location method. For the data processed at 1.031 Hz over the same window, a 16-degree CCW rotation is observed by the plane-wave method but no rotation by the source location method. The final data window of 0315/0333 again destroys the continuity of rotation by registering a significant clockwise (CW) rotation of 20 degrees for the plane-wave methods and 2 degrees for the source location method. The polarization rotation tendency inferred from Table 6 for the three data windows spanning time interval 0241/0310 indicates CW rotation for the NY, IL, and FL sites. The rotations for the MD and WV sites are not consistently unidirectional and are oppostie each other. The second data window for MD indicates a CW rotation relative to the first, and the third indicates a CCW rotation. The WV data show a CCW rotation for the second window and a CW rotation for the third. The rotation sense for the polarization ellipse axes does not complement the rotation sense of the direction of arrival directrix computed from propagation time differences between sites for the two days of data for which an overlapping time sequence of data windows was analyzed. It should be recognized that the large standard deviation associated with the average polarization orientations precludes a high degree of confidence in any conclusions based on them. It is our opinion that this problem would be inherent in polarization data collected in the same latitudes by any other system of measurement. Conclusions on orientation trends can be obtained only

by statistical studies of a large number of well-behaved events. Since our data samples were obtained by highly selective standards with most consideration given to cross-correlation characteristics and only secondary consideration given to polarization characteristics, these samples are insufficient for such a statistical study of polarization orientations.

Much more significance, however, is attributed to the following observations. For each of the three wave propagation methods, rms time-delay errors indicating the deviation of the input data from the equivalent "exact" solution values were calculated for each data window. In all but two instances the source location method had slightly better internal consistency (i.e., lower rms error). This property is also apparent in the lower standard deviations in computed velocities for this model. The average rms time error for each of the three methods was

Plane wave, flat earth:	0.306 ± 0.158 s
Plane wave, spherical-earth:	0.335 ± 0.151 s
Source location:	0.186 ± 0.105 s.

The average azimuthal angle of arrival at the FL site was calculated for each method. These were found to be

Plane wave, flat earth:	5.5 ± 15.4°E
Plane wave spherical earth:	3.2 ± 15.2°E
Source location:	9.9 ± 6.7°E.

The source location method, which is internally more consistent, is also much more consistent in average azimuth of arrival. We have determined that the geomagnetic meridian passes through the FL reference site at an azimuthal angle of approximately 11°E.* The close proximity of the average direction of arrival by the source location method with the geomagnetic meridian is in strong support of the theoretical determination by Greifinger and Greifinger [3] that propagation along the meridian is most favorable. The plane-wave methods support this finding somewhat less convincingly, primarily because of the large deviation of the computed directions of arrival from the average value. It must be recalled, however, that the two plane-wave methods do not fit the observed data as well as the source location method. We interpret these observations as evidence that it is necessary to take nonplanar wave fronts into account in propagation calculations.

The concept of ducted Pc1 micropulsations being constrained to propagate along the geomagnetic meridian is not new. In fact it was originally assumed by workers in this field that this was the only possible direction a ducted wave could travel (see for example Ref. 6 and 17). It was not until the report of observations of E-W propagation by Campbell and Thornberry [18] and Fraser [19] that off-meridian propagation was given serious consideration.

Finally, it must be stated that the possibility of purely E-W propagation cannot be examined with the data from our five-station network. Because our stations are at mid-latitudes, strict E-W propagation would pass by undetected. Correspondingly, no data

---

*The geomagnetic meridian passing through the FL site follows a path that intersects the L-shell contours at right angles. The 11°E inclination was determined by manually sketching this path and measuring the azimuth at the FL site with a protractor.

41

ALTHOUSE AND DAVIS

windows analyzed for this report have ever indicated propagation in an E-W direction. The largest off-meridian propagation angles observed were $31°$E and $33°$W relative to the geomagnetic meridian or $42°$E and $22°$W relative to the geographic meridian. These values were obtained using the plane-wave propagation model, which as mentioned previously gave the larger diversity of directions of arrival. The largest off-meridian propagation angles observed using the source location model were $16°$E and $12°$W relative to the geomagnetic meridian, or $27°$E and $1°$W of the geographic meridian. Although the geographical location of the sites makes detection of east-west propagation improvable, the results above show that at midlatitudes there is a strong tendency toward meridianal propagation.

Attenuation

It is desirable to interpret the attenuation constant data in Table 5 in relation to the twilight-sunrise curves shown in the illustrations in Appendix E. Our observations are in agreement with those of other reports that optimum ducting conditions appear to occur in late night to early morning hours. The latest time at which a quality event was recorded was about 0930 UT or 0430 local standard time. Observation of Pc1's at all five stations have in a few cases existed until 0830 local standard time. However, the effects of severe attenuation, which are characteristic of daylight conditions, have by then become apparent in terms of very poor signal-to-noise ratio at the FL site. Over the local time interval (UT–5 hr) of 2130/0430 within which our data are clustered, the observed attenuation rates appear to be determined by existing ionospheric conditions much more strongly than the location of the twilight-sunrise swath relative to the five-station network. For example, the data taken on day 338 have the largest attenuation values observed, even though the sunrise line is the farthest east of the site network. The far eastward location of the sunrise terminator places the ionosphere above the network in the darkest and potentially optimum condition of low-attenuation ducting. The lowest attenuation rates (with the exception of the anomalous result on 196 0440/0448) were obtained on day 106, when the ionosphere above most of the sites was experiencing twilight conditions. Hence, in the optimum late-night, early-morning ducting time interval the attenuation rates depend only weakly on the proximity of the dawn terminator and are probably more strongly dependent on ionospheric properties. A study of attenuation constant vs ionospheric electron density data was not attempted because of the unavailability of ionosonde data in the appropriate geographical areas.

The magnitudes of the attenuation constants are considerably larger than those calculated by Greifinger and Greifinger [3] for nighttime minimum sunspot conditions, which indicated attenuation rates of 2 dB or less per 1000 km for propagation up to 15 degrees off the geomagnetic meridian and 4.5 dB or less per 1000 km for propagation at angles up to 30 degrees from the meridian. However, our values are in the same range as those measured by Bagnall [39]. The anomalous (amplification) result for day 196 is indicative of the unpredictability of relative signal amplitudes at two given sites and suggests that leakage or transmission of the hydromagnetic wave energy from the ionospheric medium to the surface of the earth may not be constant over the dimensions of our network of stations. This hypothesis is also supported by the large standard deviation found for all data windows.

42

Velocity

The velocities of propagation computed for all data windows ranged from 444 to 1523 km/s. The magnitude of the velocity, unlike the computed direction of arrival, was not a strong function of the computational model. The maximum variation in predicted velocity among the three models was 16%, and the average was 9.6%. The velocities observed span the range of values reported in most other reports contained in the references, but are all considerably smaller than the 2300 km/s velocity reported by Campbell and Thornberry [18] in their observation of E-W propagation. Where several adjacent or overlapping sequences of data were analyzed, the temporal progression of values found was slow and smooth. Most of the sequences (notably those for days 106 and 338) seem to indicate a trend of increasing velocity with duration of the event; however, the data collection is too small to support this statistically.

Phase Analysis

A considerable portion of the data analysis effort was directed toward phase correlation and consequent phase velocity and direction-of-arrival determination. Initial attempts to cross-correlate undetected single-axis components of the Pc1 signal from two different sites led to conflicting results when various combinations of NS and EW components were used. The reasons for this are not difficult to understand. If the wave is elliptically polarized, which is generally the case, and if the major axes of the polarization ellipses aline with the NS axis direction at each site, then cross-correlation of NS vs NS or EW vs EW would give identical results. However, cross-correlation of NS at one site vs EW at the other site would be in error by an amount characteristic of rhe ellipticity of the wave. This could be as large as $\pm 1/4$ cycle. If the polarization ellipses are not inclined at identical angles relative to the sensor axes at the various sites, which again is the usual situation, then cross-correlation of NS vs NS at any two sites would be in error for the same reason as given above by an amount depending on the ellipticity of the wave and the inclination of the polarization ellipses. For site pair separations of the order of 500 to 1000 km this source of error is too large to ignore for reasonably accurate results. This problem has always been ignored in previous reports by other workers because of the use of site separation of several thousand kilometers and because in most cases only envelope correlations and consequent group velocity parameters were determined. The envelope detection removes the phase information and reduces some of the sensitivity to the above problem.

In our phase-correlation work this problem was eliminated by squaring and summing the NS and EW signal components at each site. The composite signal was then cross-correlated with the equivalent at another site. The squaring processes, however, created a 180-degree phase ambiguity in the composite signal. Cross-correlation of the composite signals results in an always-positive correlation function with successive relative maxima representing alternately in-phase and out-of-phase conditions. The amplitude of the correlation function drops slowly rather than abruptly with time lag on either side of a broad "envelope" maximum. The narrower the bandwidth of the presquared signal components the broader the cross-correlation function "envelope" maximum becomes. The 180-degree phase ambiguity can be resolved by resorting back to cross-correlations between single axis components. The maxima in the composite cross-correlation function, which represent the desired in-phase conditions, can be identified by association with the

43

nonsquared-component correlation function between the largest amplitude components at each site. When a site has nearly equal amplitudes for both NS and EW axes, several sets of component correlations must be performed. The locations of the in-phase correlation peaks for these sets will bracket the position of the correct peak relative to zero time lag. It frequently happened, however, that although an in-phase maximum occurred close to an envelope correlation function maximum for one site pair, at another pair two in-phase maxima straddled and were nearly equidistant from the envelope maximum. Hence a dilemma occurred as to which phase-correlation peak to choose. In an effort to retain objectivity, direction of arrival and phase propagation velocity calculations were carried out using various combinations of the somewhat ambiguous cross-correlation time-lag parameters. In the five-station analysis method with all correlations relative to the FL reference site, if two phase correlation lags are used as candidate input parameters for each of the four site paris for direction of arrival calculations, then 16 "candidate solutions" result. The candidate solutions were thinned by arbitrarily retaining only those solutions that had standard deviations in the velocity (computed between individual site pairs along the determined direction of arrival) of less than 30% of the average velocity. These remaining solutions were then compared to the nonambiguous group-wave solution to determine whether it was possible to obtain at least one phase solution within reasonable bounds of the group solution. This procedure was performed only with the plane-wave, flat-earth method. The results for a few examples are summarized in Table 8. Multiple entries for phase-wave results are due to unresolvable ambiguities, as discussed above.

It was found that for many candidate phase solutions the normalized standard deviation in velocity (standard deviation per unit velocity) is as good as or better than that for the group velocity determination. In general, however, the computed direction of arrival and velocity for the candidate phase solutions bear so little resemblance to the group-wave solution that it is not possible to be certain which, if any, of the phase solutions is the correct one. Particularly disturbing was the tendency to obtain candidate phase solutions with velocity considerably smaller than that of the group solution. According to theory (see Sec. 2) the phase velocity should be larger than the group velocity. For days 105 and 106, which had group velocities in excess of 1000 km/s, no candidate phase solutions were obtained with velocities greater than or equal to the group value. For day 196, data window 0440/0448, there are two candidate phase solution velocities greater than the group velocity value of 517 km/s. The value of the one possibility, 592 km/s, is 15% larger than the group velocity and is a quite reasonable value. The other value found, 1601 km/s, is 3.1 times larger than the group velocity and is probably not the correct solution. In the following time window, 0510/0518, the 1366-km/s candidate phase solution is 81% faster than the group velocity solution of 754 km/s. It may be that the relatively faster phase velocity for this window is caused by a closer proximity of the analysis center frequency to the lower cutoff point frequency in the spectrum (Fig. A6). For the rest of the examples, for which only one value of phase velocity greater than group velocity was obtained, the ratio of phase velocity to group velocity ranged from 1.49 to 2.21. These rather large values for the ratio may indicate that the analysis center frequency was close to the ionospheric waveguide cutoff frequency, at which point there is a wide divergence between phase and group velocity. As mentioned in Sec. 2, near the cutoff point the phase velocity will approach infinity.

Table 8—Comparison of Group-Wave and Phase-Wave Determinations of
Velocity and Direction of Arrival

Day	Time	Frequency (hz)	Group	Phase	Azimuth (deg)	Velocity (km/s)	Standard Deviation (km/s)	Normalized Standard Deviation
105	0915/0923	1.242	X		6	1373	79	.058
				X	-3	736	50	.068
				X	-9	622	135	.217
				X	-14	462	95	.206
106	0630/0648	.878	X		6	1187	86	.072
				X	-4	536	22	.041
	0650/0708	.878	X		27	1202	46	.038
				X	-7	543	37	.068
				X	20	529	90	.170
				X	21	461	94	.204
	0700/0718	.878	X		42	1495	249	.167
				X	-7	543	35	.064
				X	41	785	167	.213
	0710/0728	.878	X		-12	1457	189	.130
				X	-6	546	33	.060
				X	-14	446	105	.235
				X	-20	319	76	.238
119	0808/0826	1.250	X		6	817	75	.092
				X	-3	492	88	.179
				X	-13	490	20	.041
				X	11	638	38	.060
				X	13	1214	202	.166
	0816/0824	1.250	X		7	758	105	.139
				X	11	638	37	.058
				X	-3	492	89	.181
				X	-14	484	20	.041
				X	12	1212	200	.165
122	0757/0805	.883	X		22	502	39	.078
				X	15	524	35	.067
				X	21	481	51	.106
				X	23	434	98	.226
				X	10	341	39	.114
				X	28	1108	79	.071
195	0754/0802	1.281	X		-4	772	83	.108
				X	0	627	47	.075
				X	-7	488	82	.168
				X	-10	429	84	.196
				X	-19	468	15	.032
				X	-17	1193	166	.139
196	0440/0448	.909	X		-20	517	92	.178
				X	1	592	57	.096
				X	-23	400	31	.078
				X	-13	410	93	.227
				X	-26	1601	251	.157
	0510/0518	1.090	X		-1	754	66	.088
				X	2	627	47	.075
				X	-22	1366	258	.189
338	0630/0648	1.259	X		-20	643	129	.201
				X	-17	437	16	.037
				X	-22	371	58	.156
				X	2	572	33	.058
				X	-13	1036	149	.144

The discussion of these results has been pursued primarily to point out the difficulty of using cross-correlations between Pc1 "carriers" to obtain estimates of phase wave parameters. Because of the inability to obtain a unique solution, the potential high precision of this method is severely compromised. This point is glossed over in all literature on Pc1 analysis procedures. The large variation in position of the phase correlation function peaks relative to the envelope or group correlation function maximum for various site pair combinations, as well as the large difference between group velocity and phase velocity estimates, indicate that dispersion may be quite significant.

6. SUMMARY OF RESULTS AND THEIR RELEVANCE TO NAVAL COMMUNICATIONS

Ducting

The results of the data analysis in the last section support the generally held contention that naturally occurring Pc1 hydromagnetic emissions are ducted in a waveguide mode at F_2-layer heights (≈ 350 km) in the ionosphere. The Pc1 emissions were seen with great regularity as far south as the Florida site, and good similarity in amplitude-time characteristics was preserved at all five sites during early morning hours. Also in agreement with other observations was our finding that the ability to obtain propagation was severely curtailed during daylight and early evening hours.

Analysis of propagation time delays between sites indicated that better agreement between data and propagation analysis method can be obtained if the method allows for curvature of the wave front toward the ionospheric secondary source region than can be obtained from a plane-wave method. When a method employing a circularly expanding wave front from the localized source region was used, it was found that the wave tended to arrive at the Florida site on paths with azimuths close to that of the geomagnetic meridian. Considering both this method, as well as the less internally consistent plane-wave method, the maximum deviations of the propagation path from the geomagnetic meridian were $31°$E and $33°$W for all data presented. Using the more internally consistent curved wave front method alone, maximum deviations of only $16°$E and $12°$W from the geomagnetic meridian were found.

Propagation Velocity

Group velocity determinations, unlike the direction-of-arrival determinations, were found to be relatively independent of the analysis methods used. Velocities observed ranged from 444 to 1523 km/s. The variation in propagation velocity from day to day is probably caused by variations in ionospheric F_2-layer plasma density as suggested by Manchester [6], although this likelihood could not be checked because of the lack of ionosonde data in appropriate geographical areas. Attempts to measure phase velocity and the difficulties involved in interpreting the results are discussed in Sec. 5.

46

Attenuation

Measurement of the attenuation constant for propagation over the five-station network during the early morning hours showed that the attenuation is highly variable from day to day and that the apparent attenuation is higher for ULF than it is for ELF. The values found were as high as 13 dB/1000 km but were more typically 6.5 dB/1000 km. Typical attenuation for ELF is 1 dB/1000 km. Our measured values of attenuation are somewhat higher than those indicated by the theoretical calculations by Greifinger and Greifinger [3] but are in relatively good agreement with the measurements by Bagnall [39].

Dispersion

No specific tests for dispersion were conducted. However, in a qualitative sense the envelope variations of the Pc1 emissions in the receiving system bandwidth of 0.39 to 2.1 Hz were quite similar to cursory visual inspection at all five sites, from New York to Florida and from Maryland to Illinois, when good ducting conditions prevailed. Correspondingly, visual comparison of the spectra at all five sites for all data shows no pronounced spectral differences as a function of latitude or longitude.

To obtain data among various site combinations of sufficient similarity to obtain cross-correlations with accuracies reliable to the order of tens to hundreds of milliseconds, required eliminating variant beating patterns characteristic of data with slightly different spectral characteristics. This was achieved by narrow-band filtering of all data with a Q of 20 to 50.

In the phase velocity study it was found that the positions of the relative maxima of the phase correlation peaks as a function of time lag in relation to the single envelope-correlation peak for cross-correlations between various pairs of sites were highly variable. Thus some dispersion did indeed occur and cast into uncertainty the reliability of phase velocity calculations.

Relevance

All the evidence of this research effort, as well as previous NRL efforts to stimulate hydromagnetic emissions in the Pc1 band, indicates that the ULF band cannot be considered an attractive alternative to the ELF band.

Previous NRL research showed that hydromagnetic emissions in the Pc1 band are not readily stimulated by methods such as artificial ionization releases in the 90- to 140-km altitude range, by ionospheric heating at E- and F-layer heights by powerful HF radars, or by VLF-ULF interaction methods using powerful naval VLF communications transmitters. Other novel and untried methods of hydromagnetic wave stimulation are certain to exist, but at present there is still no practical way to generate waves capable of transmitting information in the ULF frequency range. Furthermore, the trouble is far from over even if a successful method for generating ULF traveling waves is discovered. Transmission of the traveling wave from a naval installation to an itinerant fleet appears fraught with problems. Current theory and experimental observations indicate that the

only practical and efficient mechanism for long-range wave transport at ULF is by ionospheric ducting. However, the apparent attenuation rate for ducted ULF waves near 1 Hz appears much larger than that for ELF waves at 40 to 80 Hz. In addition, a communications system at ULF could not operate effectively with the prevalent variability in attenuation from day to day, the variability in propagation speed, and the directional preference of propagation along the geomagnetic meridian. Dispersion would probably further reduce the already small information rate achievable at ULF frequencies. Attempts to use the ionospheric duct for communications during periods when ducting conditions are favorable will have to contend with interference caused by the natural background. One of the greatest single drawbacks to the ULF ducting mechanisms is its apparent complete failure during daylight conditions over the propagation path. A communications system attempting to radiate ULF energy during the summer season through latitudes higher than 70 degrees via the ionospheric duct would most likely experience nearly complete loss of signal at all times of day because of continual sunlight at those high latitudes and altitudes characteristic of the duct.

ACKNOWLEDGMENTS

REFERENCES

1. J. Galejs, *Terrestrial Propagation of Long Electromagnetic Waves*, Pergamon Press, Oxford, 1972.

2. C. Greifinger and P. S. Greifinger, "Theory of Hydromagnetic Propagation in the Ionospheric Waveguide," *J. Geophys. Res.* 73, 7473 (1968).

3. C. Greifinger, and P. S. Greifinger, "Wave Guide Propagation of Micropulsations out of the Plane of the Geomagnetic Meridian," *J. Geophys. Res.* 78, 4611 (1973).

4. R. N. Manchester, "Propagation of Pc1 Micropulsations from High to Low Latitudes." *J. Geophys. Res.* 71, 3749 (1966).

5. L. Tepley and R. K. Landshoff, "Waveguide Theory for Ionospheric Propagation of Hydromagnetic Emissions," *J. Geophys. Res.* 71, 1499 (1966).

6. R. N. Manchester, "Correction of Pc1 Micropulsations at Spaced Stations," *J. Geophys. Res.* **73**, 3549 (1968).

7. J. R. Davis, J. W. Willis, and E. L. Althouse, "Magic Mode: Investigations of Artificial Stimulation of ULF Waves in the Ionosphere and Magnetosphere," NRL Report 7552 (AD 759012), Mar. 12, 1973.

8. J. W. Willis and J. R. Davis, "Investigation of the Stimulation of ULF Waves," NRL Report 7925 (AD A 018245), Nov. 13, 1975.

9. A. C. Fraser-Smith and C. A. Cole, Jr., "Initial Observations of the Artificial Stimulation of ULF Pulsations by Pulsed VLF Transmissions," *Geophys. Res. Lett.* **2**, 146 (1975).

10. J. A. Jacobs, *Geomagnetic Micropulsations*, Springer-Verlag, New York, 1970.

11. D. R. Criswell, "Pc1 Micropulsation Activity and Magnetospheric Amplification of 0.2 to 5.0 Hz Hydromagnetic Waves." *J. Geophys. Res.* **74**, 205 (1969)

12. W. A. Campbell, "Geomagnetic Pulsations," in *Physics of Geomagnetic Phenomena*, p. 822-909, Academic Press, New York, 1967.

13. V. A. Troitskaya and A. V. Gul'elmi, "Geomagnetic Micropulsations and Diagnostics of the Magnetosphere," *Space Sci. Rev.* **7**, 689 (1967).

14. T. Watanabe, "Quasi-Linear Theory of Transverse Plasma Instabilities with Applications to Hydromagnetic Emissions from the Magnetosphere," *Can. J. Phys.* **44**, 815 (1966).

15. A. J. Dessler, "The Propagation Velocity of World Wide Sudden Commencements of Magnetic Storms." *J. Geophys. Res.* **63**, 405 (1958).

16. M. Kawamura, "Short-period Geomagnetic Micropulsations with Period of About 1 Second in the Middle and Low Latitudes," *Geophys. Mag.* **35**, 1 (1970).

17. R. C. Wentworth, L. Tepley, K. D. Amundsen and R. R. Heacock, "Intra- and Interhemisphere Differences in Occurrence Times of Hydromagnetic Emissions," *J. Geophys. Res.* **71**, 1492 (1966).

18. W. H. Campbell and T. C. Thornberry, "Propagation of Pc1 Hydromagnetic Waves Across North America," *J. Geophys. Res.* **77**, 1941 (1972).

19. B. J. Fraser, "Ionospheric Duct Propagation and Pc1 Pulsation Sources," *J. Geophys. Res.* **80**, 2790 (1975).

20. C. Altman and E. Fijalkow, "Mechanism of Transmission of Hydromagnetic Waves Through the Earth's Lower Ionosphere," *Nature* **220**, 53 (1968).

21. C. Altman and E. Fijalkow, "The Transmission of Electromagnetic Waves Through the Ionosphere at Micropulsation Frequencies," *Alta Freq.* **38**, 183 (1969).

22. P. Greifinger, "Ionospheric Propagation of Oblique Hydromagnetic Plane Waves at Micropulsation Frequencies," *J. Geophys. Res.* **77**, 2377 (1972).

23. P. Greifinger, "Micropulsations form a Finite Source," *J. Geophys. Res.* **77**, 2392 (1972).

24. L. N. Baranskiy, "Some Characteristics of the Polarization of Pc1 Pulsations Associated with their Waveguide Propagation," *Geomagn. Aeronomy*, **10**, 86 (1970).

25. V. B. Lyatskiy and V. P. Selivanov, "Time Variation of the Vector of Preferred PP Polarization According to Observations at Lovozero," *Geomagn. Aeronomy* **6**, 126 (1966).

26. J. H. Pope, "An Explanation for the Apparent Polarization of Some Geomagnetic Micropulsations (Pearls)," *J. Geophys. Res.* **69**, 399 (1964).

27. V. A. Troitskaya, L. N. Baranskiy, P. A. Vinogradov, A. V. Sobolev and S. I. Solov'yev, "Some Properties of the Earth's Electromagnetic Field Oscillations of the Pc1 Type Observed Simultaneously Over a Wide Area," *Geomagn. Aeronomy*, **8**, 579 (1968).

28. W. R. Summers and B. J. Fraser, "Polarization Properties of Pc1 Micropulsations at Low Latitudes," *Planet. Space Sci.* **20**, 1323 (1972).

29. W. R. Summers, "Production Mechanisms for the Observed Behaviour of the Low Latitude Pc1 Polarization Ellipse," *Planet. Space Sci.* **22**, 801 (1974).

30. L. Tepley, "Low-Latitude Observations of Fine-Structured Hydromagnetic Emission," *J. Geophys. Res.* **69**, 2273 (1964).

31. H. W. Smith, "Some Observations and Characteristics of Type Pc1 Geomagnetic Micropulsations," *J. Geophys. Res.* **69**, 1875 (1964).

32. B. J. Fraser and W. R. Summers, "Simultaneous Observations of Pc1 Micropulsation Polarization at Four Low Latitude Sites," *Ann. Geophys.* **28**, 697 (1972).

33. E. G. Stassinopoulos, "World Maps of Constant B. L. and Flux Contours," NASA Publ. SP-3054, Washington, D.C., page 114, 1970.

34. W. H. Campbell, "Induction Loop Antennas for Geomagnetic Field Variation Measurements," ESSA Technical Report ERL 123-ESL6, U.S. Department of Commerce, Boulder, Colo. page 30, 1969.

35. "Transmission Specifications for Voice Grade Private Line Data Channels," Bell System Tech. Ref. Publ. 41004, 1969.

36. S. Akasofu and S. Chapman, *Solar-Terrestrial Physics*, Oxford University Press, New York, page 553, 1972.

37. C. O. Hines, I. Paghis, T. R. Hartz, and J. A. Fejer, eds., *Physics of the Earth's Upper Atmosphere*, p. 17, Prentice-Hall, Englewood Cliffs, N.J., 1965.

38. *Tables of Sunrise, Sunset, and Twilight* (Nautical Almanac Office, U.S. Naval Observatory), U. S. Government Printing Office, Washington, D.C., 1945

39. F. T. Bagnall, "A Contribution to Pc1 Propagation Concepts," Ph.D. Thesis, Univ. of Newcastle, Newcastle, Australia, 1971.

Appendix A

DATA SPECTRAL CHARACTERISTICS

51
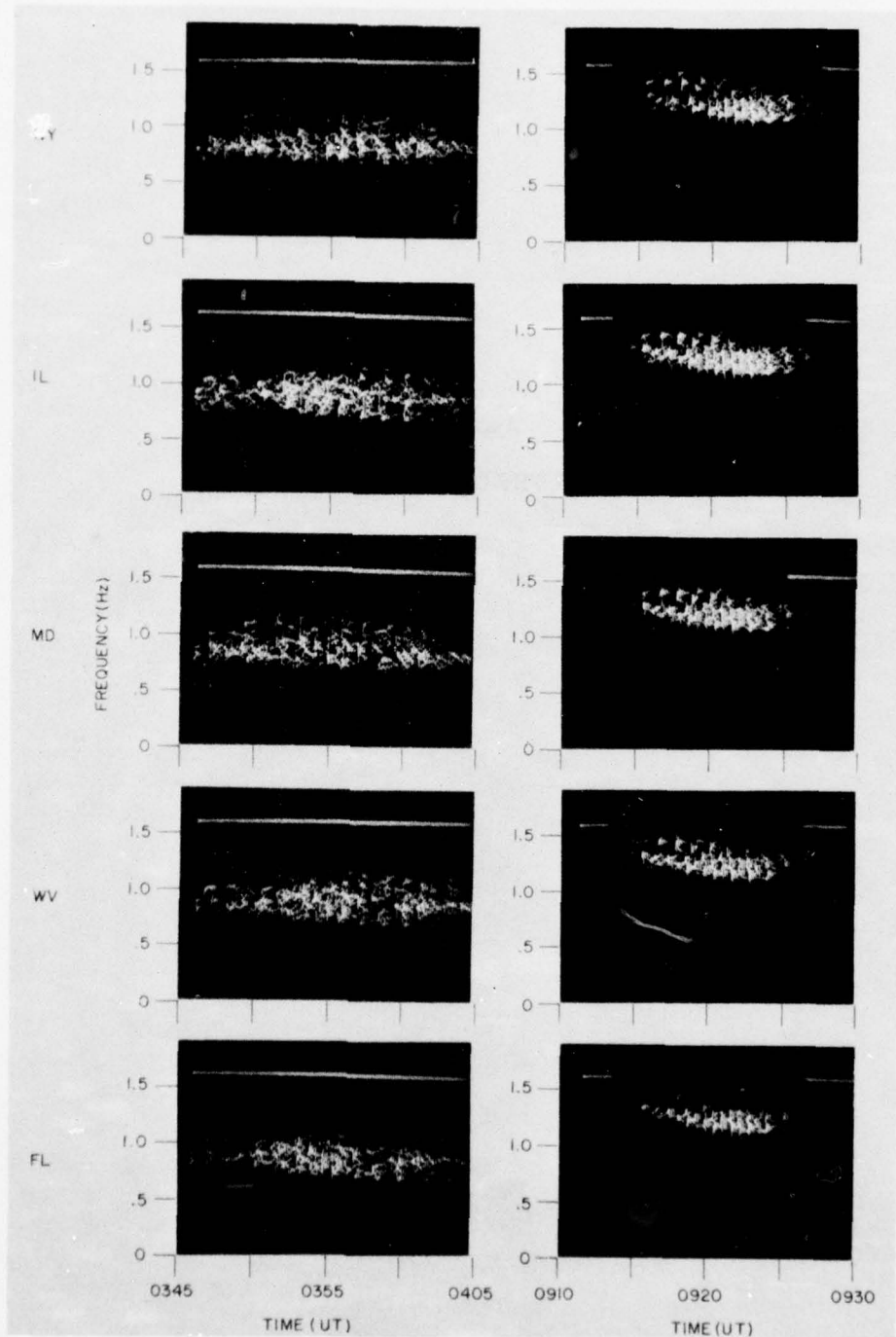
Fig. A1—Julian day 105

52
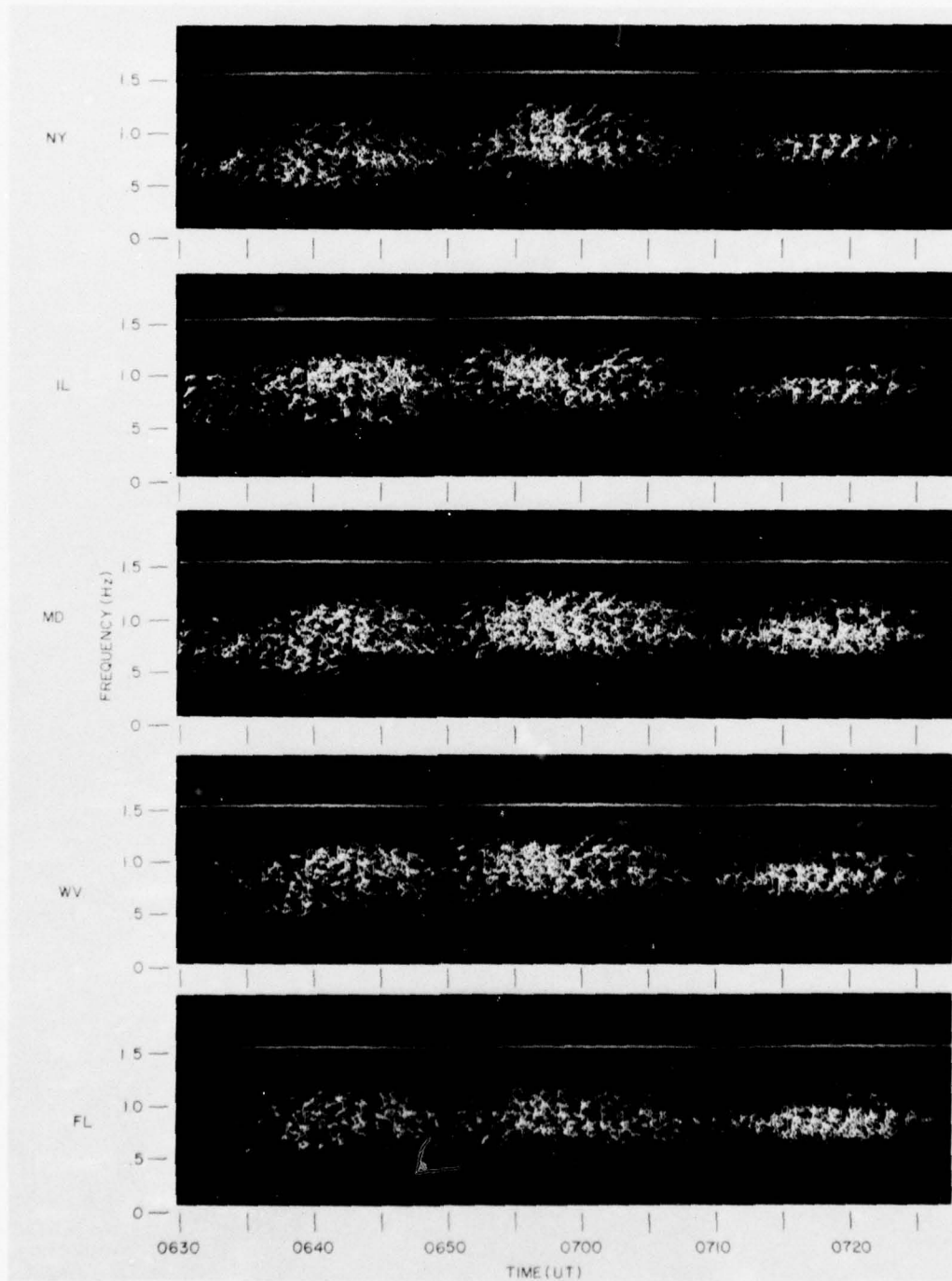
Fig. A2—Julian day 106

Fig. A3—Julian day 119

54
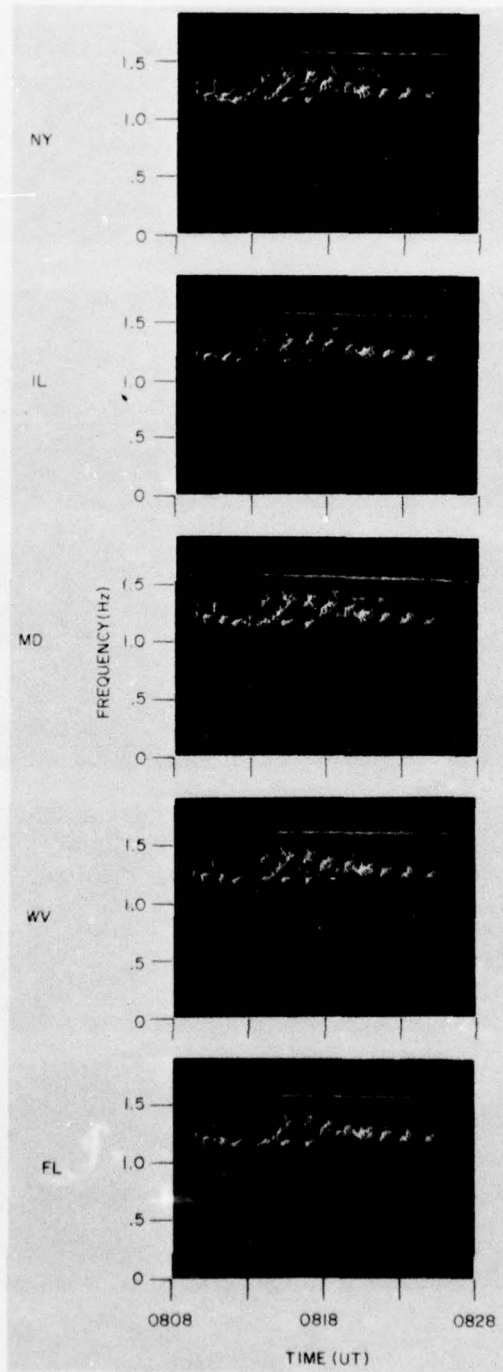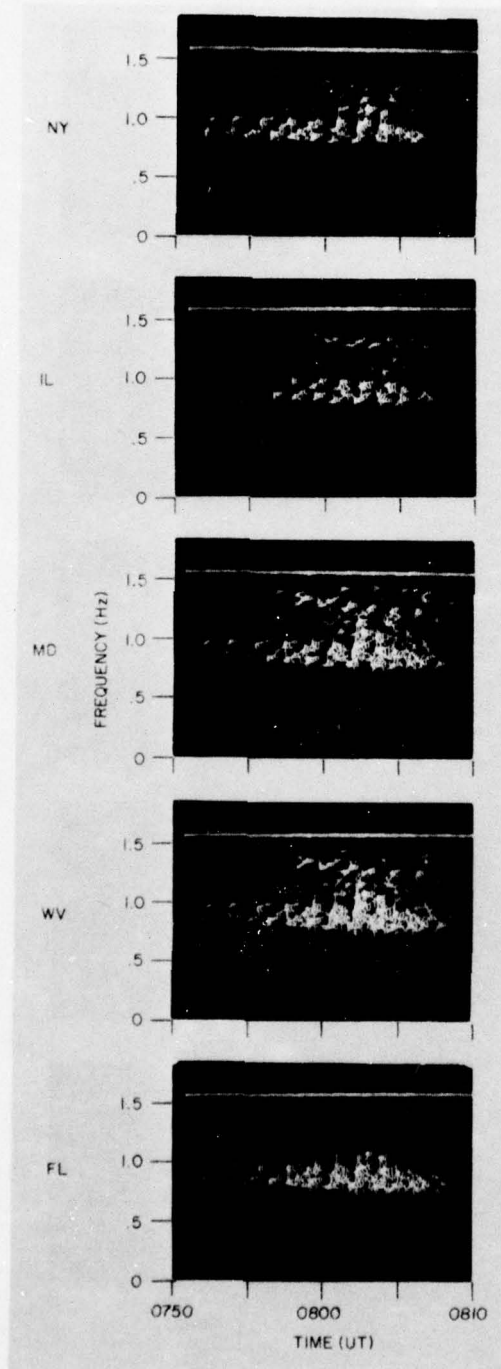
Fig. A4—Julian day 122
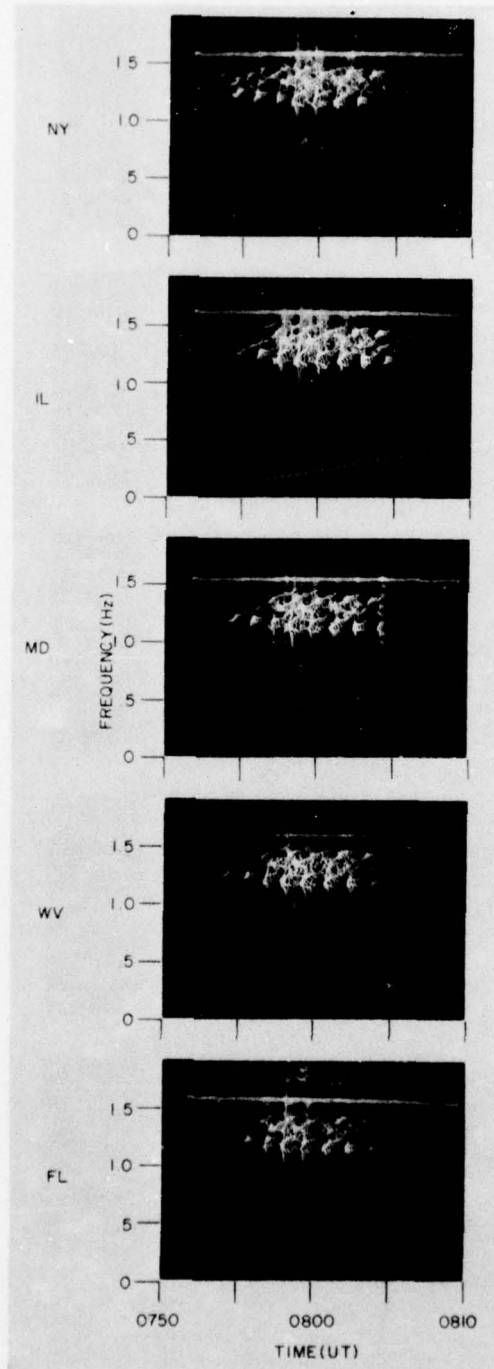
Fig. A5—Julian day 195

56
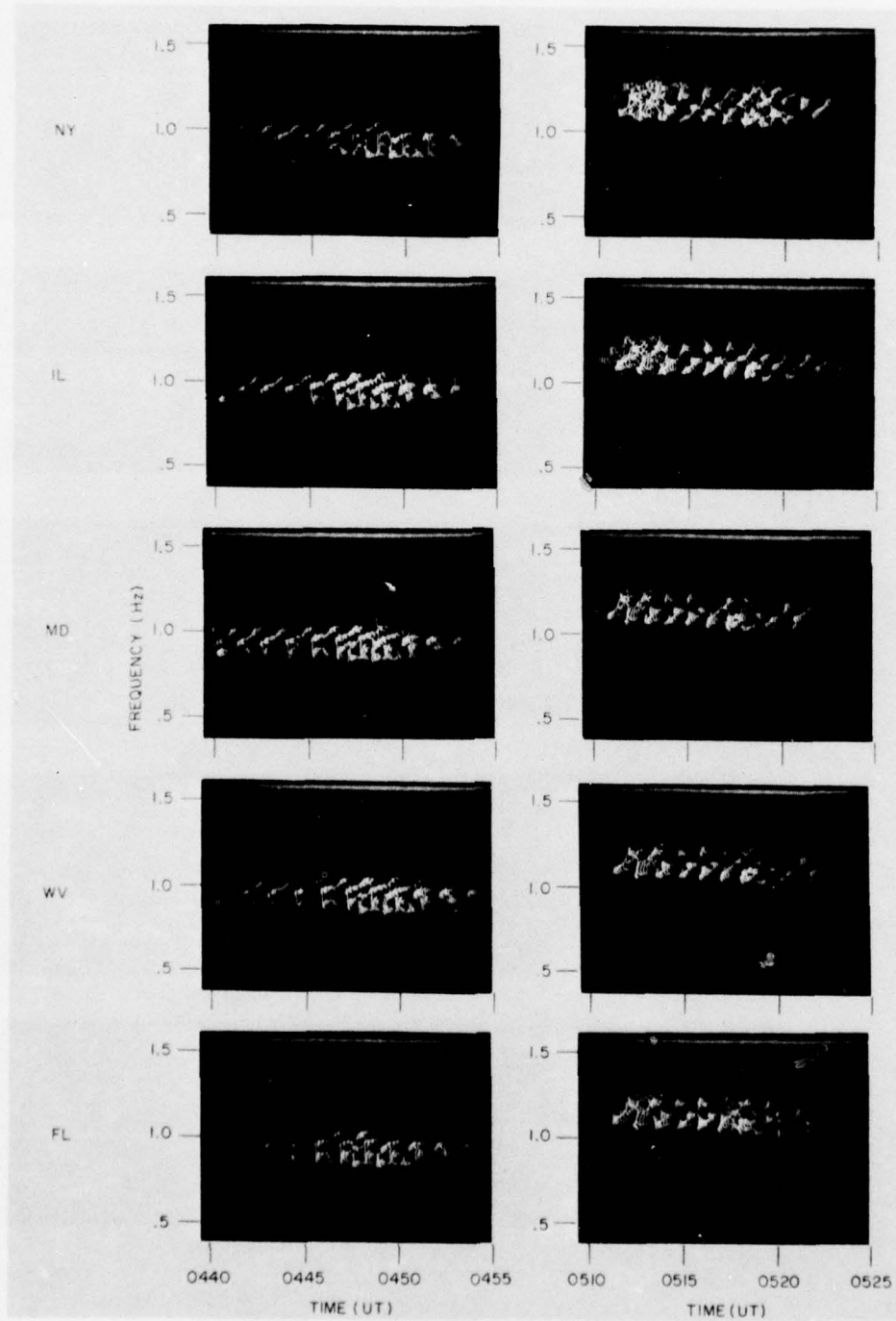
Fig. A6—Julian day 196
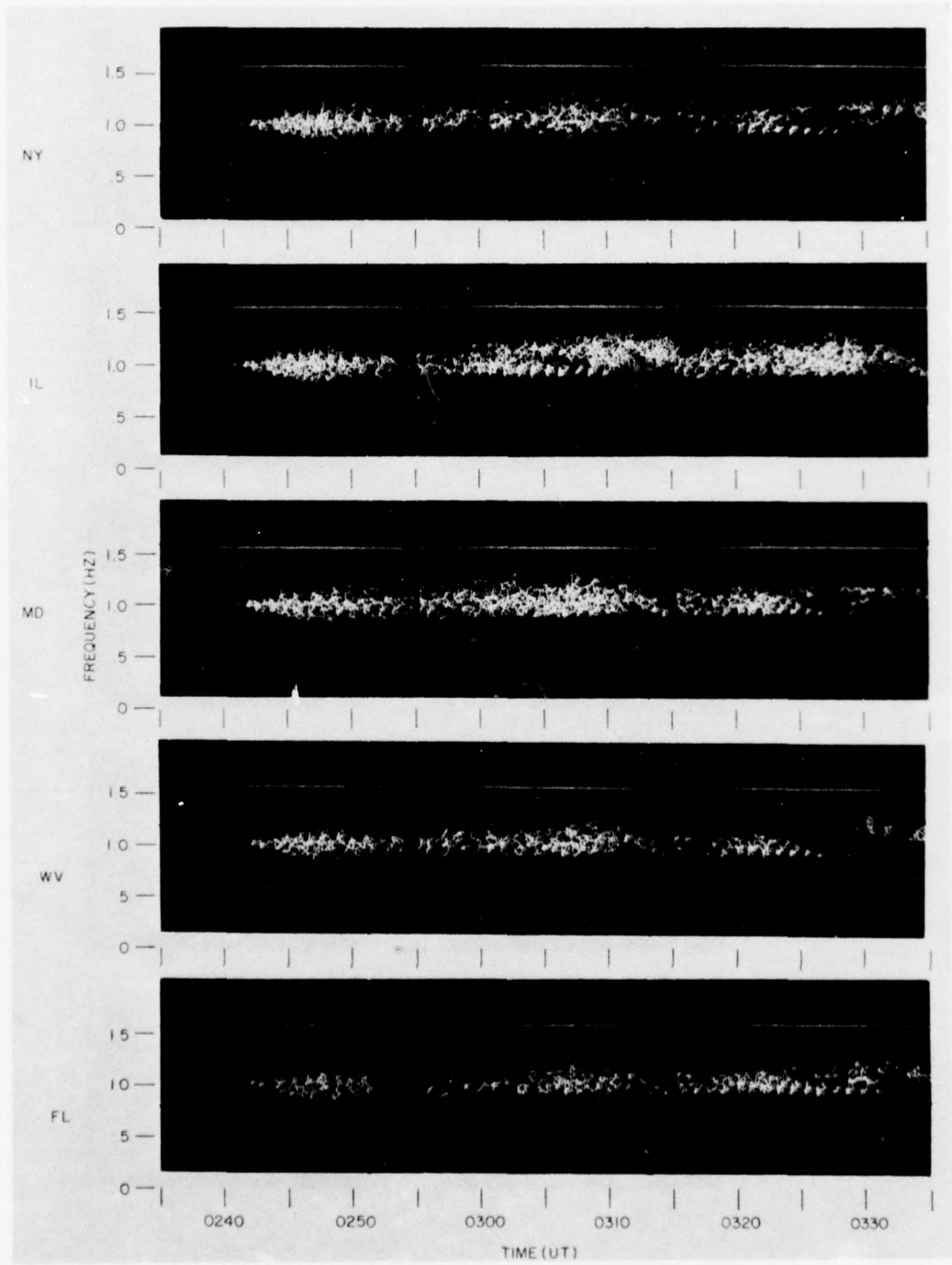
Fig. A7—Julian day 338
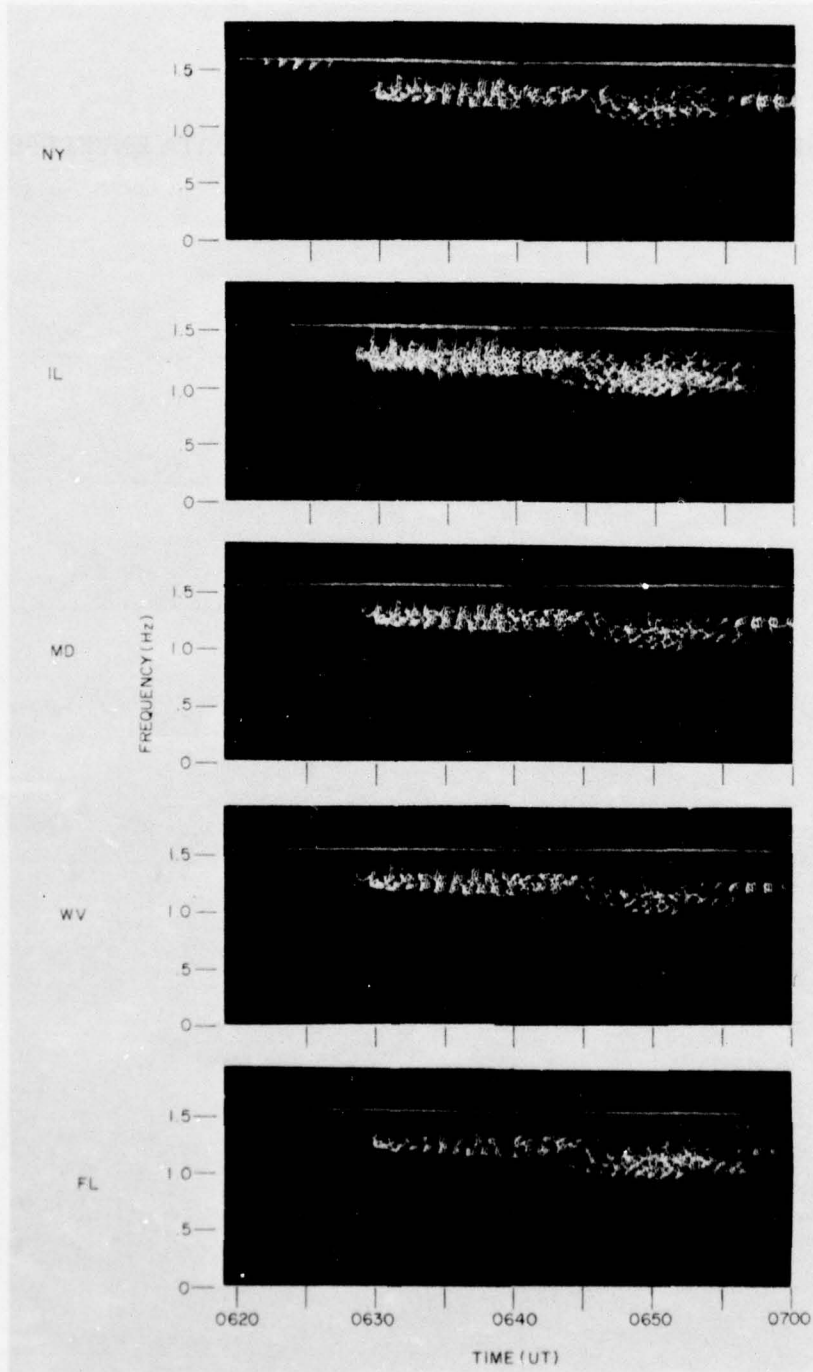
Fig. A8—Julian day 338

Appendix B

AMPLITUDE-TIME CHARACTERISTICS OF THE DATA ENVELOPE
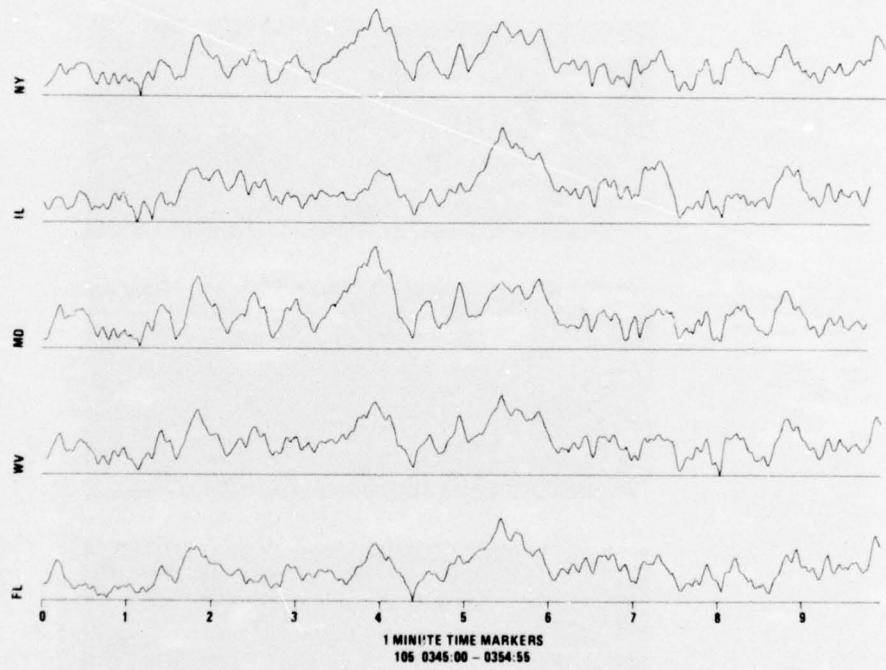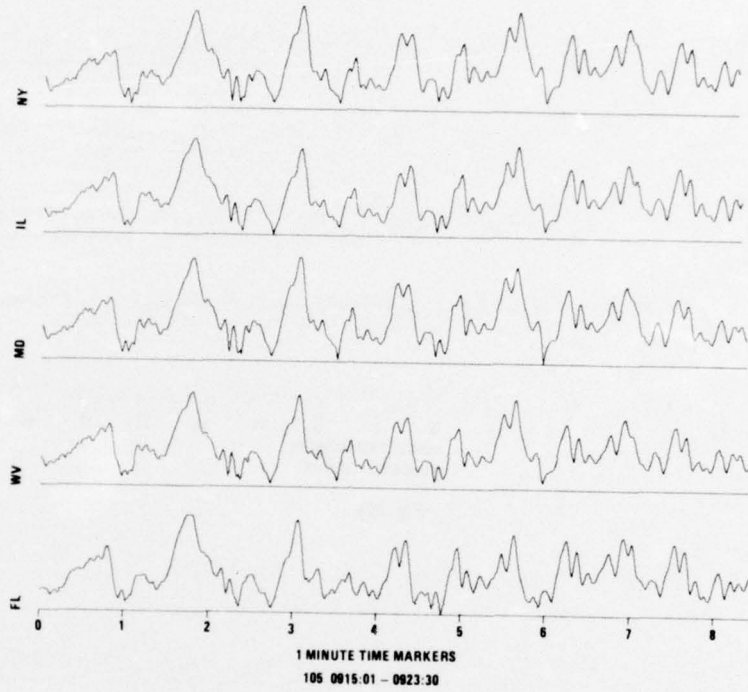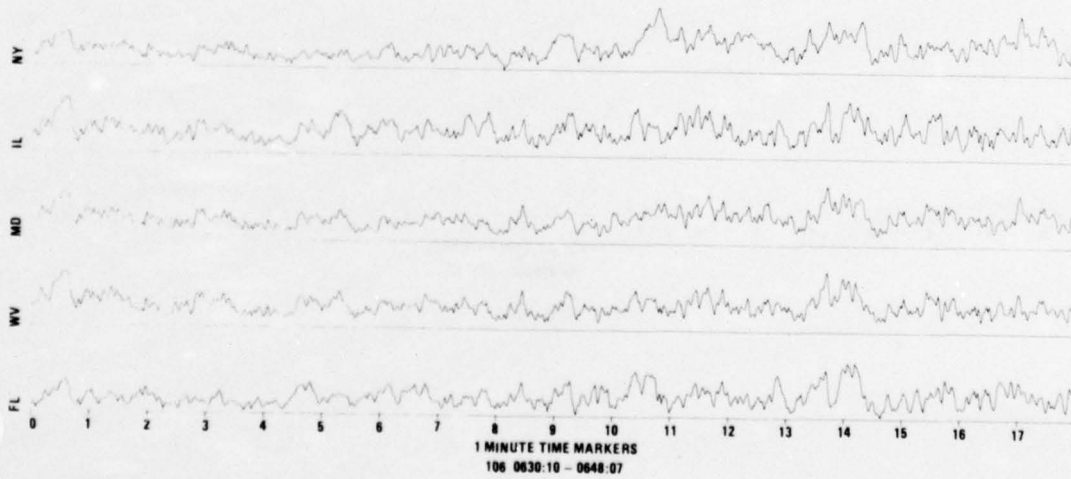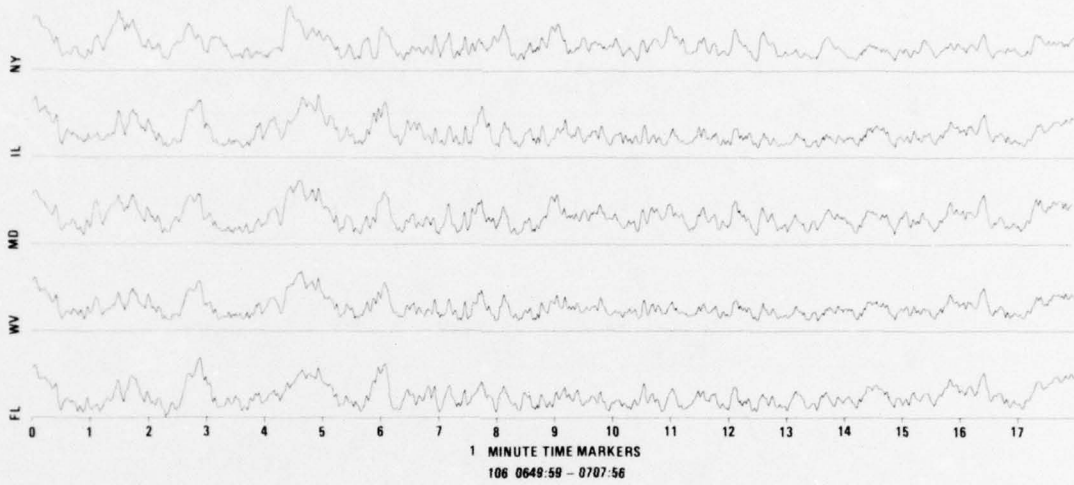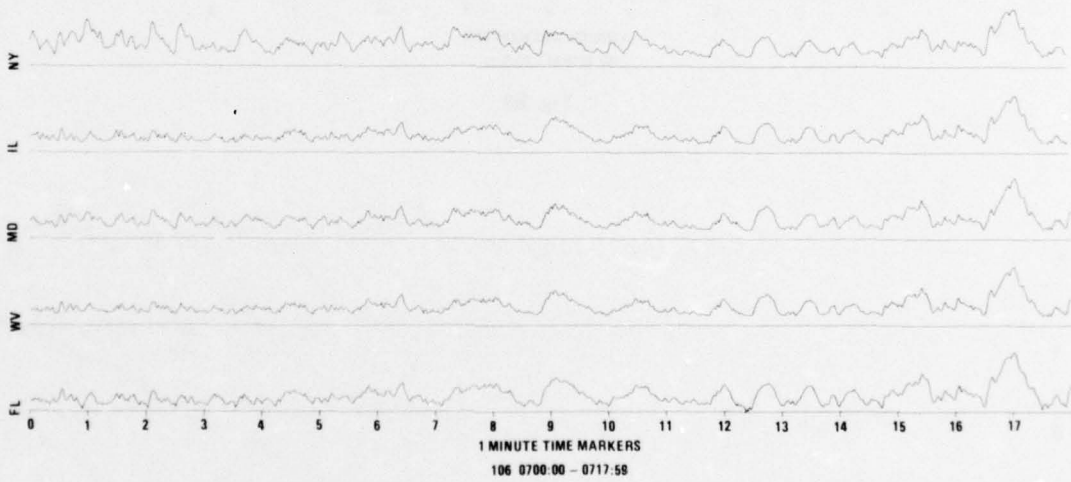
1 MINUTE TIME MARKERS
106 0345:00 — 0354:55

Fig. B1

1 MINUTE TIME MARKERS
105 0915:01 — 0923:30

Fig. B2

1 MINUTE TIME MARKERS
106 0630:10 — 0648:07

Fig. B3

1 MINUTE TIME MARKERS
106 0649:59 – 0707:56

Fig. B4

1 MINUTE TIME MARKERS
106 0700:00 – 0717:59

Fig. B5

1 MINUTE TIME MARKERS
106 0709:55 – 0727:50

Fig. B6

1 MINUTE TIME MARKERS
119 0807:50 – 0826:00

Fig. B7

1 MINUTE TIME MARKERS
122 0756:57 – 0805:55

Fig. B8

1 MINUTE TIME MARKERS
195 0753:57 – 0803:54

Fig. B9

1 MINUTE TIME MARKERS
196 0440:01 – 0448:57

Fig. B10

1 MINUTE TIME MARKERS
196 0509:54 – 0518:47

Fig. B11

65

Fig. B12

Fig. B13

66

1 MINUTE TIME MARKERS
338 0250:54 – 0317:42

Fig. B14

1 MINUTE TIME MARKERS
338 0314:54 – 0332:50

Fig. B15

1 MINUTE TIME MARKERS
330 0020:47 – 0030:19

Fig. B16

68
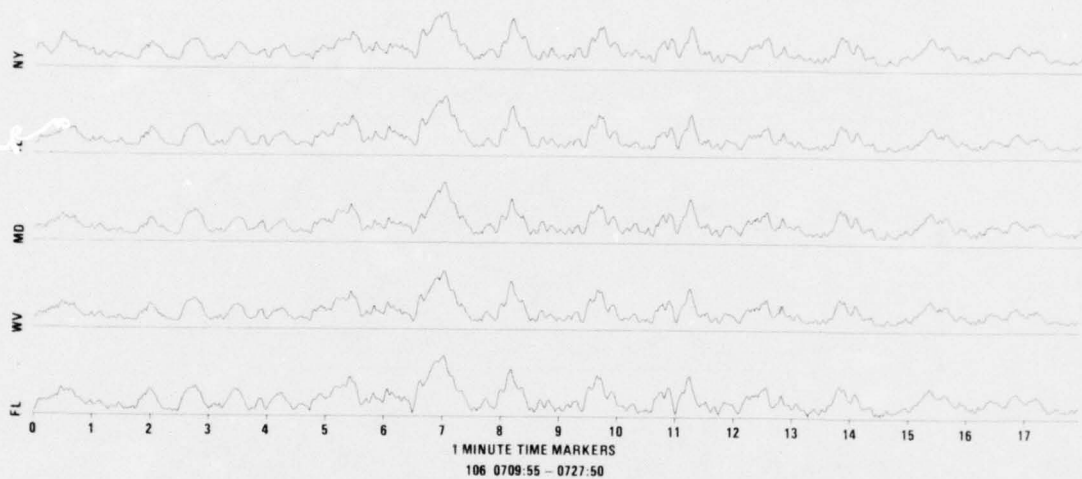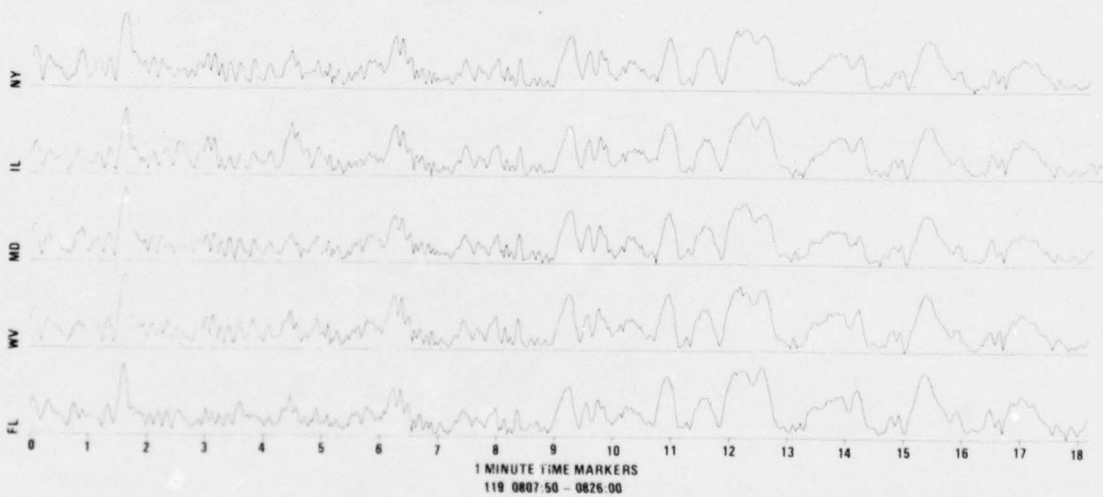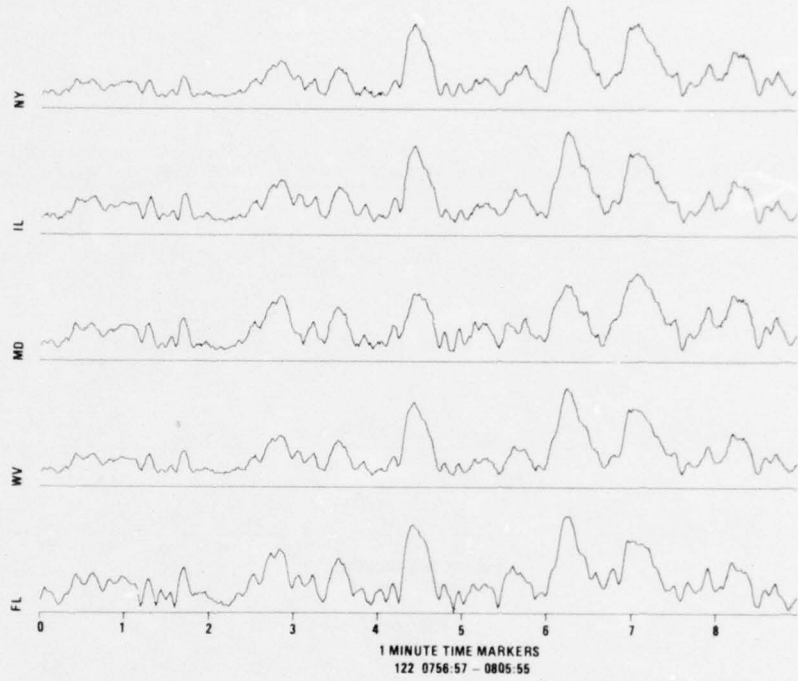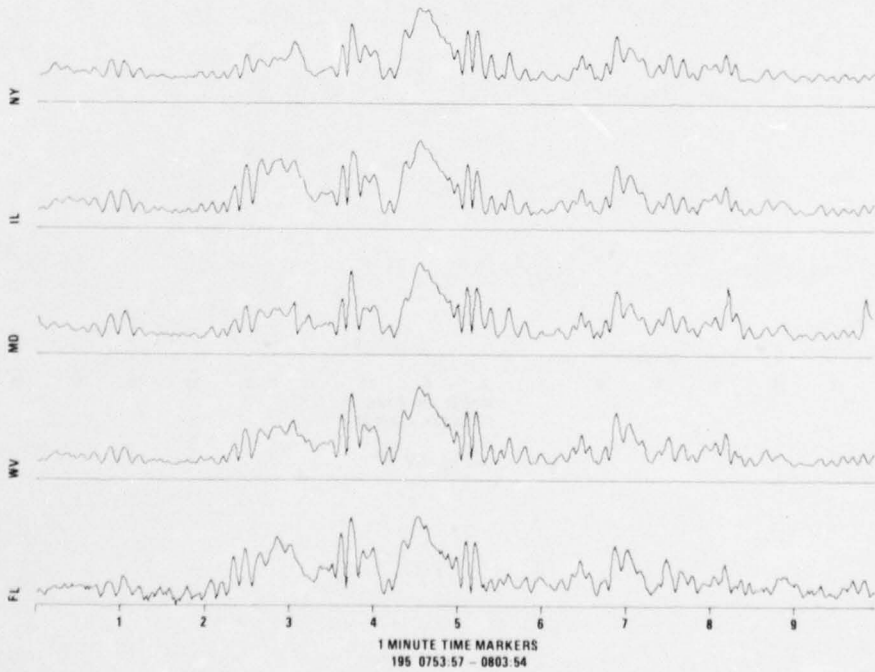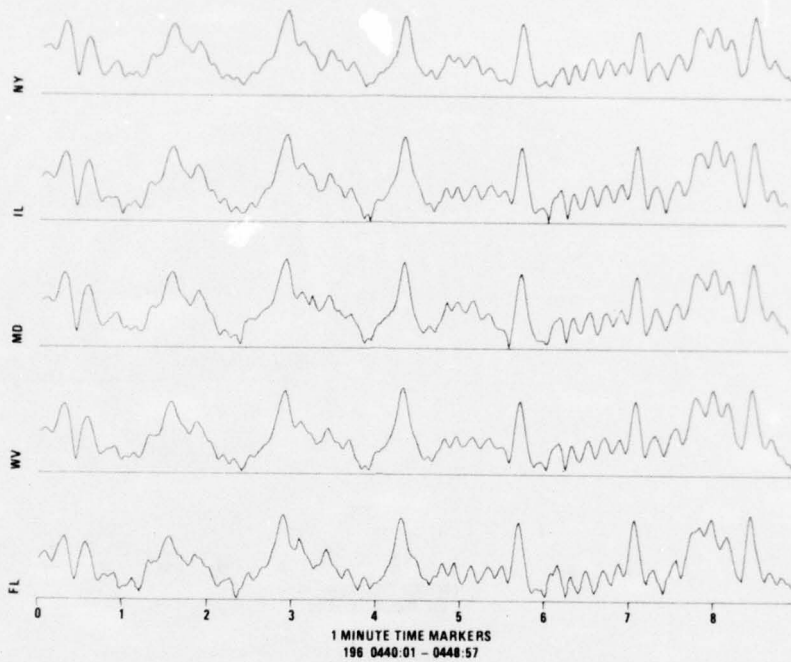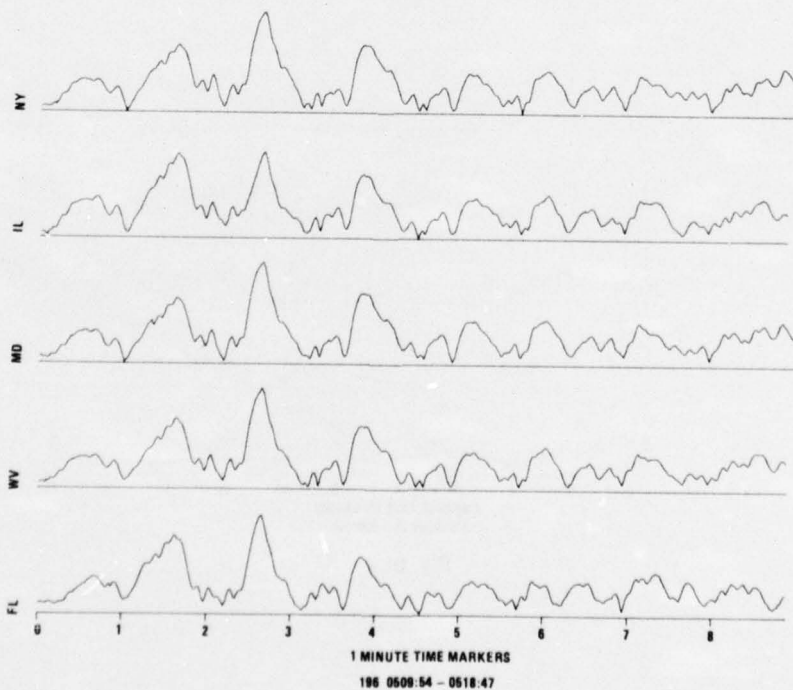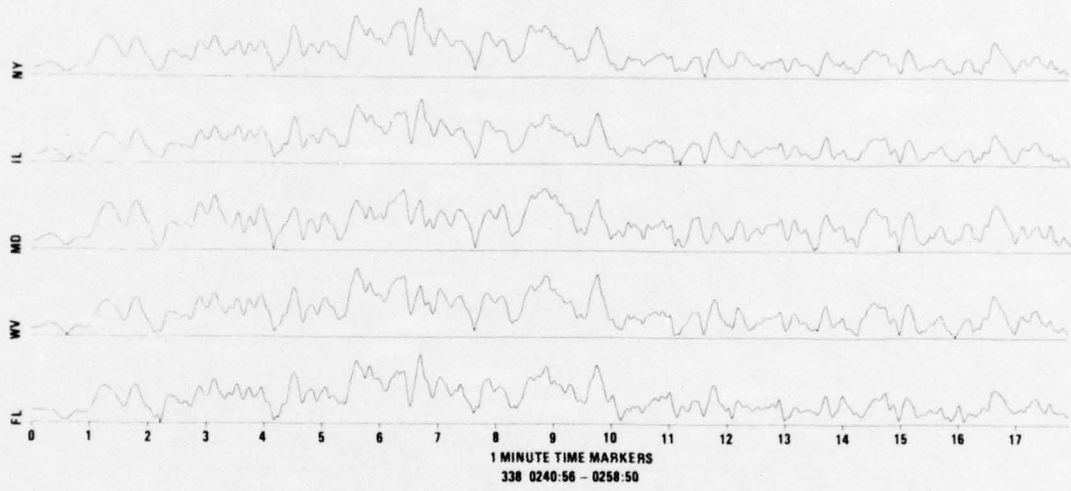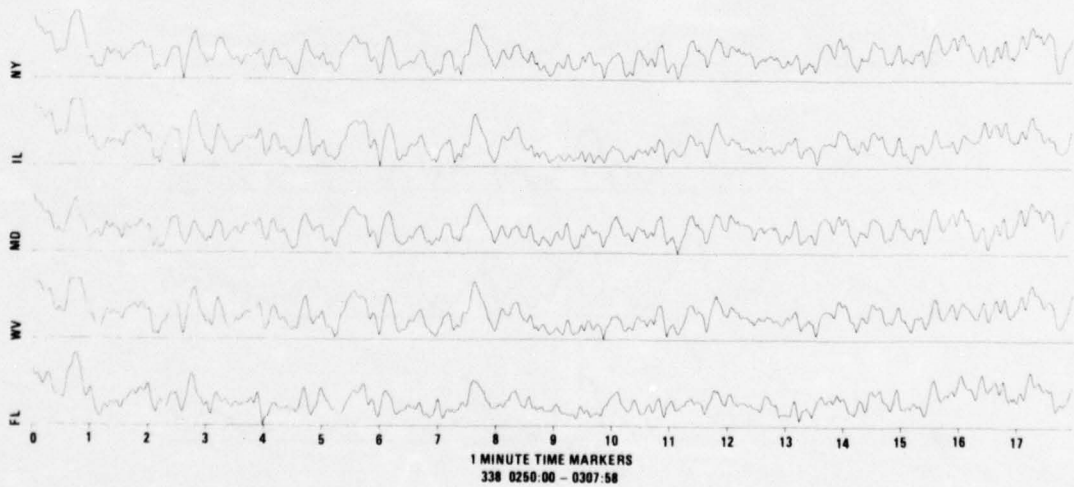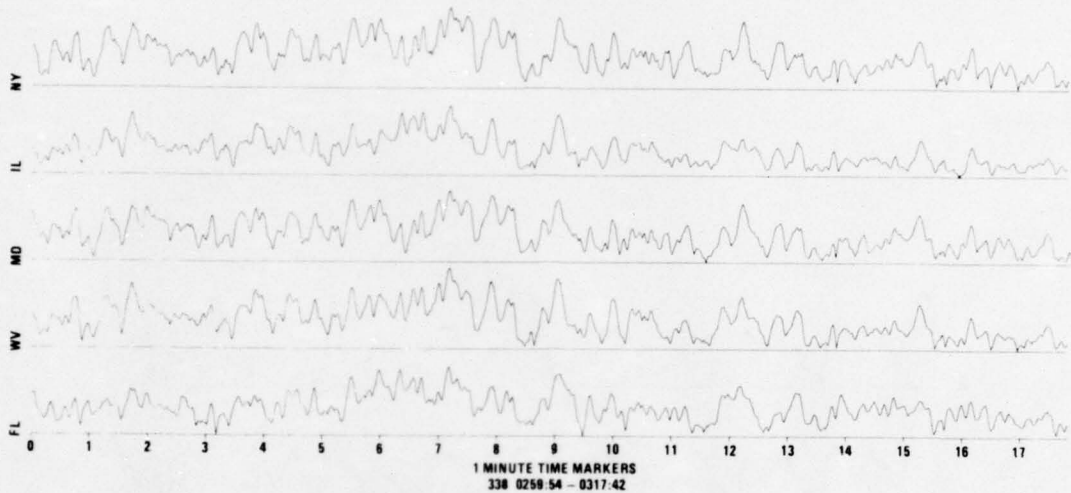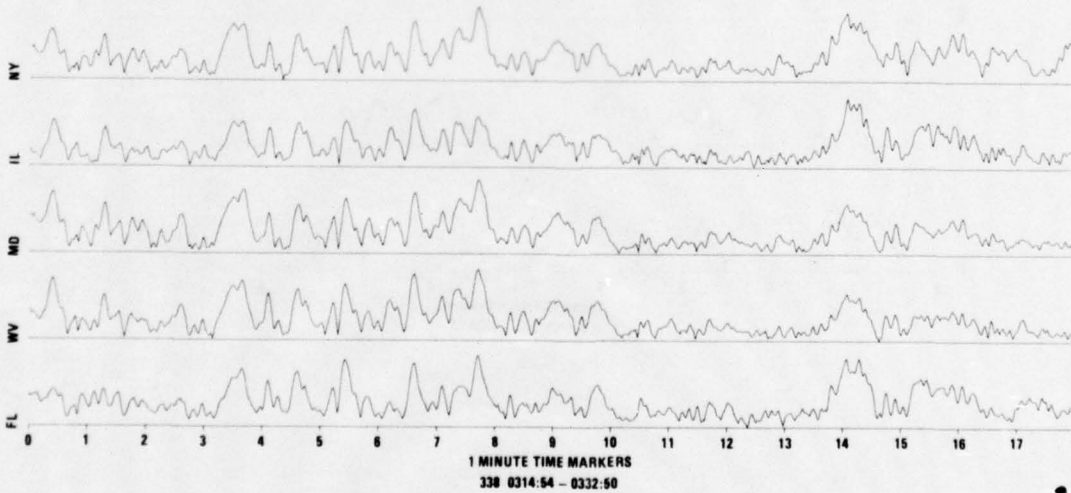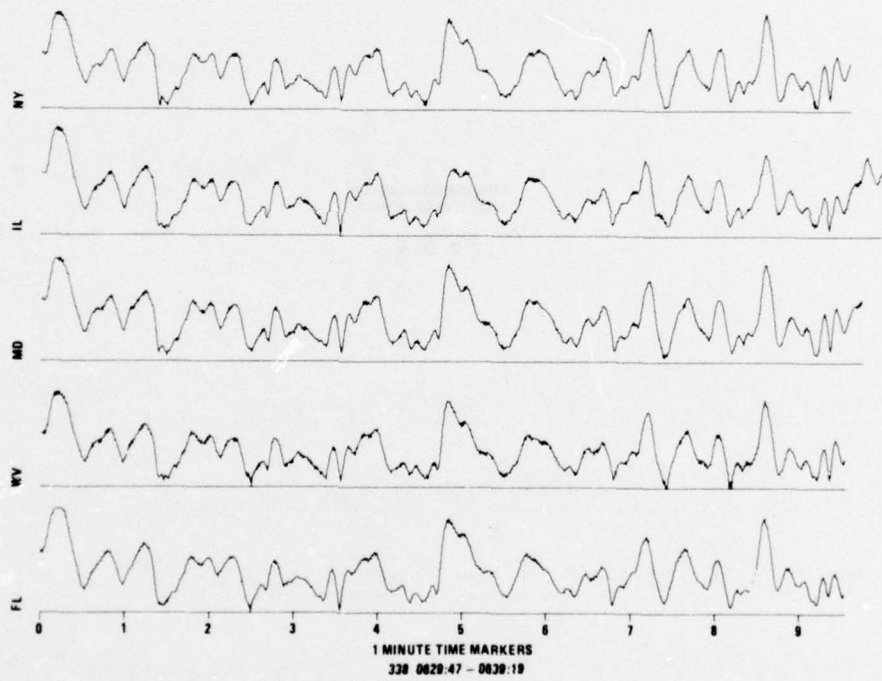
Appendix C

POLARIZATION CHARACTERISTICS OF THE DATA

The polarization ellipses were obtained by plotting the north-south data component on the ordinate direction against the east-west data component on the abscissa direction. Both components were band-pass filtered at a Q of 50 and at a center frequency indicated in Table 2. The filters were carefully adjusted to equalize phase shift characteristics. The polarizations are plotted in a time sequence from left to right. Each ellipse represents exactly 5 s of data, and the start of each new ellipse is exactly 1 min displaced from the start of the former one.
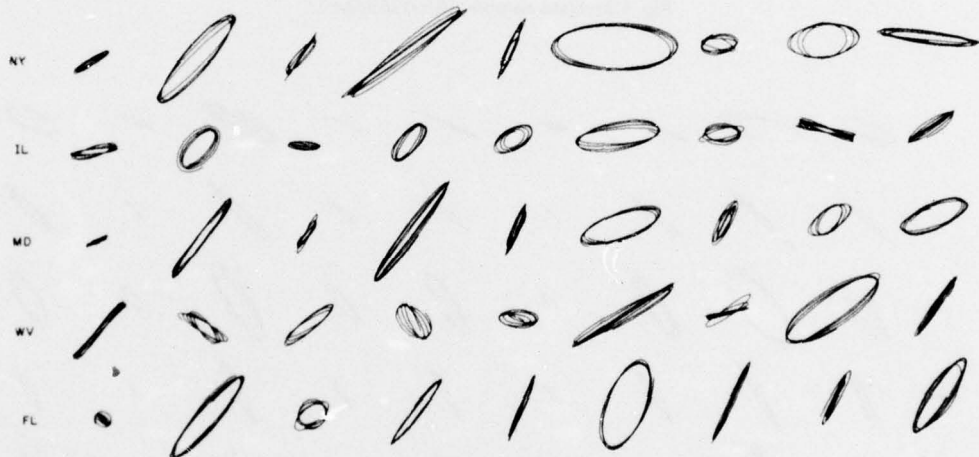
Fig. C1—Data sample 105 0346/0354

69
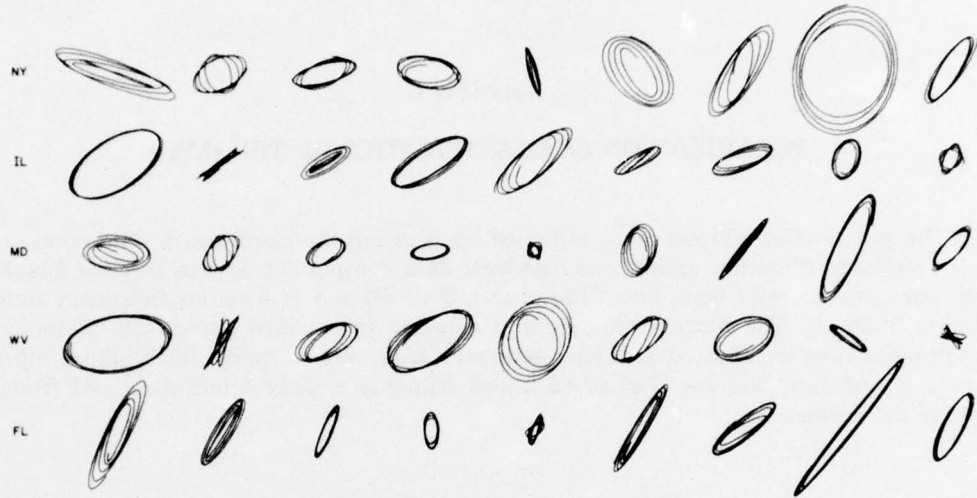
Fig. C2—Data sample 105 0355/0403
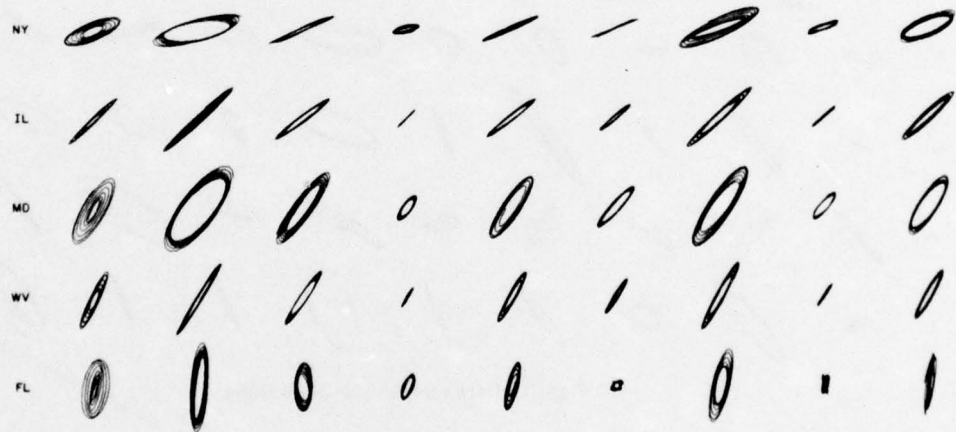
Fig. C3—Data sample 105 0916/0924

70
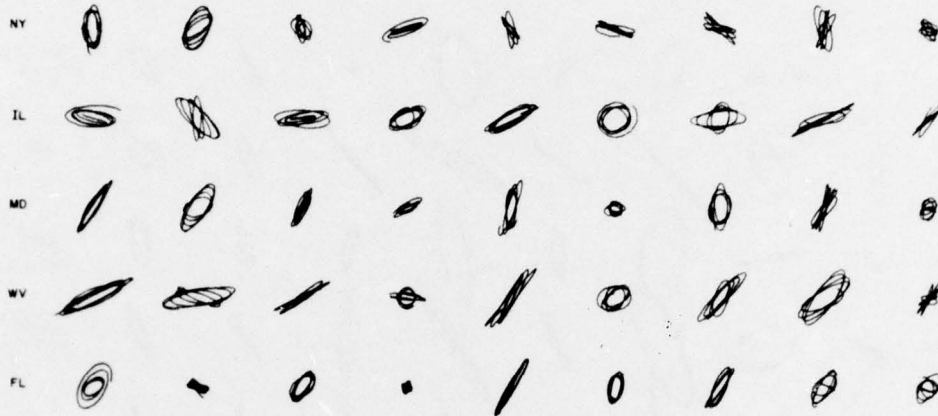
Fig. C4—Data sample 106 0631/0639
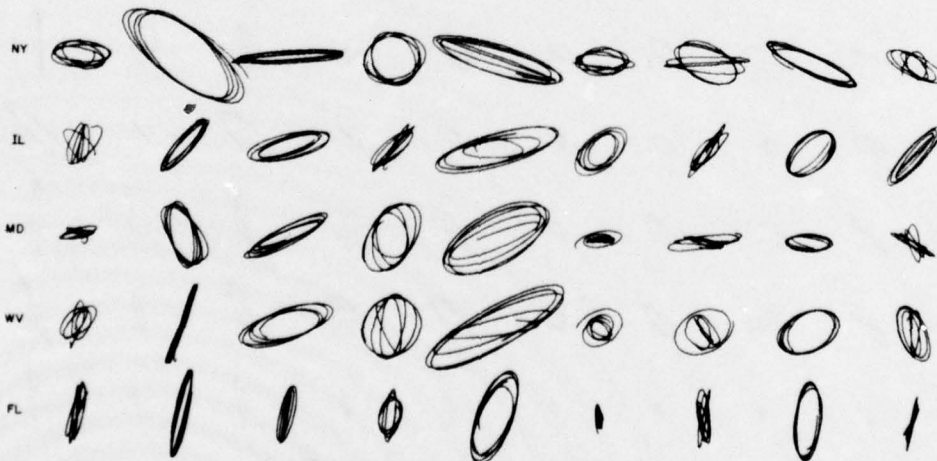
Fig. C5—Data sample 106 0640/0648
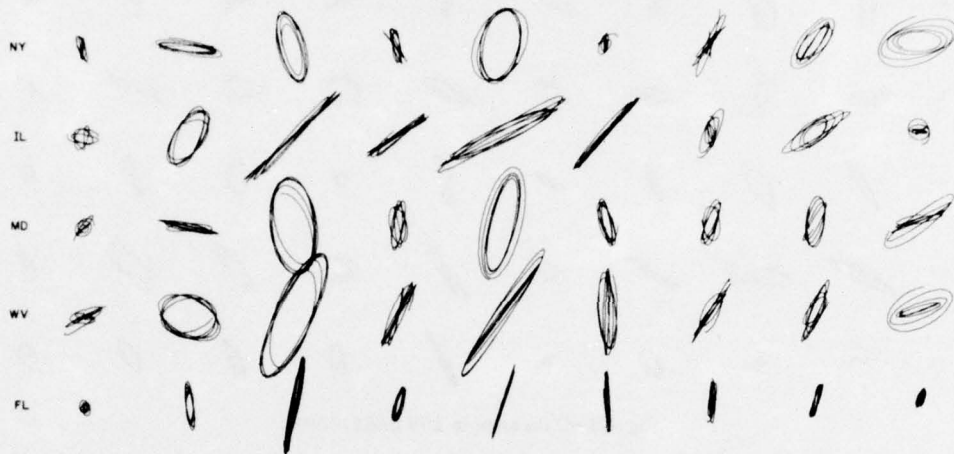
Fig. C6—Data sample 106 0651/0659
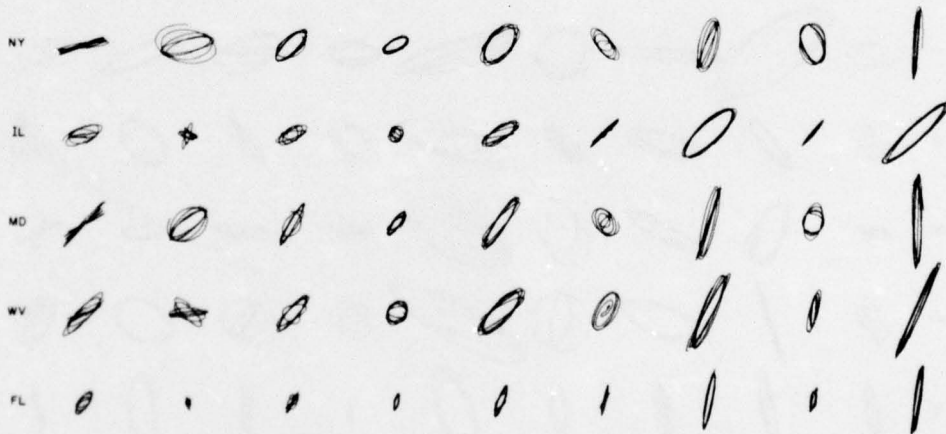
Fig. C7—Data sample 106 0700/0708
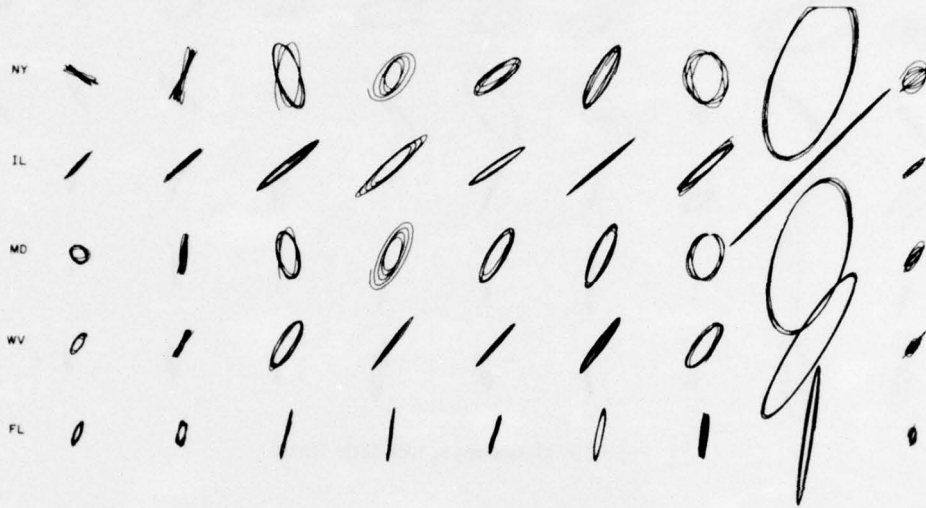
Fig. C8—Data sample 106 0710/0718
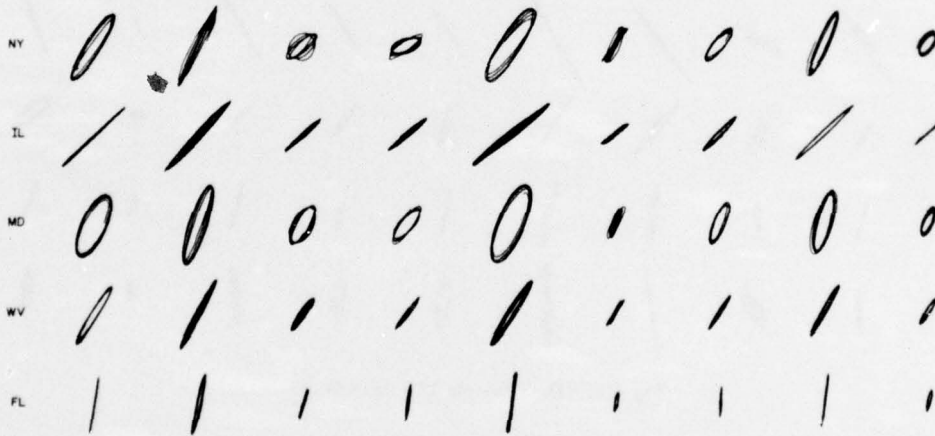
Fig. C9—Data sample 106 0720/0728

Fig. C10—Data sample 119 0809/0818
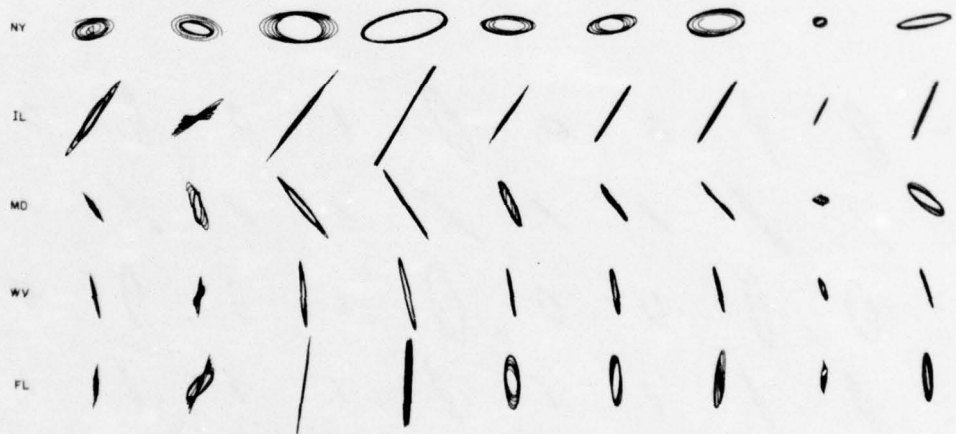
Fig. C11—Data sample 119 0819/0827
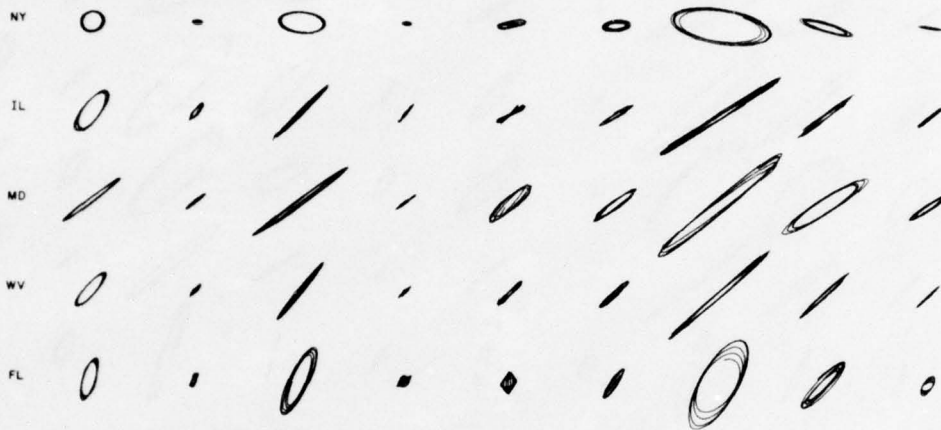
Fig. C12—Data sample 122 0800/0808
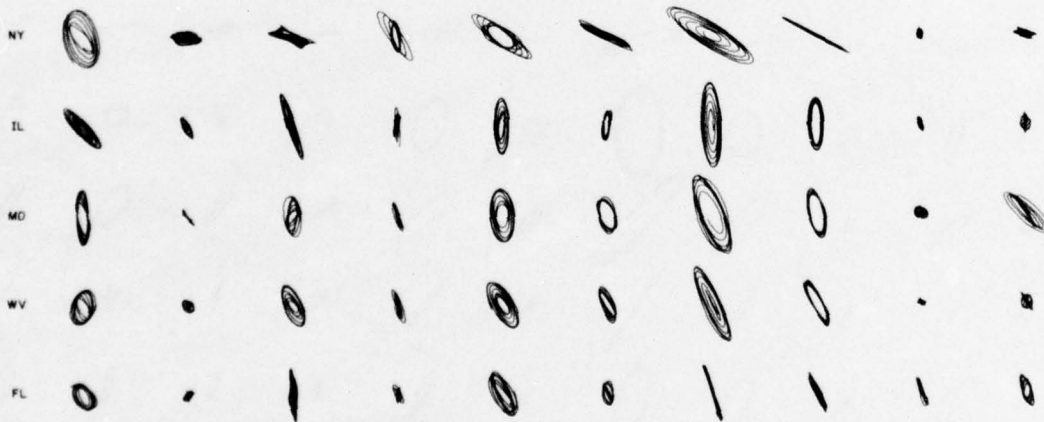
Fig. C13—Data sample 195 0755/0804
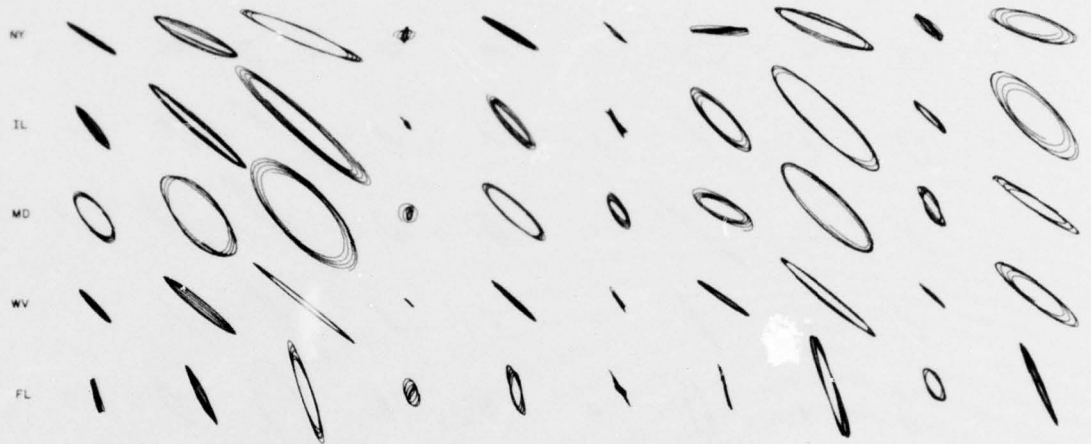
Fig. C14—Data sample 196 0441/0450
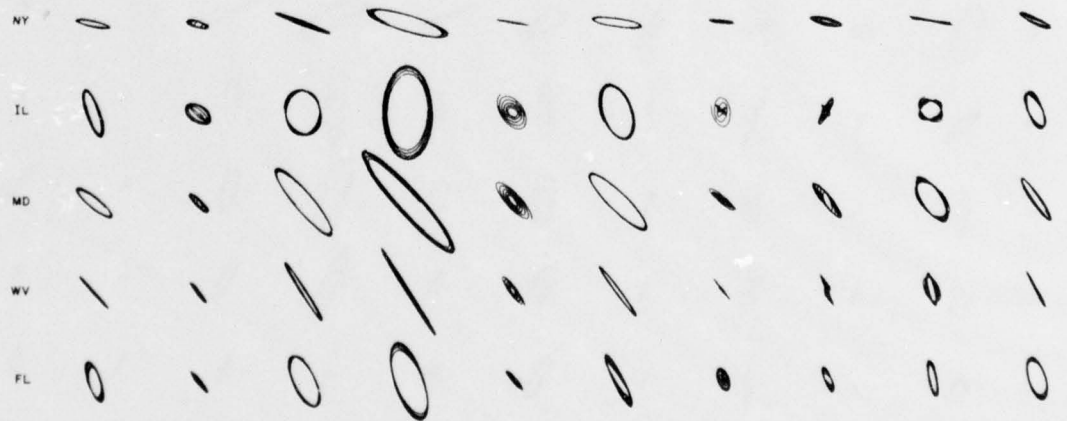
Fig. C15—Data sample 196 0511/0520
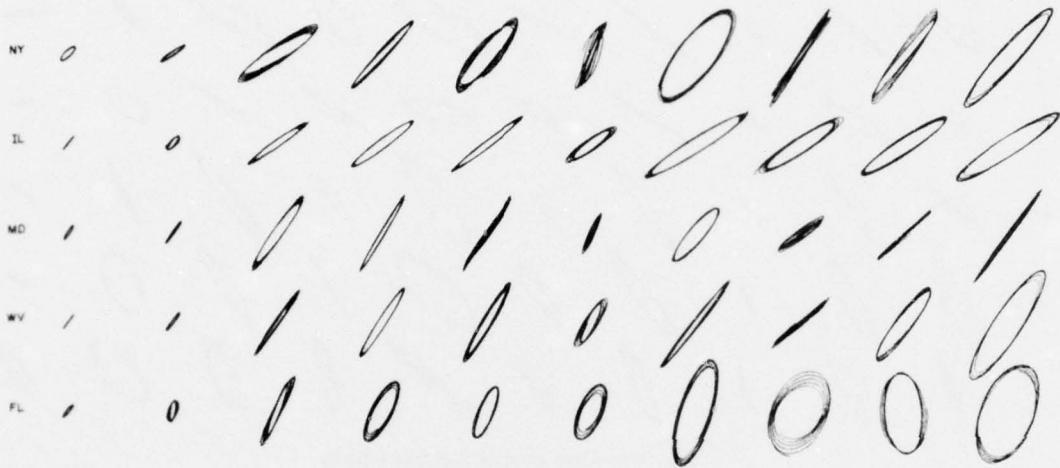
Fig. C16—Data sample 338 0241/0250
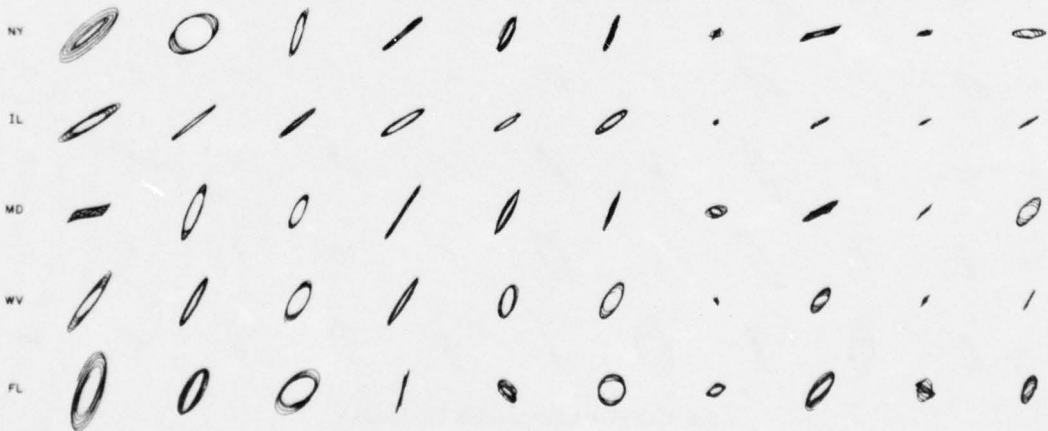
Fig. C17—Data sample 338 0251/0300
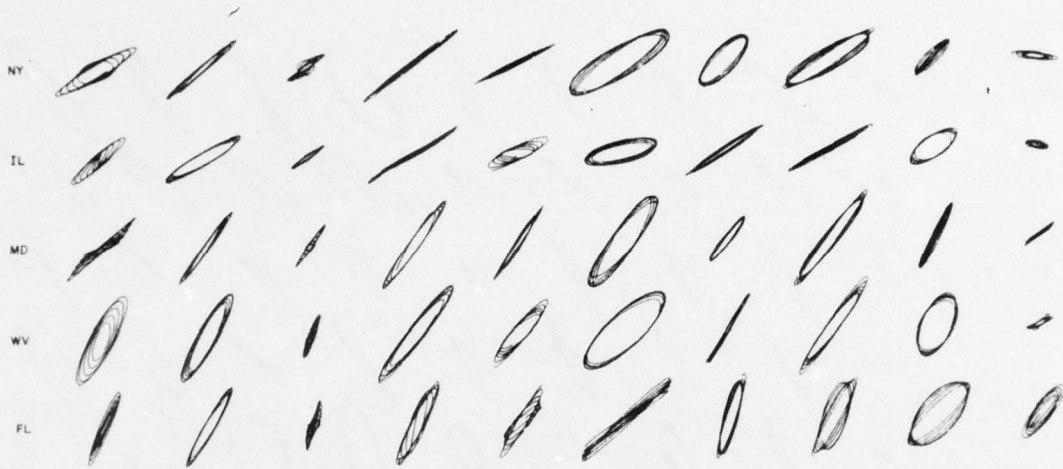
Fig. C18—Data sample 338 0301/0310
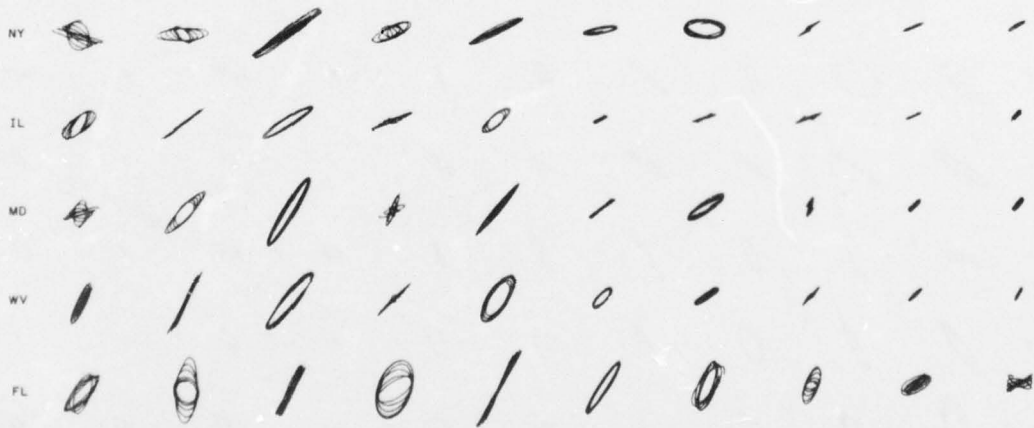
Fig. C19—Data sample 338 0311/0320
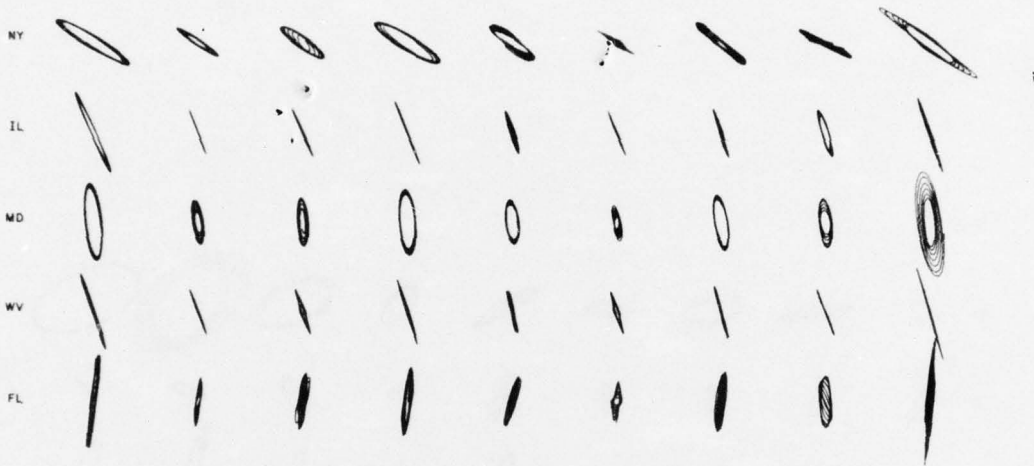
Fig. C20—Data sample 338 0631/0639
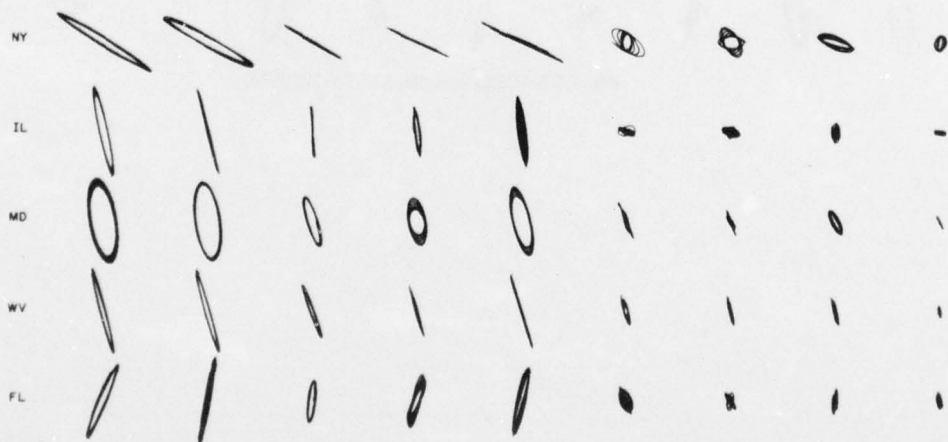
Fig. C21—Data sample 338 0640/0648
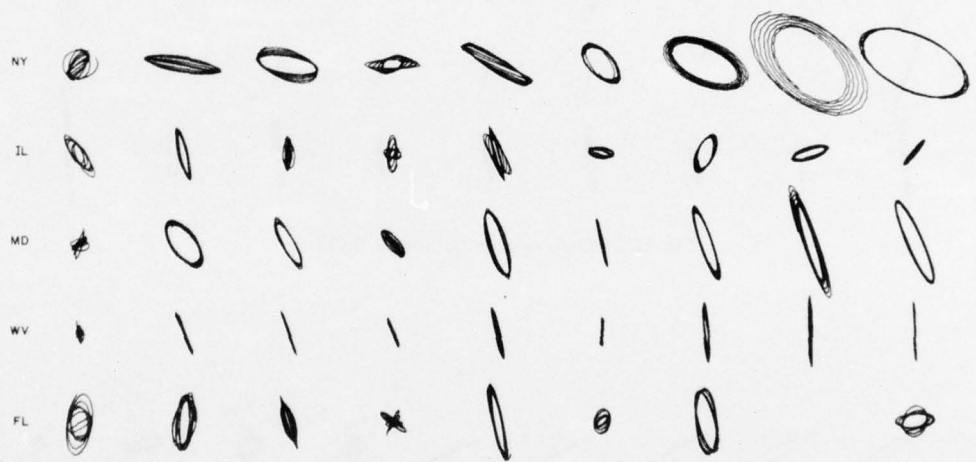
Fig. C22—Data sample 338 0652/0700

Appendix D

POLARIZATION PROJECTION MAPS

The average inclinations of the polarization ellipses at each site are projected to test the hypothesis that the projections point to the secondary source region. For comparison direction of arrival for the group-wave solution is shown for the plane-wave, flat-earth method (dashed line) and for the source location method (dotted line).

105 0916/0924

106 0720/0728

119 0809/0818

119 0819/0827

Fig. D1

122 0800/0808   196 0441/0450

196 0511/0520   338 0241/0250

Fig. D2

338 0251/0300

338 0301/0310

338 0631/0639
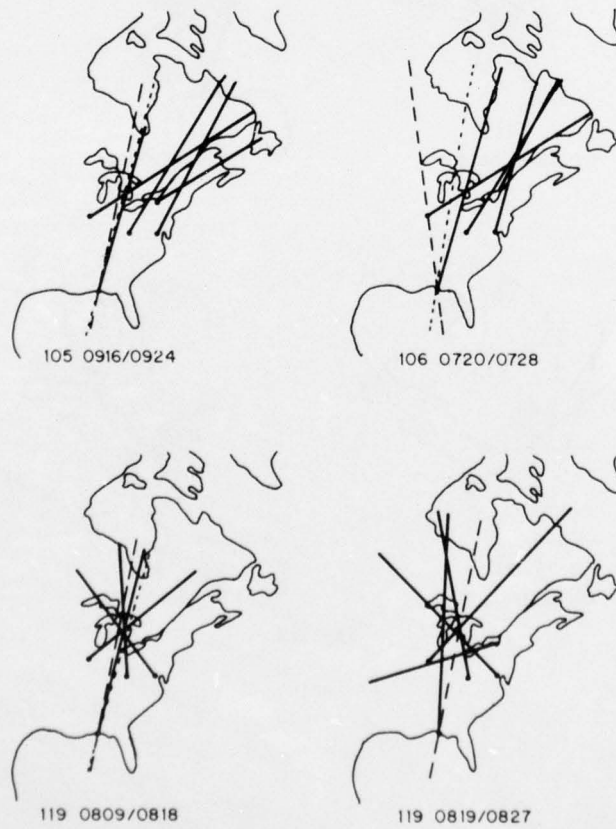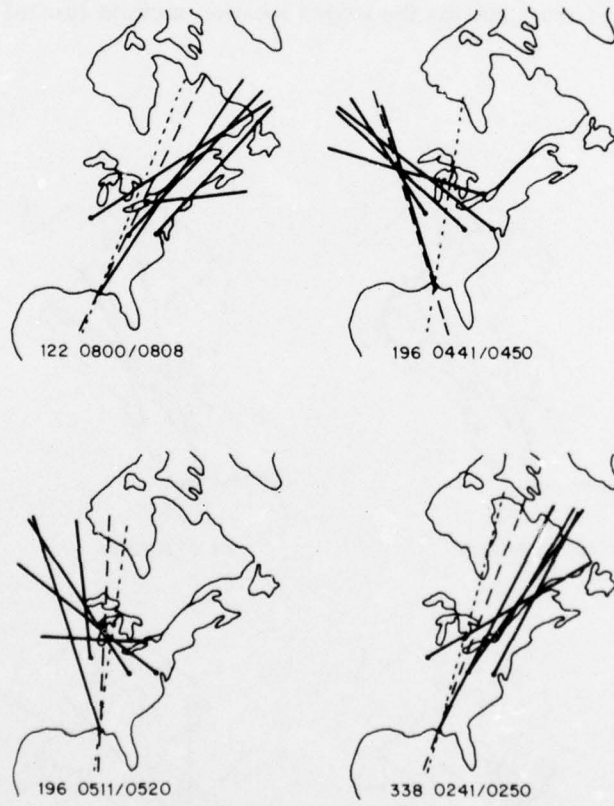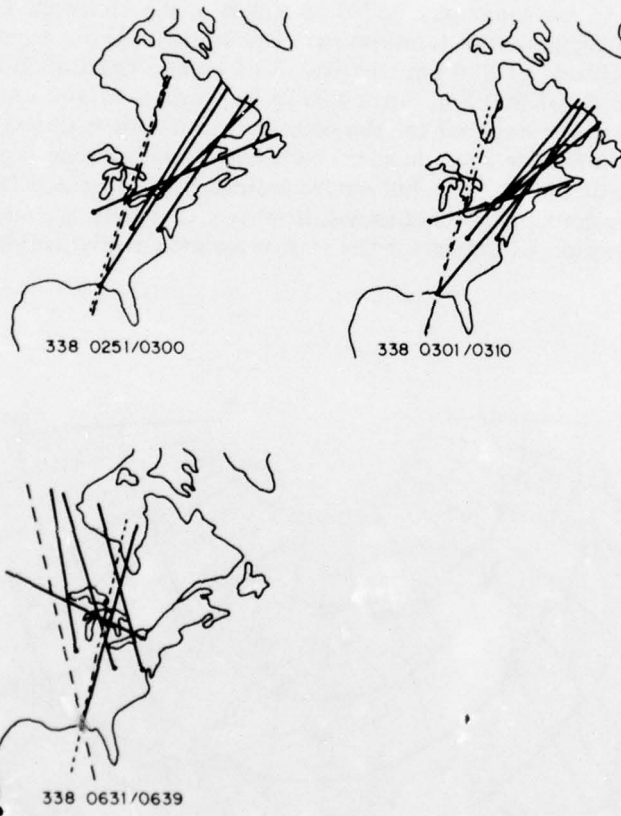
Fig. D3

Appendix E

RESULT SUMMARY MAPS

The directions of arrival and source locations determined for the group velocity solutions using the plane-wave, flat-earth method and the source location method are plotted in relation to the geography of North America, the McIlwain L-shell contours, and the astronomical twilight-sunrise terminators. The twilight-sunrise terminators were calculated for an altitude of 350 km (see Sec. 5 of text). The L-shell contours are plotted for an altitude of 200 km, but a change in position to 350 km is not significant. The direction of arrival computed for the plane-wave method is shown as a line terminating at the Florida reference site. In some instances these lines are tagged with numbered half-circles for identification. The full circles indicate the computed locations of the secondary source regions. It is emphasized, however, that they are most reliably used as an indicator of direction of arrival for the source location model (refer to Sec. 4 and 5).
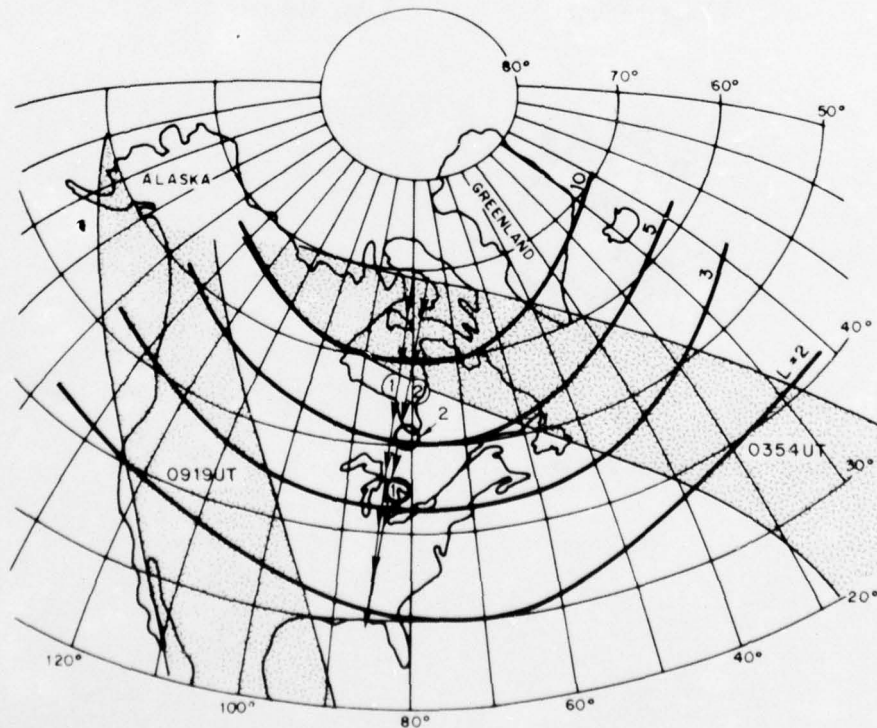
Fig. E1—Day 105. Twilight-sunrise contours computed at times indicated. Label indentification: (1) 0345/0403 UT; (2) 0915/0923 UT.
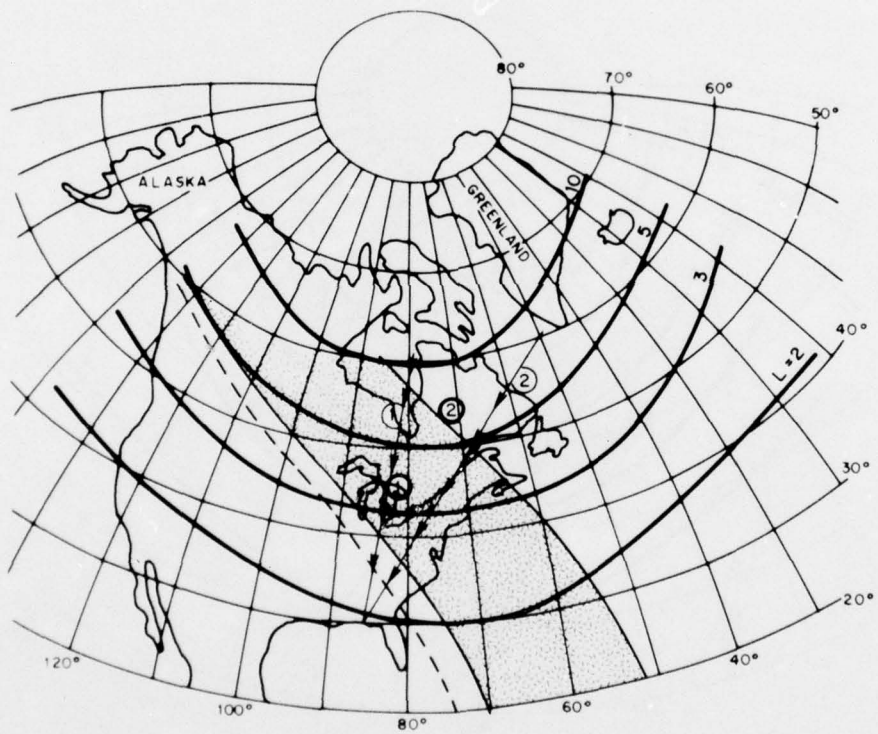
Fig. E2—Day 106. Twilight-sunrise contours at 0639 UT (stippled) and twilight contour at 0659 UT (dashed line). Label identification: (1) 0630/0648 UT; (2) 0650/0708 UT
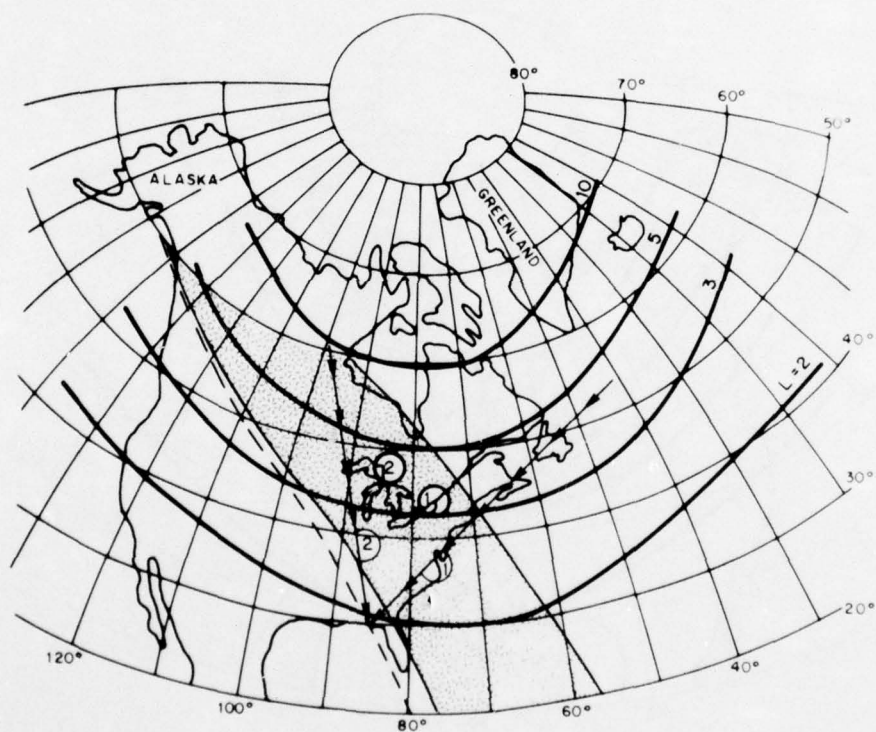
Fig. E3—Day 106. Twilight-sunrise contours at 0709 UT (stippled) and twilight contour at 0719 UT (dashed line). Label identification: (1) 0700/0718 UT; (2) 0710/0728 UT
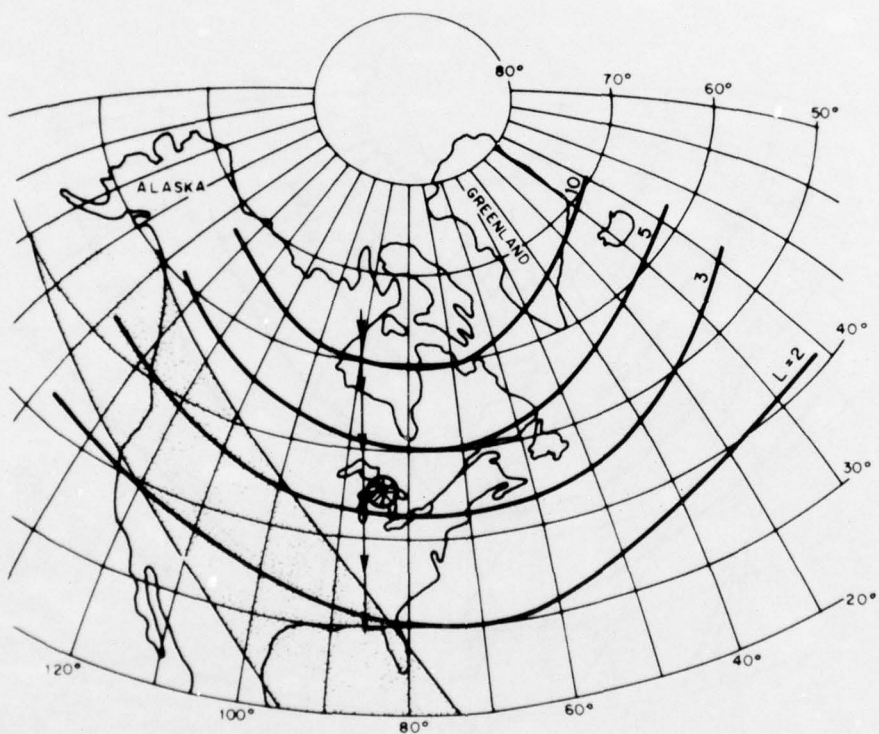
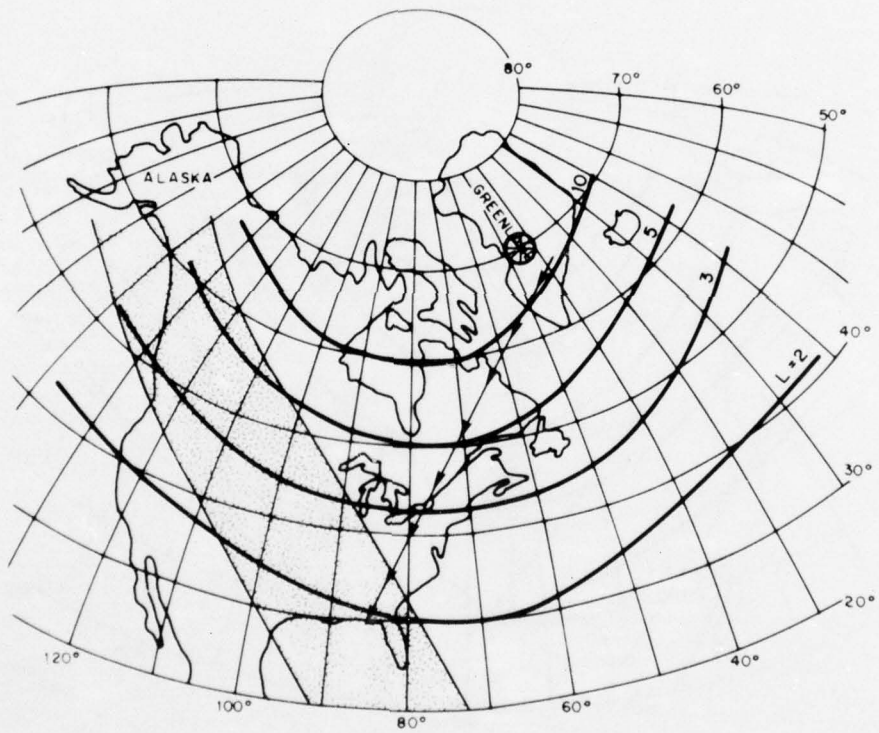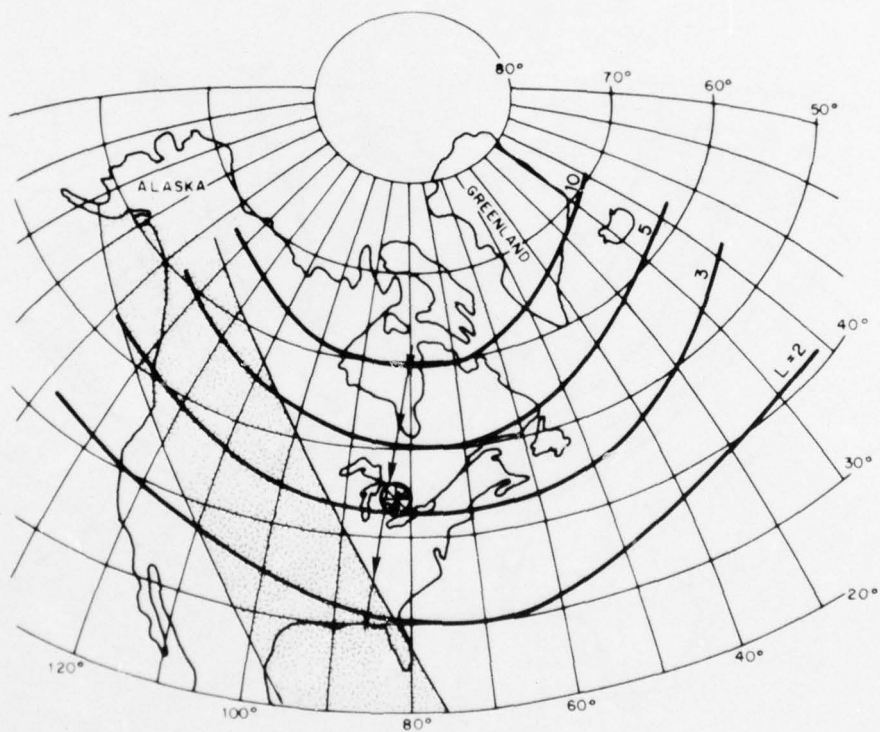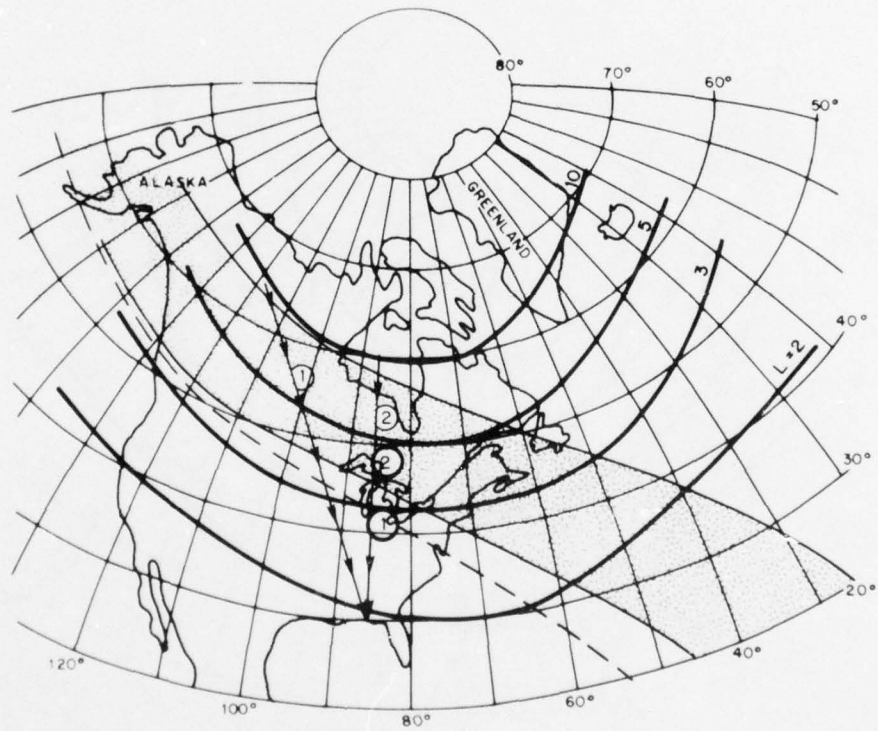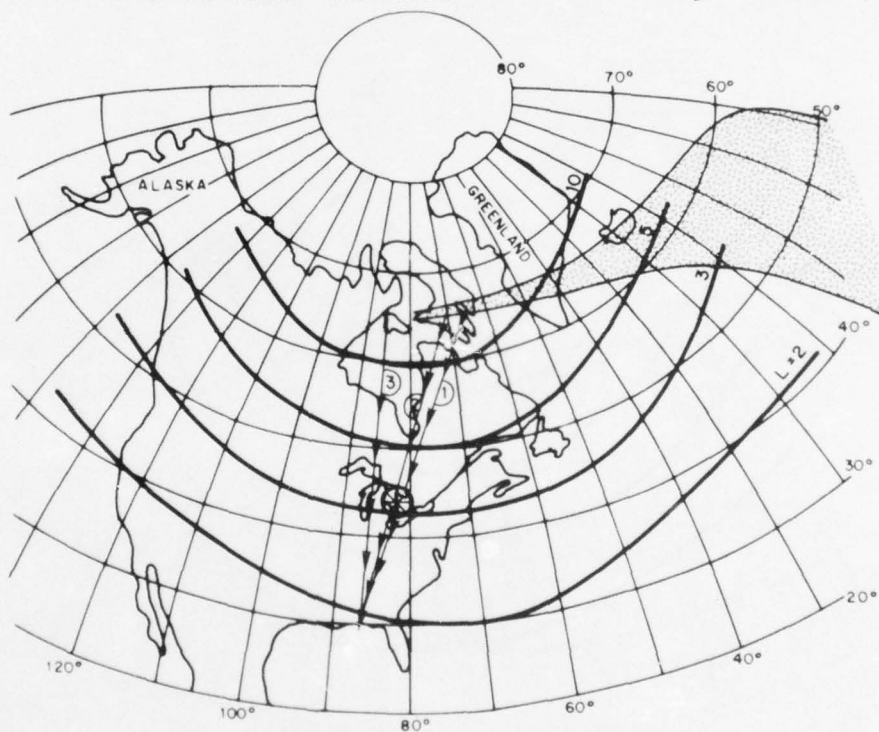Fig. E4—Day 119. Twilight-sunrise contours at 0817 UT. Analysis interval, 0808/0826 UT

Fig. E5—Day 122. Twilight-sunrise contours at 0801 UT. Analysis interval,
0757/0805 UT

Fig. E6—Day 195. Twilight-sunrise contours at 0759 UT. Analysis interval,
0754/0802 UT

Fig. E7—Day 196. Twilight-sunrise contours at 0440 UT (stippled) and twilight contour at 0513 UT (dashed line). Label identification: (1) 0440/0448 UT; (2) 0510/0518 UT

Fig. E8—Day 338. Twilight-sunrise contours at 0250 UT. Label identification: (1) 0241/0259 UT (1.019 and/or 1.031 Hz); (2) 0250/0308 UT (1.019 Hz); (3) 0250/0308 UT (1.031 Hz). Common source location for 1, 2, and 3.
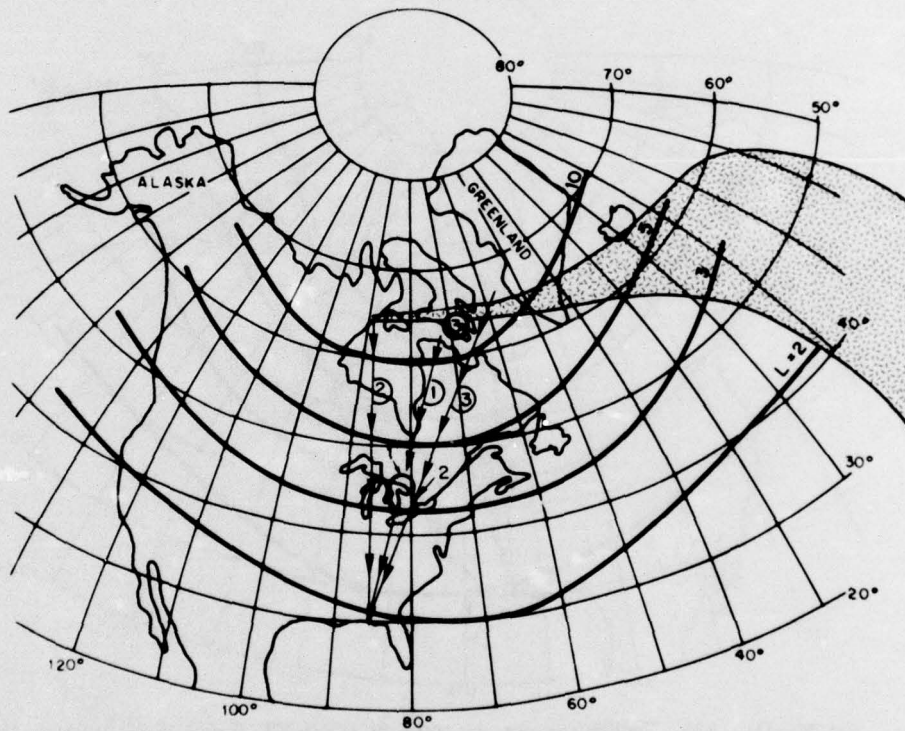
Fig. E9—Day 338. Twilight-sunrise contours at 0324 UT. Label identification: (1) 0300/0308 UT (1.019 Hz); (2) 0300/0318 UT (1.031 Hz); (3) 0315/0333 UT (1.031 Hz)
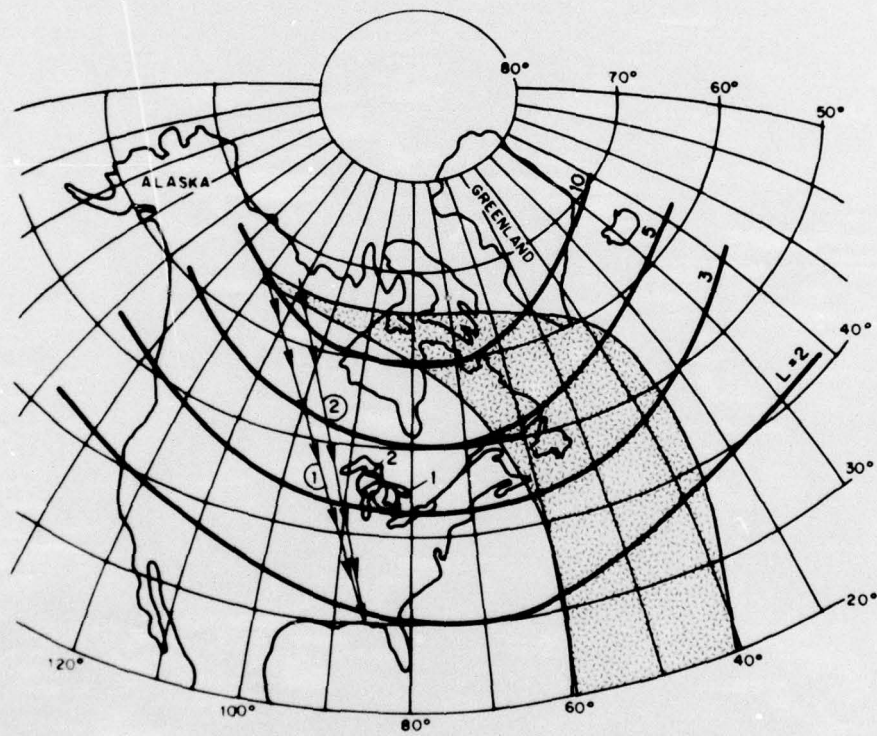
Fig. E10—Day 338. Twilight-sunrise contours at 0639 UT. Label identification:
(1) 0630/0648 UT; (2) 0642/0700 UT